R. & M. No. 3286

MINISTRY OF AVIATION

AERONAUTICAL RESEARCH COUNCIL
REPORTS AND MEMORANDA

An Investigation of the Flow about a Plane Half-Wing of Cropped-Delta Planform and 6 per cent Symmetrical Section at Stream Mach Numbers between 0·8 and 1·41

By E. W. E. Rogers, M.Sc., I. M. Hall, Ph.D. and C. J. Berry
of the Aerodynamics Division, N.P.L.

LONDON: HER MAJESTY'S STATIONERY OFFICE
1962
PRICE £1 14s. 0d. NET

An Investigation of the Flow about a Plane Half-Wing of Cropped-Delta Planform and 6 per cent Symmetrical Section at Stream Mach Numbers between 0·8 and 1·41

By E. W. E. Rogers, M.Sc., I. M. Hall, Ph.D.* and C. J. Berry
of the Aerodynamics Division, N.P.L.

Reports and Memoranda No. 3286†
September, 1960

Summary. A study has been made of the flow development over the wing as the incidence and stream Mach number vary and this is illustrated by surface pressure distributions and oil-flow patterns. The growth and movement of the two main surface shocks (the rear and forward shocks) is discussed, and conditions for flow separation through these shocks are considered. For the rear shock, which has little sweep, these conditions are similar to those for shock-induced separation on two-dimensional aerofoils. The forward shock is comparatively highly swept and separation seems to correspond to two rather different but simultaneously-attained conditions, one related to the component Mach number normal to the shock front and the other to the position of the reattachment line.

The flow in the region between the leading edge and the forward shock is shown to have certain characteristics analogous to those found upstream of the shock on two-dimensional aerofoils. To the rear of the forward shock, but ahead of the rear shock, the flow at low supersonic speeds resembles in some respects that about a simple cone.

The general flow development is related in the text to the wing lift and pitching moment, and the drag. The first two are most affected by the aft movement of the rear shock, which also stimulates the transonic drag rise. The lift-dependent drag is shown to be influenced by the appearance of leading-edge separation and possibly also by some stage in the development of the forward shock.

The flow over the cropped-delta planform is noteworthy for the absence of the strong outboard shock and this is attributed partly to the cropped tip and partly to the unswept trailing edge. A comparison is made with results obtained during preliminary tests in which the wing planform closely resembled that of a true delta.

1. *Introduction.* The flow about a plane sweptback wing at transonic and low supersonic speeds is quite complex, and only in recent years has substantial progress been made towards understanding the problems involved. At the N.P.L., early work in this field included an extensive investigation[1, 2] of the behaviour of a tapered, sweptback half-wing, having a leading-edge sweep

* Now Department of the Mechanics of Fluids, Manchester University.

† Previously issued as A.R.C. 22,191. Published with the permission of the Director, National Physical Laboratory.

of 53·5 deg, a trailing-edge sweep of 32·9 deg and an aspect ratio of 2·83*. Subsequently, tests have been made on another half-wing having the same leading-edge sweep and streamwise section (6 per cent thick RAE 102), but with an unswept trailing edge. The present report considers the results obtained with this delta planform.

The main sequence of tests was made with the wing cropped so that the taper ratio was 0·2. The tip chord is then almost the same fraction of the semi-span as for the earlier tapered wing (for a comparison, *see* Fig. 1a). Some preliminary tests, however, were made with a very small tip chord (taper ratio = 0·01) so that the true delta planform was closely approached. These results are also considered (Section 5 below).

The observations discussed in this report were obtained at intervals between September, 1958 and April, 1959.

2. *Experimental Details.* 2.1. *The Model.* The model planform is shown in Fig. 1b. The model itself was made by tangent-plane methods and has a tolerance on the circumscribing envelope of 0·001 in. The material used was free-machining 'Leadloy'. Four pressure-plotting stations are provided, at 0·15, 0·45, 0·70 and 0·90 of the cropped semi-span; it is sometimes convenient to refer to these as stations A to D respectively.

The chordwise distribution of holes was identical at each station (Table 1).

TABLE 1

Chordwise Distribution of Pressure Holes

Hole No.	1	2	3	4	5	6	7	8	9	10	11	12	13	14	15	16
(x/c) %	0	2	5	10	18	26	34	42	50	58	66	74	82	88	90	100

Except for certain check holes, all were located on the upper surface of the wing with respect to the convention used in defining incidence.

In most cases corresponding holes at each spanwise station were connected to a common pressure tube which passed through the root of the model to the outside of the tunnel. Thus only one station at a time could be tested, the holes at the other three stations being sealed with a solution of cellulose in acetone. To ease both the manufacture of the model and sealing difficulties when in the tunnel, some of the holes close to the leading edge were interconnected to only one other hole; in addition the trailing-edge pressure holes were all independent.

2.2. *The Tunnel.* The half-wing was mounted directly on a turntable forming part of one sidewall of the 18 in. × 14 in. High-Speed Wind Tunnel. No provision was made to reduce the wall boundary layer just upstream of the model position, partly because earlier experience had shown that the layer apparently had little effect on the pressures measured at the most inboard station, A. For the transonic speed range (stream Mach number, M_0, < 1·22) walls with longitudinal slots were fitted above and below the model, the ratio of open to total area of these walls being one-eleventh[3]. Solid, shaped liners replaced the slotted walls for tests at $M_0 = 1·41$. In both configurations the sidewalls were formed from solid interchangeable panels, some containing windows.

* Wing 12 of Warren's series of planforms.

The operation and performance of the tunnel at transonic speeds is described in Ref. 3. At $M_0 = 1{\cdot}41$, the variation in stream Mach number at the model position is less than $\pm 0{\cdot}01$; the majority of disturbances present are weak and originate from junctions in the sidewalls.

The wing surface pressures were recorded on two multitube mercury manometers, and the wing forces and moments measured by means of a four-component strain-gauge balance mounted externally on the turntable.

All measurements were made with the tunnel stagnation pressure (H) held constant at 31 in. mercury absolute.

2.3. *Experimental Procedure.* As was mentioned earlier it was necessary to measure the distribution of surface pressure at each spanwise station in turn for the required range of M_0. Results were obtained at both positive and negative incidences in order to simulate the effect of an upper and lower surface. Normally the wing incidence was varied from + 12 to − 12 deg in steps of one degree, but, where required, distributions were measured at incidences outside this range or at closer intervals. The zero incidence was found by using the lower-surface check holes provided on the model; the variation with Mach number was negligible. It was considered that a given incidence could be set and reset to an accuracy better than 0·05 deg.

All the results discussed in this report were obtained with a leading-edge roughness band extending over the initial 0·1 of the local chord on both surfaces. The band was formed from No. 320 grade carborundum powder set in a thin band of proprietary lacquer*. Boundary-layer transition was found to occur at the band on both surfaces for the complete range of Mach number and incidence. The transition band was broken for a small part of the semi-span at each pressure-plotting station in order to obtain reliable pressure readings from the holes close to the leading edge. The patch of laminar flow which may occur as a result of this is quite small and the technique is one that has been found satisfactory on other models.

The transition band was continuous for the balance measurements of wing lift, drag, pitching and rolling moments, which were obtained for similar values of incidence and stream Mach number as the chordwise pressure distributions.

In the balance tests a small gap existed close to the model root to allow for the deflection of the balance system. In addition, a gap occurred between the model root and the tunnel wall near the root trailing and leading edges. These gaps were made as small as possible to minimise the effects of leakage either into the balance box (itself connected to the tunnel static pressure) or from one surface of the model to another. It is felt that errors introduced by such leaks are small, although it is not possible to estimate them with any accuracy.

The force and pressure measurements were supplemented by an extensive series of surface oil-flow patterns so that the general flow development with incidence or Mach number could be studied. The material used was a 1:2 mixture of titanium oxide and a suitable oil,† with the addition of lauric acid. A satisfactory pattern could be obtained, and subsequently photographed, after about two minutes running time.

No corrections have been applied to the present results to allow for wall-interference effects at subsonic and transonic speeds. Some allowance has been made however for the Mach number

* For details of the roughness band itself and the techniques used in its preparation, *see* Ref. 4.

† Shell Vitrea 72 (kinematic viscosity 720 centistokes at 20° C.).

gradient along the working section known to be present at low supersonic speeds. This effect is relatively small, a nominal Mach number of 1·10 becoming 1·11, when corrected. In this speed range the flow about the model is influenced by wave reflections from the tunnel walls; this matter is discussed further below (Section 7).

2.4. *Reynolds Number.* The test Reynolds number (R_c), based on the mean aerodynamic chord ($\bar{c}$), varies with stream Mach number. Typical values are given in Table 2, for a stagnation pressure of 31 in. mercury.

TABLE 2

Test Reynolds Number

M_0	0·80	1·00	1·20	1·41
$R_c \times 10^{-6}$	2·5	2·8	3·0	2·8

3. *Results and Discussion of Flow Development.* 3.1. *Presentation of Results.* The measured distributions of pressure at the four spanwise stations are listed in Table 3 as the ratio of the observed pressure (p) to the tunnel stagnation pressure (H). Some of these results are plotted in Figs. 2 and 3; the former shows the effect of changes in stream Mach number at constant incidence, the latter the variation in surface pressure with incidence at a given value of M_0. The development of the flow on the wing surface, as indicated by typical oil-flow photographs, is contained in Fig. 4. Each section of this Figure depicts results at constant Mach number and is placed next to the corresponding section of Fig. 3 so that flow patterns and pressure distributions can be compared easily.

The wing lift, drag and pitching moment, expressed in the usual coefficient form, are included as Table 4, and a graphical presentation is made in Figs. 5a, b and c. Further data derived from the balance tests, including lift-curve slope, centre-of-pressure position and lift/drag ratio are set out in the various sections of Fig. 6. The basic information from the present tests is completed by Fig. 5d which shows the various flow-development boundaries deduced from the complete set of oil-flow photographs.

The subsequent Figures are concerned with a more detailed analysis of the results and will be referred to as required in the discussion.

3.2. *Summary of Flow Development.* It is perhaps convenient at this stage to describe briefly the flow development over the wing as stream Mach number and incidence are increased. In subsequent sections some aspects of the wing flow will be discussed further.

At the lowest test Mach number (0·80) and low incidence the local supervelocities near the leading edge increase markedly towards the tip and there is an accompanying forward movement of the chordwise loading. The resultant flow velocity becomes supersonic at station D ($\eta = 0{\cdot}90$) at an incidence of about 1·5 deg. Just below $\alpha = 4$ deg, separation occurs near the tip (Fig. 4a (i)), the separated flow rolling up to form a part-span vortex. This moves inboard with increasing incidence, causing a small rise in pressure on the inboard edge, near the reattachment line, and a

reduction in pressure beneath the vortex. When the vortex has moved inboard sufficiently, station D becomes outboard of the secondary separation line (*see* Fig. 4a (iv)) and hence lies in a region of low surface shear.

The general sequence is similar at $M_0 = 0{\cdot}90$, and is not greatly influenced by the presence of a shock wave which at moderate incidences lies across all but the most inboard region at about $0{\cdot}4$ of the local chord. As can be seen in Fig. 3b this shock wave (which corresponds to the rear shock in the nomenclature of Ref. 1) is stronger and slightly nearer the leading edge at station D for a given incidence. The shock wave can be detected from the oil-flow pattern at $\alpha = 5$ deg in Fig. 4b (i) the direction of the filaments changing most markedly at station C. The most outboard station (D) is influenced at this incidence by the vortex associated with the leading-edge separation and the effects of the rear shock in this region are obscured. With increase in incidence the vortex moves inboard as at $M_0 = 0{\cdot}80$. At $\alpha = 12$ deg, the two outboard stations lie beyond the secondary separation line and hence have only slight chordwise pressure gradients on the upper surface. Station B is largely beneath the part-span vortex and exhibits a characteristic 'hump' in the surface pressure distribution at $x/c = 0{\cdot}4$. Station A at $\eta = 0{\cdot}15$ is little influenced by the leading-edge separation and still has a pronounced suction peak near the nose. The rear shock in this region has become a diffuse, continuous compression.

The rear shock can be clearly seen in the oil patterns and pressure distributions obtained at $M_0 = 0{\cdot}95$ (Figs. 4c and 3c). At $\eta = 0{\cdot}90$, the shock exists on both the upper and lower surface for incidences between 0 and 4 deg and the surface pressure just downstream of the shock is close to that for local sonic flow, a feature also found in tests on two-dimensional aerofoils. Leading-edge separation once again occurs just below $\alpha = 4$ deg and the resulting part-span vortex moves, with increasing incidence, across the wing thus diminishing the region influenced by the rear shock. The rear shock in fact is eliminated at station D before it has grown sufficiently in strength to induce boundary-layer separation to the rear; moreover the rate at which the part-span vortex moves inboard with incidence is sufficiently large to prevent the conditions for shock-induced separation building up farther inboard. As a result the wing is free of this phenomenon at $M_0 = 0{\cdot}95$.

Just above a stream Mach number of $0{\cdot}95$ at an incidence close to 4 deg, a forward shock can be detected near the tip, and the onset of leading-edge separation is delayed slightly. As Fig. 5d shows, the latter effect becomes more marked as M_0 increases and at a Mach number of unity the forward shock is clearly visible at $\alpha = 5$ deg (Fig. 4d (v)) whilst the flow breakdown at the tip occurs a little below $\alpha = 6$ deg. The corresponding development of the surface pressures at station D can be seen in Fig. 3d; the forward shock appears as a strong recompression at about $x/c = 0{\cdot}23$. Once again with increasing incidence the part-span vortex sweeps inboard across the wing.

The rear shock at $M_0 = 1{\cdot}00$ is comparatively unswept and its position on the wing surface changes little with incidence. Flow separation between the shock and the trailing edge would appear to occur by $\alpha = 2$ deg, but the exact incidence is not easy to determine from the oil-flow patterns alone. The bow wave first appears at this speed, but does not directly affect the flow on the model surface, except where it is reflected on to the wing surface from the tunnel walls.

The rear shock almost reaches the trailing edge by $M_0 = 1{\cdot}05$; the forward shock appears at a slightly lower incidence than at $M_0 = 1{\cdot}00$ (Fig. 5d) and separation to the rear of this can be seen at $\alpha = 5$ deg in Fig. 4e (iii). The flow separation develops into a vortex, the characteristic oil-trace being well defined for example in Fig. 4e (v) at $\alpha = 8$ deg. At this incidence tip leading-edge separation begins, the separated flow joining the vortex formed behind the forward shock; with

increasing incidence separation spreads rapidly along the leading edge. The forward and rear shocks disappear or are reduced in extent as the vortex moves inboard.

This type of flow development with incidence, characterised by attached flow around the leading edge to a forward shock, the presence of the rear shock at the trailing edge, and the ultimate spread of the tip separation inboard, persists at stream Mach numbers of 1·11 and 1·16. The incidence at which the forward shock can be detected behind the roughness band, or induces separation, or at which tip separation occurs, changes however as shown in Fig. 5d. Thus the delay in tip separation allows the vortex behind the forward shock to grow sufficiently to cause significant regions of relatively low pressure on the wing surface, as for example in Fig. 3g, station C, at incidences between 6 and 10 deg.

The surface pressure distributions and oil-flow patterns obtained at $M_0 = 1{\cdot}41$ are shown in Figs. 3h and 4h. In general the flow development is similar to that applicable to the upper end on the transonic range; the forward shock appears at a somewhat smaller incidence and its influence can be seen even at station A at $\alpha = 12$ deg. Above $\alpha = 5$ deg the forward shock intersects the wing trailing edge, the intersection point moving inboard with increasing incidence. Thus by $\alpha = 8$ deg (Fig. 4h (iv)) station D is almost clear of the influence of this shock, the surface pressure remaining nearly constant along the chord (Fig. 3h). The oil patterns show however a tip shock originating close to the tip leading edge and crossing station D at about mid-chord, and the forward shock at about 0·8 semi-span. This tip shock is weak and has only a small effect on the pressure distribution and the direction of the oil filaments. By $\alpha = 9$ deg the intersection between the forward and tip shock is more marked and a triangular region of separated flow exists between the intersection point and the trailing edge. The forward shock has a pronounced kink, the portion behind the tip shock becoming less swept. This effect is sufficient to cause station D to be influenced once more by the forward shock, which results in the pressure changes observed at this station close to the trailing edge at $\alpha = 12$ deg (Fig. 3h). Station C is affected by the flow separation which may be responsible for the larger pressure recovery observed close to the trailing edge at high incidence.

The vortex formed from the flow separating behind the forward shock is most marked at these high incidences (*e.g.*, Fig. 4h (vi)) and as the leading-edge separation develops and moves inboard it changes into the part-span vortex associated with the leading-edge separation (Fig. 4h (viii)).

The foregoing description of the flow development does not reveal any novel feature, except for the flow separation at $M_0 = 1{\cdot}41$ associated with the intersection of the forward and tip shocks. The most significant aspect is perhaps the apparent absence of an outboard shock (*i.e.*, a strong compression outboard of the intersection of the forward and rear shocks which is frequently associated with severe flow separation to the rear). The unswept trailing edge of the present planform ensures that the rear shock reaches the trailing edge at a comparatively low Mach number (about 1·05); the development of the forward shock with incidence at speeds below this is restricted by the onset of leading-edge separation. Intersection between the forward shock and the rear shock only occurs therefore when the latter is at the trailing edge, and was detected in fact only at $M_0 = 1{\cdot}41$. No results were available between Mach numbers of 1·16 and 1·41 for the correct range of incidence and it seems likely that an intersection will occur above about $M_0 = 1{\cdot}20$. The cropped tip of course helps to delay this event. The resultant outboard shock will form close to the trailing edge and thus its significance in promoting extensive flow separation would seem to be reduced; indeed by $M_0 = 1{\cdot}41$ the marked flow separation is associated more with the intersection of the rear and tip shocks.

The initial tip shock[1], which sometimes forms close to the tip of a swept wing near sonic stream speed, would also appear to be absent for the present planform. In fact, however, it can be detected in the oil-flow photographs at $M_0 = 0{\cdot}95$, $\alpha = 1$ deg. The rear shock which is swept back crosses station D at about $0{\cdot}4$ chord; a second shock (the initial tip shock) is visible normal to the oncoming flow at about $0{\cdot}45$ chord. The two shocks are so close that their separate effects cannot be distinguished in the surface pressure distribution (Fig. 3c); moreover the rear-shock movement and growth with incidence and Mach number are sufficient to swamp the initial tip shock when the flow conditions are changed and hence the latter exists independently in only a very limited flow régime.*

This brief survey of the flow development over the wing with increasing stream speed and incidence will now be followed by a more detailed study of some of the points which are of general interest in considering the behaviour of sweptback wings.

3.3. *Flow Development in the Leading-edge Region.* The inboard spread of leading-edge separation with increasing incidence suggests that this movement is controlled by the attainment progressively of some critical condition in the leading-edge region. The determination of such a condition probably requires a detailed experimental investigation; the present model which has pressure holes at the leading edge, $0{\cdot}02$ and $0{\cdot}05$ chord is obviously unsatisfactory. In Fig. 7a, the variation of observed pressure at hole 2 ($x/c = 0{\cdot}02$) at the four spanwise stations is plotted for a stream Mach number of $0{\cdot}80$. The lowest pressure achieved is similar at stations B, C and D; station A is unaffected by the part-span vortex within the incidence range of the tests. It is not possible to determine exactly at what incidence leading-edge separation took place at each station, partly because of the roughness band which extends over the first $0{\cdot}1$ chord. The incidence at which the vortex reattachment line first reaches the rear of the roughness band can be found however and the values for stations B, C and D are indicated. These too correspond to an approximately constant pressure ratio; reattachment at $x/c = 0{\cdot}02$, if it occurs, will take place at lower incidences.

The magnitude of the lowest pressures reached by hole 2 in Fig. 7a is perhaps of no great significance in itself. The peak occurs when the hole lies beneath the vortex; further increase in incidence leads to a more rearward position of the vortex 'centre' along the particular spanwise station, and rise in pressure at hole 2.

In Fig. 7b, the pressure variation for this hole at station C is shown for various stream Mach numbers. Up to $M_0 = 0{\cdot}925$, the peak suction occurs at about the same incidence, suggesting that the local vortex development has some similarity. Of more significance perhaps is the fact that above $M_0 = 0{\cdot}925$ the observed pressures tend to be almost independent of Mach numbers between $\alpha = 5$ deg and the incidence at which the tip separation spreads inboard to affect station C. Above the latter value the pressure rises as the pressure hole enters the region outboard of the secondary separation line.

This dependence of local pressure largely on wing incidence occurs of course in the attached-flow régime ahead of the forward shock and its inception may be estimated from the change in slope which occurs in the curves at about $\alpha = 5$ deg for example in Fig. 7b, and 4 deg in Fig. 7c, an event which may be related to the development of a supersonic type of flow around the leading edge

* It is of course debatable whether the shock which forms near the tip at low incidence at $M_0 = 0{\cdot}90$ (Fig. 3b) is a rear shock or an initial tip shock; the present evidence is insufficient to determine this. The tip flow is soon dominated by the rear shock however, and it is convenient to describe the complete process simply as a development of the rear shock.

and which has a marked similarity to certain two-dimensional aerofoil flows. It is shown again in Fig. 7c this time for station D. Once again the beginning of the final pressure rise at each Mach number corresponds to the tip separation reaching this spanwise position. In both cases the measured pressures for a given incidence are not entirely constant, but rise very slightly with increasing M_0, a trend consistent with the curve obtained at $M_0 = 1{\cdot}41$, which is somewhat different from the transonic set of curves.

Farther back along the chord at $x/c = 0{\cdot}18$, a similar group of curves may be obtained (Fig. 7d). The slight trend with Mach number is now not so simple in form, but the results are consistent with reaching the broken line as the stream Mach number approaches $1{\cdot}41$.

There is some similarity between this pressure freeze on the swept wing and that observed in the transonic flow about two-dimensional aerofoils where the local pressures upstream of the shock do not change greatly with stream Mach number; this is the so-called 'sonic freeze'. On a swept wing the phenomenon only applies to the region ahead of the forward shock where, in fact, the flow most closely approaches that on an infinite yawed wing, because the roof and tip influences are greatly diminished.

By taking a mean line through the relevant points the approximate shape of the transonic pressure-freeze curves of Figs. 7b, c and d can be obtained, as shown in Fig. 8a. For hole 2, the shape of the two lines is similar but that at the more inboard station is displaced to incidences about $1{\cdot}5$ deg higher. This must be due to the delay in flow development as the roof is approached. The conditions for which flow breakdown occurs at each station might be expected to be similar however. This event corresponds approximately to the attainment of the minimum pressure for a given Mach number and the actual values of the lowest pressure ratio $(p/H)_{\min}$ from Figs. 7b and c have been plotted in Fig. 8b. Except at $M_0 = 1{\cdot}00$ the same minimum pressure (or maximum velocity) is reached at the breakdown condition at the two stations. This suggests that the inboard spread of the separated region is controlled by the speed at which a given pressure distribution is reached near the leading edge at each spanwise station. The critical pressure, $(p/H)_{\min}$, seems to depend on stream Mach number, but at a given Mach number is achieved by measuring the wing incidence.

In addition to the transonic pressure 'freeze' mentioned above, the position of the part-span vortex over the wing surface is also affected only a small amount by stream Mach number. It is not easy to define the vortex position accurately and for convenience the position of the reattachment line has been used, though even this is not always well-defined. Its approximate position at various angles of incidence is shown in Fig. 9a. The left-hand diagram confirms that up to 10 deg incidence at least, the reattachment-line position is almost unchanged by increasing M_0 from $0{\cdot}8$ to $1{\cdot}0$. This Mach number range is representative of conditions where the flow is dominated by a part-span vortex for most of the incidence range above about 5 deg*.

The right-hand diagram gives results for incidences of 10 deg and above, after leading-edge separation has developed. Though a direct comparison at different Mach numbers and constant incidence is not possible, the results suggest that vortex position is largely determined by the model incidence alone, even at $M_0 = 1{\cdot}41$. At incidences below those shown in this diagram the flow is attached around the leading edge. Separation, with an attendant vortex, may still be

* At $M_0 = 1{\cdot}0$, a forward shock exists between incidences of 4 and 5 deg, but leading-edge separation and the resultant vortex have formed by $\alpha = 6$ deg (Fig. 4d (v) and (vi)).

present behind the forward shock however and it seems that the reattachment line of this vortex is at about the same position as for a leading-edge vortex at the same incidence at lower Mach numbers. This point is illustrated in Fig. 9b. It is thus as if the wing geometry and incidence fix in some way the position of the reattachment line; any separation ahead of this is forced to conform to the general pattern, irrespective of the cause of the separation or the stream Mach number. At $M_0 = 1{\cdot}41$ the forward shock is swept a little behind the reattachment region appropriate to 8 deg at the lower Mach numbers, except outboard of about $0{\cdot}7$ semi-span. The flow through the shock is attached up to this position and separates outboard.

To investigate this point further the positions of the reattachment lines at incidences of 6, 7 and 8 deg for $0{\cdot}7$ semi-span were plotted against stream Mach number (Fig. 10a). It is not possible to obtain great accuracy but as far as can be judged the positions of these lines varied little with Mach number*, and thus were independent of whether the separation sprang from the leading edge or from a forward shock well back on the wing surface. The position of the latter has also been plotted in this Figure and the use of filled symbols indicates that the flow separates through the shock. Two cases of incipient separation occur at this station; at $M_0 = 1{\cdot}16$, $\alpha = 6$ deg and at $M_0 = 1{\cdot}41$, $\alpha = 8$ deg. These are denoted by half-filled symbols. Both are close to the intersection of the forward-shock locus and an extrapolation of the reattachment-line position, the latter being assumed to be independent of stream Mach number. These intersections, and one deduced for $\alpha = 7$ deg, are plotted in Fig. 10b and not unexpectedly agree well with the separation line at $\eta = 0{\cdot}7$ obtained from the oil-flow patterns.

Similar results can be obtained at other spanwise stations (except very close to the tip), though accuracy is lost farther inboard, as the shock approaches the leading edge.

Fig. 10 would seem to lead to the suggestion that separation through the forward shock depends on whether this is ahead of, or behind, a reattachment line fixed only by the wing incidence. This criterion is difficult to interpret physically and moreover appears to be unrelated to an alternative but more conventional approach discussed in the next section when the forward shock will be considered in more detail.

3.4. *The Forward Shock.* At constant wing incidence, and with increasing stream Mach number the forward shock moves rearward at any particular station. This is shown in Fig. 10a and also in more detail in Fig. 11, where the curves are drawn to show the movement in shock position with incidence at constant M_0. The variation is approximately linear except at $M_0 = 1{\cdot}41$, where the intersection between the forward shock and the tip shock causes the former to cross station D ahead of the trailing edge again for incidences greater than 9 deg. At station C too, the rear shock remains stationary for incidences between 11 deg and the onset of leading-edge separation at this position.

This rearward movement could be due to an increase in shock sweep (ϕ_F) with incidence or Mach number. Fig. 12 suggests that the former effect is negligible and the variation of ϕ_F with M_0 is small enough at transonic speeds to be attributed mainly to difficulties in measuring this quantity from the photographs. Thus it is probably true to say that the forward-shock movement with

* Except at $M_0 = 0{\cdot}90$ and $0{\cdot}95$ at $\alpha = 8$ deg where the vortex position over the outer part of the wing seems to be influenced by the rear shock and the tip flow, and acquires a larger sweep. This may be unrepresentative of the general pattern, when the rear shock is absent or is close to the trailing edge. This distortion is less marked for an analysis made at $\eta = 0{\cdot}5$.

incidence is mostly due to an inward displacement of the point along the leading edge at which the shock turns back over the wing surface, a displacement associated with the increase in the general level of local velocities with incidence, and the spanwise velocity gradient*.

At constant incidence and increasing stream Mach number the pressures ahead of forward shock change only slowly (Fig. 7).

In earlier tests on sweptback wings there has been some interest in the conditions for which flow separation takes place through the forward shock. In Ref. 2, for example, it appeared that separation occurred when the component Mach number normal to the shock front (M_n) exceeded about 1·39. M_n may be found from a knowledge of the geometric shock sweep, ϕ_F, the local Mach number just upstream of the shock (M_1) and the direction of this flow relative to the stream direction θ. Thus

$$M_n = M_1 \cos(\phi_F - \theta).$$

The flow deflection θ can be related theoretically[2] in a simple manner to M_1, but is best found from the oil-flow patterns and is taken as the filament direction just ahead of the shock. This is permissible since both the spanwise and chordwise pressure gradients are small in this region and the oil probably gives a realistic indication of the flow direction outside the boundary layer. This type of analysis has been applied to the most suitable results on the cropped-delta wing, where the forward shock is sufficiently behind the roughness band for the flow direction θ to be measured accurately. This means that only station D can be used at transonic speeds; at $M_0 = 1{\cdot}41$, the shock reaches the trailing edge at this station before separation occurs but the data at stations B and C are satisfactory. The results are shown in Fig. 13, and agreement with the tentative criterion of Ref. 2 is quite good. Two points are shown with half the symbol filled to indicate that separation appeared to be just beginning (*i.e.*, the oil filaments behind the shock were almost parallel to the shock front[2, 6]); both points lie close to the broken line representing $M_n = 1{\cdot}39$.

This agreement with the results of Ref. 2 is not unexpected since the leading-edge sweep and streamwise section of the two wings are identical. Further investigation would be required to establish whether such a criterion has a wider validity. Its relationship to the other apparent criterion shown in Fig. 10 is unknown at present, though it is possible that both are aspects of some more fundamental condition. One further point should perhaps be mentioned; the shock movement on the wing is unaffected by the onset of separation, as is shown in Fig. 11.

Pressure distributions were also obtained at $M_0 = 1{\cdot}16$, for station C at incidences between 5 and 8 deg, in intervals of 0·25 deg. Those for the upper surface are shown in Fig. 14. Separation first occurs at $\alpha = 6$ deg, this curve being shown as a broken line. The pressure ratio just upstream and downstream of the shock (p_1/H and p_2/H respectively) can be defined approximately by the lines sketched in the Figure. The shock pressure ratio p_2/p_1 is plotted in the lower diagram, which shows that this reaches a maximum value well after separation. The local Mach number ahead of the shock (M_1) continues to increase steadily with incidence, the rearward shock movement and chordwise reduction in local Mach number being insufficient to compensate for the general rise in surface velocity with incidence. These two quantities do not seem to be directly related to the onset of separation in the way that M_n is, for example.

* This assumes a simple flow model in which the forward shock exists close to the leading edge for some part of the wing span inboard and turns back over the wing when local flow conditions are appropriate. Such conditions may be reached progressively nearer the leading edge as the incidence is increased.

Unfortunately, the forward shock at station C for $M_0 = 1{\cdot}16$ is too close to the roughness band to enable the flow deviation θ to be measured accurately from the oil-flow photographs over most of the incidence range which is of interest. However with care a reasonably reliable estimate can be made and M_n calculated. The results are given in Fig. 15. Separation was considered to be just beginning at $\alpha = 6$ deg, when $M_n = 1{\cdot}35_5$; by $\alpha = 6{\cdot}5$ deg, $M_n = 1{\cdot}39_5$, the oil-flow pattern clearly indicated that separation had occurred. Note that incipient separation was considered to be present at $\alpha = 6$ deg at station D, the value of M_n then being $1{\cdot}39$.

Fig. 15 does not really enable a more precise assessment to be made of a separation condition in terms of M_n than has already been obtained. The accuracy of determining this quantity is unlikely to be very high, and in addition the estimate of the 'beginning' of separation depends to some extent on the quality and number of the relevant flow patterns. It is felt however that Fig. 15, as well as Fig. 13, provide further evidence that a critical value of M_n for this range of leading-edge sweep and section lies near $1{\cdot}39$*.

In the upper part of Fig. 14, the position of the reattachment line is shown for incidences between 6 and 8 deg. The value of p/H at reattachment is fairly constant in this case, but generally the reattachment pressure rises slightly as the position moves rearward with increasing incidence. Some reattachment-line loci are sketched in the various parts of Fig. 3, where they are shown as broken lines and labelled with a ringed R. The reattachment pressure is lower inboard for a given incidence (*see* Fig. 3f, for example). Thus a simple explanation for the reattachment-line position in terms of a constant reattachment pressure does not seem valid.

The wing surface between the shockwave and the reattachment point lies beneath the vortex, and the pressure in this region should be reduced accordingly. In Fig. 16 the pressure at two holes ($x/c = 0{\cdot}34$ and $0{\cdot}42$) is plotted against incidence, the data being for the same flow conditions as Fig. 14. At the more rearward hole the fall in pressure continues to be linear beyond the incidence at which separation occurs at the shockwave (at $x/c = 0{\cdot}19$) but a more rapid decrease takes place as the reattachment line approaches the hole. When the hole is beneath the vortex the rate again becomes uniform until ultimately the shock passes the hole. There is no apparent rise in pressure (or more strictly a reduction in the rate at which the pressure decreases with incidence) in the region of the reattachment line. Such a reduction might in fact have been expected since this line represents quasi-stagnation conditions. Moreover there appears to be no marked suction 'peak' under the 'centre' of the vortex. Both these effects are however found at subsonic speeds with vortices formed from leading-edge flow separations and their absence in the region of the forward-shock separation may be associated with the more limited (and hence weaker) nature of the vortex flow behind the forward shock.

The difference in the surface pressure distribution for separated and attached flow is sketched in the lower part of Fig. 16. In the latter case the pressure rise through the shock would be larger and, assuming that the shock position is not influenced by the separation (Fig. 11), the lift is slightly lower.

3.5. *The Rear Shock.* The two main shock waves present on the cropped-delta planform are the forward and rear shocks, the latter developing away from the leading-edge region and moving

* The simple nature of this concept of a 'critical' value of M_n which is independent of M_0, M_1 or ϕ_F must mean that it is only a rough approximation to the real locus governing boundary-layer separation. It is put forward however as a convenient simplification.

back to the trailing edge as the Mach number increases. Its growth with Mach number and incidence can be seen in the various parts of Figs. 2 and 3.

The position of the rear shock can be defined without difficulty from the oil-flow patterns or pressure distributions for the outer part of the wing. Farther inboard however it becomes more diffuse until at the root only a gradual flow recompression may exist; this effect is diminished as the incidence or stream Mach number is increased.

The position of the rear shock at one particular Mach number changes only slowly with wing incidence, as shown for example in Fig. 17. There is nevertheless a substantial rearward movement with stream Mach number, the trailing edge being reached at $\eta = 0{\cdot}9$ near $M_0 = 1{\cdot}05$. In terms of the local chord the rear shock appears to be farther aft inboard over most of the Mach number range. This may be misleading as the shock sweep relative to the free-stream direction (ϕ_R) is small but positive (Fig. 18), so that the trailing edge is reached just near the tip. Fig. 18 also suggests that the shock sweep, like the shock position, does not depend greatly on incidence.

ϕ_R is the geometric shock sweep; the effective shock sweep (ϕ_{RE}) depends on the local inclination of the surface flow at the shock front. The oil-flow patterns suggest that the latter quantity is small and perhaps directed towards the wing centre-line, thus causing the effective sweep to be somewhat smaller than the measured geometric sweep. The direction of the oil-flow filaments in this region may not be an entirely reliable guide to the flow direction outside the boundary layer, but it would certainly seem that on the present planform the rear shock is virtually unswept, since $\cos\phi_{RE}$ (or $\cos\phi_R$) is close to unity.

This particular aspect makes the question of the required conditions for boundary-layer separation at the rear shock of considerable interest, because of the obvious similarity with the shock on two-dimensional aerofoils at transonic speeds; separation conditions for this type of flow has received considerable attention, particularly from Pearcey (*see*, for example, Ref. 6).

Pressure distributions at station C on the wing upper surface at $\alpha = 4$ deg are shown in Fig. 19a for close intervals of Mach number between $0{\cdot}90$ and $1{\cdot}05$. The development of the rear shock can be seen clearly. Because the shock lies normal to the stream the onset of separation is not easy to detect from the oil-flow patterns. At $M_0 = 0{\cdot}95$ (Fig. 4c (iii)) the flow is certainly attached; by $M_0 = 1{\cdot}00$ (Fig. 4d (iv)) separation has probably occurred between the shock and the trailing edge. The oil patterns at $\alpha = 4$ deg and intermediate Mach numbers suggested that separation was first evident at $M_0 = 0{\cdot}97$ and certainly this was the lowest Mach number for which reverse flow at the surface was observed. Between $M_0 = 0{\cdot}95$ and $0{\cdot}97$ the boundary layer appears to thicken appreciably behind the shock and to drift towards the tip. Though uncertainty exists in distinguishing between a very thick and a separated boundary layer in this particular case, it seems likely that the critical condition occurs close to $M_0 = 0{\cdot}97$. From the family of curves drawn in Fig. 19a, it might be inferred that at $M_0 = 0{\cdot}96$ a small amount of separated flow, with subsequent reattachment, exists to the rear of the shock, causing a sudden decrease in the value of the pressure ratio, p_2/H, downstream*, and a decrease in the pressure ratio p_2/p (Fig. 19c).

The local Mach number upstream of the shock (M_1) is also given in Fig. 19c. This increases rapidly until $M_0 = 0{\cdot}95$, but the subsequent increase is comparatively slow. Separation, assumed

* The locus of p_2/H depends a great deal on the way the curves are drawn and is thus to some extent arbitrary. The pressure at hole 12 ($x/c = 0{\cdot}74$) to the rear of the shock diverges at $M_0 = 0{\cdot}96$, and this may be regarded as an indication of separation. This divergence spreads downstream with increasing Mach number.

to take place at $M_0 = 0{\cdot}97$, corresponds to a value of M_1 of about $1{\cdot}23$ which is near the range ($1{\cdot}23$ to $1{\cdot}25$) accepted for two-dimensional flow. The shock sweep for the cropped-delta wing is only about 10 deg (Fig. 18) and hence has little effect in reducing the component Mach number normal to the shock front.

A similar analysis may be made when the wing incidence is increased at constant Mach number (Fig. 20). Separation in this case is considered to take place near $\alpha = 3$ deg, when the local Mach number ahead of the shock is $1{\cdot}24$.

For the present wing, separation occurs behind the rear shock for a comparatively limited range of flow conditions. At subsonic stream speeds (say $M_0 = 0{\cdot}90$) the shock is influenced by the leading-edge separation before it has grown to the critical strength; the rate of inboard movement of the vortex with incidence is larger than the growth of shock strength inboard and thus shock-induced separation never develops. This can be seen from the pressure distributions of Fig. 3b; the lowest local pressure ratio (p_1/H) ahead of the shock before leading-edge separation modifies the flow remains above the value ($0{\cdot}397$), and thus the local Mach number remains below the value $1{\cdot}23$, the critical for shock-induced separation.

As the stream Mach number increases, the local surface Mach numbers increase too and leading-edge separation occurs at progressively higher incidences (Fig. 5d). Thus the chances of shock-induced separation are higher. At $M_0 = 0{\cdot}95$ however the flow is still apparently attached behind the rear shock (Fig. 4c). At $\alpha = 4$ deg, for station D, the local Mach number just upstream of the rear shock is $1{\cdot}35$, which is well above the critical value mentioned earlier. The trailing-edge pressure for this case is close to that obtained at zero incidence (Fig. 3c) suggesting, in common with the appropriate oil pattern that the flow in the trailing-edge region is attached. Indeed the evidence suggests that separation, if it occurs, must be limited to a small region just behind the shock. The geometric sweep of the shock is about 15 deg so that the Mach number component normal to the shock front is about $1{\cdot}31$. Inboard, at station C, the value of M_1 has fallen to $1{\cdot}21$ and the flow there is certainly attached.

The local Mach number ahead of the rear shock at stations C and D is shown diagrammatically in Fig. 21 for a range of incidence and Mach number. Where possible the state of the flow through the shock is indicated, based on the evidence of the oil patterns. The heavy lines in both diagrams show possible boundaries between attached and separated flows; in the latter case separation is assumed to exist over an appreciable fraction of the chord and hence very local separation regions are excluded. At $\eta = 0{\cdot}70$, the separation boundary corresponds roughly to the condition $M_1 = 1{\cdot}23$*, although this value is in fact attained at $\alpha = 5$ deg, $M_0 = 0{\cdot}95$ and the flow remains attached. The shock sweep is about 15 deg (so that $M_1 \cos \phi_R = 1{\cdot}19$) and this may explain why this point lies outside the boundary. The discrepancy is probably small enough to be unimportant. Of more significance however are the comparatively high values of M_1 at $\eta = 0{\cdot}90$ at incidences between 2 and 4 deg and Mach numbers of $0{\cdot}95$ and $0{\cdot}975$. The highest local Mach number ($1{\cdot}35$) has already been noted. Even if this point should strictly be counted as producing local separation, it is noticeable that complete separation develops with an increase in stream Mach number, but for a decrease in M_1. This trend however is consistent with results obtained on two-dimensional aerofoils which show that the critical Mach number for separation tends to decrease slightly with increasing stream Mach number and also to decrease as the shockwave causing the separation

* Unfortunately no oil pattern was available for the critical case of $\alpha = 5$ deg, $M_0 = 0{\cdot}975$, where $M_1 = 1{\cdot}26$.

moves rearward. It seems unlikely that the present results are due entirely to either an arbitrary definition of, or detection of, separation, or to an inability to determine correctly the effective shock sweep.

It is tempting to attribute the apparent anomaly to the presence of the wing tip. If Figs. 4c (iii) and 4d (iv) are compared it will be seen that upstream of the shock, the inboard influence of the tip vortex is smaller at the higher stream Mach number. The flow near the shock is not greatly different at stations C and D and separation extends outboard of the former position. Though spanwise drift occurs behind the shock, the local conditions are approximately two-dimensional. At $M_0 = 0{\cdot}95$ separation may only occur close to the tip because of the larger transverse velocity gradient. But the tip-vortex influence extends inboard almost to station D and it seems possible that flow separating behind the rear shock is induced to flow towards the tip and onto the tip vortex, and that the apparent (and effective) attachment behind the shock at station D is due to spanwise drift of flow farther inboard. Thus the highly three-dimensional nature of the flow in this region is effective in minimising the shock-induced separation. A similar situation might arise farther inboard when the spread of the tip separation with increasing incidence suppresses an already existing separation. Fig. 4d between $\alpha = 5$ and 10 deg may show an example of this.

It is suggested therefore that where the rear shock is reasonably two-dimensional in form and the effective sweep is low separation will occur for similar flow conditions to those appropriate to two-dimensional aerofoils. When marked three-dimensional effects are present, the development of the separation, if not the actual inception, will be delayed by the presence of a flow component along the shock front due perhaps to the influence of the tip. Whether this argument can be extended to explain the comparatively high value of M_n (about $1{\cdot}39$) at the apparent separation condition through the forward shock is uncertain at present. It might be expected though that the critical value of M_n would vary somewhat with shock sweep, increasing from the value of about $1{\cdot}23$ appropriate to unswept shocks.

An assessment of separation conditions at the two inboard stations is difficult because the rear shock is close to the trailing edge by the time critical conditions are reached and it is more difficult to determine from the oil patterns whether separation has occurred. In general the available results confirm those found at station C. For example at $\alpha = 6$ deg, Fig. 2d, the flow is just about to separate at station B at $M_0 = 1{\cdot}00$ (M_1 is then $1{\cdot}23$) and is fully separated at $M_0 = 1{\cdot}05$ when $M_1 = 1{\cdot}25$. Similar results may also be obtained at station A despite possible influence from the closely-adjacent wall boundary layer.

One interesting feature of the flow revealed by Fig. 21 is that the Mach number upstream of the shock does not necessarily increase as the stream Mach number or wing incidence is raised. Some loci of M_1 at constant incidence but changing M_0 have been drawn on the various sections of Fig. 2 as broken lines labelled with a ringed A. There appear to be two main types of curve. In the first, M_1 increases steadily with M_0; an example of this is shown in Fig. 2c, at $\eta = 0{\cdot}45$. The second type occurs at this incidence at $\eta = 0{\cdot}90$; the shock strength at first increases rapidly with Mach number but as it moves rearward M_1 falls. Curves of form intermediate between these types exist, as for example at $\eta = 0{\cdot}70$ in the same Figure.

Type I curves seem to be characteristic of the inboard stations at moderate incidences; Type II curves occur near the wing tip and above 4 deg incidence are influenced by the development of leading-edge separation. The fall in the value of M_1 with increasing stream Mach number at station D is associated with the characteristic form of the pressure distribution over the wing at

transonic speeds, when the pressure on the surface ahead of the rear shock tends to rise behind about 0·45 chord at all but the most inboard station. Fig. 2c shows this effect well. The pressure rise is more noticeable at station D, and the rearward-shock movement with Mach number is a little larger than inboard. The two effects combine to cause M_1 to decrease with M_0. Inboard, the effects are less marked but the rate of increase of M_1 with M_0 is smaller than might be expected. This type of development is favourable in that it may reduce the chances of flow separation over the outer part of the wing. The wing profile must influence the development to some extent and hence a section leading to the present type of flow changes would seem to be preferable to one which in similar circumstances allows the flow to expand continually back to the rear shock.

A curious locus of M_1 occurs at $\alpha = 6$ deg, $\eta = 0{\cdot}70$ (Fig. 2d), where the expected development of the rear shock with increasing stream Mach number appears to have been arrested between $M_0 = 0{\cdot}95$ and $1{\cdot}00$. This seems to be due to the influence of the adjacent part-span vortex (*see* Fig. 4d (vi)), which softens the shock. Between stream Mach numbers of $1{\cdot}00$ and $1{\cdot}025$ the leading-edge flow attaches right to the tip at this incidence, and the rear-shock growth and movement proceeds normally. A similar effect occurs at $\alpha = 8$ deg, $\eta = 0{\cdot}45$ (Fig. 2e).

3.6. *The Tip Shock.* The shock which originates from close to the tip leading edge and passes back over the wing surface is seldom distinct in the oil-flow patterns obtained at transonic speeds. Its presence can sometimes be inferred from a change in the direction of the oil filaments in the tip region ahead of the forward shock (Fig. 4g (ii) for example) and from a characteristic kink in the latter shock at its intersection with the tip shock. Its effect on the surface pressures at $\eta = 0{\cdot}9$ is very small and it is concluded that the shock itself is generally weak.

At $M_0 = 1{\cdot}41$, however, the tip shock is more in evidence and contributes to the triangular separation region visible in parts of Fig. 4h. Its effect as it crosses station D is still small (Fig. 3h). The approximate position of the shock, as deduced from the oil-flow photographs, is indicated and this moves forward with increasing incidence. The actual positions are shown in the upper half of Fig. 22. This movement is perhaps at first sight the opposite from that which might be expected from a weak shock propagating in a flow whose Mach number rises steadily with incidence. However the shock, if weak, will propagate at nearly the local Mach angle relative to the direction of the local flow. The latter is inclined inboard at an angle θ which increases with, and is related to, the local surface Mach number. The tendency for the geometric shock sweep (ϕ_T) to increase due to rising local flow velocities is less than that reducing ϕ_T because the local Mach number, and hence θ, is increasing. The net result is that ϕ_T slowly falls with incidence and the shock intersects station D at progressively more forward stations.

The angle between the tip shock and the local flow direction is $\{(\pi/2) - \phi_T - \theta\}$ and as Fig. 22 shows this is only slightly greater than the Mach angle (μ) appropriate to the local Mach number at the intersection with station D. This merely confirms that the tip shock is weak. There is however a small flow deflection through the tip shock so that the inboard deflection θ is increased. This may mean that the component Mach number normal to the forward shock outboard of the intersection between the forward and tip shocks (and hence to the rear of the tip shock) is increased too, and separation becomes more severe. Moreover the forward shock in this region loses sweep as well so that in fact the flow approaches this shock almost normally. Because separation exists behind the forward shock the flow is also nearly normal to the inboard part of tip shock. In both cases the flow leaves the surface in a 'sheet' form (as in the case of rear-shock separation), though above the wing surface the flow must be complex.

3.7. *Conditions for the Appearance of Surface Shock Waves.* It is perhaps relevant to consider briefly the flow conditions under which the various shock waves associated with the wing surface may appear.

3.7.1. *The forward shock.* In Ref. 5 there is some discussion of the local flow conditions in the leading-edge region which are required before the forward shock moves rearward over the wing surface. Tentatively, it was suggested that the local Mach number M_1 must be large enough for the local Mach angle (μ_1) to be less than the angle between the leading edge and the local flow directions; *i.e.*,

$$\mu_1 < \frac{\pi}{2} - \phi_{LE} + \theta$$

where ϕ_{LE} is the leading-edge sweep and θ is the inboard flow deflection relative to the free-stream direction. If this is true, then the leading edge is effectively 'supersonic' in type† and the forward shock is equivalent to a boundary between the flow influenced by the root and the flow influenced mainly by the sweep of the leading edge.

In the above inequality, both μ_1 and θ may be expressed in terms of the local Mach number M_1 and thus the required condition is that some critical value of M_1 (say $M_1{}^*$) shall be exceeded‡. In looking at the present results it is convenient to use the corresponding critical pressure ratio $(p/H)^*$.

The forward-shock positions shown in Fig. 11 for stations C and D can be used to estimate the incidence at which the forward shock first moves back from the leading edge. The pressure ratio (p/H) near the leading edge at this incidence can then be compared with the theoretical critical value deduced from the simple flow model outlined above. This comparison is made in Figs. 23a and b. The former diagram shows that variation of the surface pressure at hole 2 ($x/c = 0{\cdot}02$) with incidence for the two stations and four stream Mach numbers, and also the theoretical and experimental estimates of critical flow conditions. These estimates, in terms of wing incidence, are plotted against stream Mach number in Fig. 23b, and the agreement is satisfactory. In particular the slow decrease in critical incidence with increasing M_0, shown in Fig. 5d, seems to be predicted. In making such a comparison, much depends on the extrapolation of the results given in Fig. 11 to the condition where the shock is at the leading edge. For station D, the shock position varies almost linearly with incidence and the extrapolation is not unduly difficult. On the other hand, at station C there is some non-linearity in the curves showing the shock position and the extrapolation is less reliable. Much of the uncertainty arises from the presence of the roughness band which covers the first tenth of the local chord, and prevents the forward shock becoming visible in this region.

It is possible then that the agreement shown in Fig. 23b may be coincidental; on the other hand until further evidence becomes available it seems reasonable to accept the suggested description and prediction of the forward-shock appearance away from the leading edge.

The forward shock may of course exist at the leading edge before flow conditions are appropriate for the rearward movement to take place. In such a condition it is difficult to detect, except by rather elaborate optical surveys[1]; from the surface pressure distributions it is not easy to say

† The analogy with the more usual use of the term 'supersonic leading edge' is convenient, but it should be remembered that the lower-surface velocities in the leading-edge region are comparatively low and that disturbances can propagate around the edge from the lower to the upper surface.

‡ $M_1{}^* = (1+5\lambda)/(1-\lambda)$ where $\lambda = M_0{}^2 \sin{}^2\phi_{LE}/(5+M_0{}^2)$ (Ref. 5).

whether a shock wave will be associated with any particular suction peak. Once critical flow conditions for the shock movement have been reached at some position near the leading edge, the shock may be detectable from the oil patterns. The effective point of origin at the leading edge can be deduced from a knowledge of the spanwise variation of pressure in that region; this origin will move inboard as the incidence increases at constant M_0. The subsequent path of the shock over the wing surface in the present case can be estimated roughly from a knowledge that the geometric sweep of the shock varies little with incidence or Mach number (Fig. 12).

3.7.2. *The rear shock.* It is generally accepted that shock waves tend to form first on a sweptback wing when the component Mach number normal to the local isobars exceeds unity. This can be regarded as an extension of well-proven two-dimensional concepts to three-dimensional flow.

Experimental proof of this hypothesis on plane sweptback wings is difficult because of the rapid loss of isobar sweep very close to the wing tip, the region where the highest surface velocities occur. It is nevertheless of interest to consider the isobar patterns in a few cases where the rear shock is developing. For simplicity, only zero incidence will be studied, and the isobars chosen will be equivalent to specified values of local Mach number, M_1.

Optical and oil-flow tests showed that a small shock, normal to the chordline and flow direction, existed near the tip at $M_0 = 0{\cdot}90$. Its inboard extent* was estimated, very approximately, to be $0{\cdot}1$ semi-span from the tip. The isobar pattern for this case is shown in Fig. 24a. Unfortunately it is not possible to decide the isobar direction between station D and the tip; if it is assumed that the contours for $M_1 = 1{\cdot}0$ and $1{\cdot}025$ close near the tip, then obviously at some position the isobars become unswept and 'supercritical' conditions exist. The spanwise extent of this region will be small however.

The rear part of the sonic contour has almost constant sweep between stations B and D at about 30 deg though the effective sweep may well be lower than this when the local flow direction is allowed for. The component Mach number normal to this line must be about $0{\cdot}86$, and it seems that no shock waves form as a result of the flow recompression in this region. By $M_0 = 1{\cdot}05$ (Fig. 24b), supersonic flow exists over a large part of the wing surface. The shock wave, as far as can be judged, extends outboard from $\eta = 0{\cdot}7$, with an average sweep not greatly different from that of the local isobars. As the same contour moves rearward with increasing stream Mach number, it loses sweep and the rear shock extends farther inboard (Figs. 24c and d). At $M_0 = 1{\cdot}41$, (Fig. 24e) the isobars are swept almost to the trailing edge, the position of the rear shock.

3.7.3. *The tip shock.* The disturbance from the tip leading-edge region should occur when the local flow becomes supersonic though it will be very weak. Unlike the forward shock the origin of the tip shock is fixed and only its direction of propagation varies with incidence and stream Mach number. This is discussed in Section 3.6 above. It is not possible to detect the tip shock at its inception but there seems no reason to doubt that it does occur when the local conditions are correct.

3.8. *Some Remarks on the General Development of the Pressure Distributions at Transonic Speeds.* The changes in the surface pressures at constant incidence as M_0 changes are shown in the sections of Fig. 2. At moderate incidence on the upper surface, when leading-edge separation is absent,

* *i.e.*, the extent of the shock deduced from oil-flow patterns. This is rather arbitrary because the discontinuous compression present at the shock became continuous farther inboard.

the sets of distributions conform to a distinct pattern, whose chief features are the backward movement of the rear shock and the steady fall in pressure over most of the chord as the Mach number increases. The latter effect is different from that found on two-dimensional aerofoils at transonic speeds, where the pressures ahead of the shock remain constant (the so-called 'sonic freeze'); a similar type of freeze to this exists for the region ahead of the forward shock on the swept wing and was discussed in Section 3.3. The present remarks are concerned with the wing surface behind the forward shock.

It is tempting to seek some method of plotting the pressure distributions so that the Mach number effect is removed, and the choice of the parameter p/p_0 (where p_0 is the stream static pressure) in place of p/H is an obvious one. Typical pressures obtained at four upper-surface holes are plotted in this form against M_0 in Fig. 25. Above sonic stream speed the values of p/p_0 change little. The large decrease in p/p_0 for the holes at $x/c = 0{\cdot}42$ and $0{\cdot}66$ corresponds to the passage of the rear shock. The incidence (2 deg) is below that at which the forward shock is apparent and hence constant p/p_0 is maintained even at $x/c = 0{\cdot}05$. Below $M_0 = 1$, the pressure ratio decreases with incidence at a somewhat greater rate than do lines representing the condition C_p = constant.

On the lower surface, the pressure ratio p/p_0 becomes constant at $x/c = 0{\cdot}42$ above $M_0 = 1{\cdot}00$, a rear shock having then formed closer to the trailing edge. At $x/c = 0{\cdot}10$, however, constant conditions are not reached. On the extreme right of the diagram are the points appropriate to $M_0 = 1{\cdot}41$ and it will be seen that in most cases these are near, though usually slightly below, the values obtained at transonic speeds. This suggests that the departure from the local condition of constant p/p_0 with stream Mach number is relatively slow.

A set of complete upper-surface pressure distributions (at $\alpha = 4$ deg, $\eta = 0{\cdot}7$) is plotted in terms of p/p_0 in Fig. 26a; the Mach numbers range from $0{\cdot}95$ to $1{\cdot}16$. The movement of the rear shock appears as a departure of the local pressures from a distribution appropriate to the rear shock at the trailing edge and in this there is a strong resemblance to the two-dimensional aerofoil and its sonic-range pressure distribution. At any particular hole there is some variation in the value of p/p_0 with Mach number. At $x/c = 0{\cdot}02$, p/p_0 rises with increasing M_0; as Fig. 7b shows, the forward shock and the constant p/H region ahead of it have not developed at this incidence. Between $x/c = 0{\cdot}1$ and $0{\cdot}4$, the largest variation occurs for the values obtained at $M_0 = 1{\cdot}11$ and $1{\cdot}16$. A plot of this type is particularly sensitive to errors in M_0 and it is just in this range that the velocity distribution along the tunnel begins to deteriorate. Thus this variation may be due to either an over-correction of the nominal stream Mach number, or to a failure to allow for local variations in the stream velocity. Despite possible shortcomings of this type, the use of the parameter p/p_0 would seem to be more revealing than the more conventional pressure coefficient C_p. Results corresponding to Fig. 26a are shown in Fig. 26c in terms of C_p.

The lower-surface pressure distributions are less satisfactory when plotted in terms of p/p_0, as can be seen in Fig. 26b. As the stream Mach number increases p/p_0 rises on the front half of the section and decreases towards the rear. In fact the condition of constant p/p_0 seems to apply only in the region ahead of a well-developed rear shock where the local Mach numbers are appreciably above unity. This aspect again has some resemblance to that for a two-dimensional aerofoil.

The physical reasons for the apparent significance of p/p_0 in certain conditions are not clear at present. There are however two possible approaches towards a tentative explanation. Firstly, the parameter p/p_0 is of importance in comparing pressure distributions obtained from related wings

having different sweepback, but tested so that $M_0 \cos \phi_{LE}$ (the Mach number component normal to the leading edge) is maintained constant. If simple sweepback theory holds then the results should be identical if plotted in terms of p/p_0. This type of analysis may be extended to the present tests by arguing that as M_0 increases, the effective sweepback in the region of interest increases too, so that the product $M_0 \cos \phi'$ remains constant. ϕ' is the local effective sweep and must be related to the local isobar sweep. This suggestion of slowly increasing isobar sweep with stream Mach number has some support from the present experimental results. A typical isobar pattern in the flow region being considered is shown in Fig. 27. Except near the leading and trailing edges, the isobars have a sweep over most of their length which increases as M_1 reduces and the root is approached. At slightly higher stream Mach numbers a given isobar moves towards the root and its sweep increases. For a particular spanwise station, the result would be similar to an overall fall in the pressure level, which apparently just balances the fall in stream static pressure accompanying the increase in M_0.

One striking feature of the isobar pattern in the region between the forward and rear shocks, if the kinks are neglected, is the resemblance to a cross-section of the flow about a cone, whose generator is the wing root chord; this region on sweptback wings in fact has sometimes been referred to as 'quasi-conical'. In true conical flow at low supersonic speeds the parameter p/p_0 changes only slowly with stream Mach number; the variation is shown in Fig. 28 for four different cone angles*. This Figure should only be regarded as illustrating the significance of p/p_0 in conical flow fields since it is not possible to obtain a numerical correlation between the fields associated with a cone and with part of a swept wing. Nevertheless, the fact that the trends with Mach number are similar is perhaps not without significance. The particular form of transonic pressure freeze which appears in the region between the forward and rear shocks may well arise from the characteristic nature of the local flow. It should perhaps be added that the two approaches to an explanation of the phenomenon which are discussed in this section are not exclusive but are related ways of simplifying the real and complex flow field.

It is interesting to note that when the majority of the wing surface is dominated by the 'quasi-conical' flow at constant p/p_0, the local pressures will not change with Mach number in flight at constant altitude. Hence the local contribution to wing lift will remain constant too. The total wing lift will only remain constant if changes on the lower surface are zero also or balance out. In such conditions, C_L falls with M_0 so that the product $C_L M_0^2$ remains constant. It is not possible to achieve this condition but some fall in C_L with M_0 at constant incidence does occur once the rear shock reaches the trailing edge ($M_0 \simeq 1 \cdot 05$). A similar trend would of course also be expected from the more conventional viewpoints of transonic and supersonic theory.

4. *Influence of Flow Development on Forces and Moments.* The preceding pages have considered in some detail the changing flow over the wing as Mach number or incidence is altered, and the knowledge gained can now be used in considering briefly the wing forces and moments.

4.1. *Lift.* Despite the wide variation in the flow pattern about the wing, the overall lift curves do not change greatly in shape as the stream Mach number is increased (Fig. 5a). The presence

* It should perhaps be pointed out that a transonic pressure freeze in terms of local Mach number (or p/H) and hence analogous to that found in two-dimensional flow does occur for cones at stream speeds very close to the sonic value, but its existence is frequently obscured by tunnel interference effects according to Page[10].

of leading-edge separation at subsonic speeds appears to cause only a small initial increase in lift-curve slope (due to the lower pressures induced under the vortex), whilst at the highest incidences there is a slight fall in slope as the vortex moves inboard and the completely separated region at the tip grows. Similarly the growth of the separation vortex behind the forward shock has only a small effect on the overall wing lift.

The most conspicuous feature of the lift curves is perhaps the marked rise in lift which occurs at constant incidences above about 3 deg between stream Mach numbers of 0·95 and 1·05. This corresponds to the aft movement of the rear shock (which appears only in the upper surface) discussed earlier, and the consequent extension of the high loading to the trailing edge which the shock reaches close to $M_0 = 1{\cdot}05$. Thereafter there is a tendency for the wing lift to fall.

These wing lift changes can be seen in Fig. 6a, which shows the approximate* lift-curve slopes at three values of wing lift. The rapid rise, and subsequent fall, in $dC_L/d\alpha$ at the highest C_L is noteworthy and corresponds to the aft movement of the rearward shock and the maintenance of attached leading-edge flow at the higher Mach numbers. The theoretical lift-curve slope at $M_0 = 1{\cdot}41$, estimated from linear theory, is also shown.

Typical spanwise loading curves are included as Fig. 29 for stream Mach numbers of 0·90 and 1·11. At the lowest incidence (2 deg), the loadings are close to the elliptic form, indicating that the lift-dependent drag should be comparatively low. By $\alpha = 6$ deg at $M_0 = 0{\cdot}90$, a part-span vortex lies across station D, with an increase in local lift; at 10 deg the vortex has passed inboard and influences stations B and C, whilst D now lies in the dead-air region outboard of the secondary separation line (*see* Fig. 4b). The loading at the highest incidence has the characteristic hump associated with a part-span vortex lying in mid semi-span.

At $M_0 = 1{\cdot}11$ and $\alpha = 6$ deg, the flow is everywhere attached with a forward shock crossing station D at about 0·3 chord. The region ahead of this augments the section lift to some extent. Between $\alpha = 9$ and 10 deg, at this stream Mach number, the leading-edge flow separates completely (*see* Fig. 4f), but the overall shape of the spanwise loading curve is not greatly altered and does not greatly resemble its counterpart at the lower value of M_0. In fact there is a tendency to approach the loading obtained at $M_0 = 1{\cdot}41$. The case shown at 12 deg incidence for this Mach number has completely attached leading-edge flow.

4.2. *Pitching Moment.* The pitching-moment curves shown in Fig. 5b, like the lift curves, are not greatly influenced by modifications in the wing flow as the incidence is increased at constant M_0. At $M_0 = 0{\cdot}85$ for example the moment curve is almost linear despite the appearance and development of the part-span vortex. There is no pitch-up as would probably be the case with a sweptback trailing edge.

The aft movement of the rear shock between stream Mach numbers of 0·95 and 1·05 produces an associated rearward movement of the centre-of-pressure positions (Fig. 6d) and a change in moment-curve slope. With the breakdown of the tip flow (*e.g.*, near $M = 1{\cdot}05$, $\alpha = 10$ deg, Fig. 4e (vi)) and the consequent development of a large part-span vortex, there is once more a change in the slope of the curves, and a forward movement of the centre of pressure.

Between $M_0 = 1{\cdot}11$ and 1·41, this slope remains almost unchanged for most of the incidence range, despite fairly severe changes in the surface flow pattern. There is no marked pitch-up such

* Because the lift curves are non-linear, the determination of accurate lift-curve slopes is difficult.

as that encountered on the Warren 12 wing[2] (which has the same leading-edge sweep and section, but a trailing edge swept at 32·9 deg) and which is attributable to the development of a strong outboard shock, with separation to its rear.

4.3. *Drag.* 4.3.1. *Drag and lift/drag ratio.* The drag polars, plotted in Fig. 5c, are similar in general shape throughout the test range of Mach number, although there is an upward displacement associated principally with the rise in minimum drag as the stream Mach number increases. At incidences of 5 deg and above there is a marked rise in wing drag coefficient up to $M_0 = 1{\cdot}11$, which could be due to the increase in C_L at constant incidence. The curves shown in Fig. 5c are not the most suitable for an analysis of lift-dependent drag, but they can be used to obtain the drag coefficient at constant lift coefficient. The variation of this with stream Mach number is shown in Fig. 6b.

At zero lift, the drag rise starts near $M_0 = 0{\cdot}9$ but no further increase occurs after $M_0 = 1{\cdot}10$. As the lift coefficient rises, the curves change shape slowly, the drag rise beginning a little earlier, and a slow increase in drag taking place at supersonic speeds. On this Figure the estimated initial appearance of the rear shock (*see* Fig. 5d) is marked at the three lowest lift coefficients. The shock remains limited in extent and comparatively weak for an appreciable range of stream Mach number and the accompanying drag increase is small. The major part of the drag rise at zero lift occurs between stream Mach numbers of 0·95 and 1·05, a region where the rear shock is growing rapidly, spreading inboard and moving towards the trailing edge.

The forward shock was first detected in a very limited range of lift coefficient (Fig. 5d). For $C_L = 0{\cdot}2$ detection occurred at $M_0 = 1{\cdot}00$, but it is difficult to assess what contribution this brings to the total wing drag. Points representing the upper limit (in stream Mach number) of the separated leading-edge flow region shown in Fig. 5d can also be included in Fig. 6b, but the change-over in flow type does not appear to alter significantly the character of the drag curves. The drag rise in the separated-flow region is most probably associated mainly with the development of the rear shock in the region between the root and the part-span vortex (Fig. 4c (vii)), for example, since the position of the latter, and perhaps its influence on wing drag, are not greatly affected by M_0. This may explain why the transonic drag rise at $C_L = 0{\cdot}4$ is smaller than that at zero lift; the fraction of the span influenced by the shock is less at the higher lift.

The lift/drag ratio for the range of test Mach number is shown in Fig. 6c, together with an inset curve of the variation with M_0 of the maximum value. The latter diagram shows the expected fall as the stream Mach number is increased; at $M_0 = 0{\cdot}80$, $(C_L/C_D)_{\max}$ is 13·3, which reduces to 8·2 at $M_0 = 1{\cdot}00$ and to 7·2 at $M_0 = 1{\cdot}41$. The chief reduction occurs between stream Mach numbers of 0·90 and 1·05, when the rear shock is developing and the wave drag growing. The increase in wing lift associated with the shock movement is not large near the maximum lift/drag condition.

At subsonic stream Mach numbers, the maximum lift/drag ratio occurs at an incidence close to that at which leading-edge separation appears (Fig. 6c). Though this may be coincidental it is perhaps significant that the onset of separation is accompanied by an increase in the lift-dependent-drag-curve slope (*see* Section 4.3.2) which may be sufficient to influence the position and magnitude of the maximum lift/drag ratio. The latter are very sensitive to the shape of the drag polar. As M_0 rises, the zero-lift drag increases and since the condition for maximum lift/drag ratio is that at

which the zero-lift drag equals the lift-dependent drag the lift coefficient at which the maximum occurs tends to increase too (Fig. 6c, inset).

The pressure drag (C_{D_p}) at each spanwise station may be obtained from an appropriate integration of the surface pressure distribution. This has been done for the present wing at zero incidence only and the section drag coefficients (multiplied by the ratio of the local chord, c, to the geometric mean chord, $\bar{c}$) are shown in Fig. 30. Because of the inadequate distribution of holes close to the leading edge on this model it is difficult to determine the magnitude of C_{D_p} accurately, though the trend with Mach number should be reliable. The thrust present at the two most outboard stations increases initially as M_0 rises, despite the formation of a shock wave at station D when $M_0 = 0{\cdot}90$. These two stations contribute pressure drag to the wing above $M_0 = 1{\cdot}0$; the shock is comparatively strong at this speed (*see* Fig. 2a). There is a tendency for the section drag rise to cease once the rear shock reaches the trailing edge ($M_0 \simeq 1{\cdot}05$). The pressure drag at the most inboard station is very large, as would be expected from the rearward shift of the velocity peak due to the root influence, and increases rapidly up to a Mach number of about $1{\cdot}1$. The rear shock is not well defined at this station.

It is tempting to use these pressure drag results to determine the pressure drag of the complete wing, by spanwise integration. Unfortunately it is uncertain how the drag should vary between the root and station A, and between the tip and station D. If it is assumed that $C_{D_p} c/\bar{c}$ falls rapidly to zero at the tip, but increases progressively into the root, very approximate values of C_{D_p} for the wing can be obtained and these are shown in Fig. 31. Once again the absolute values of the pressure drag are doubtful but the increase with Mach number may be represented at least approximately. The drag rise obtained in this way is about two-thirds of that measured on the balance which suggests some error in the analysis. The initial part of the drag rise does seem to be correctly represented however.

4.3.2. *Lift-dependent drag.* In analysing lift-dependent drag, it is convenient to consider the variation of the drag-due-to-lift (ΔC_D) with C_L^2, where ΔC_D is the difference between the measured drag and that obtained at zero lift*. Curves of this type are contained in Fig. 32 for a range of stream Mach number.

The curves have large linear sections joined by regions where the slope changes rapidly. Such a change occurs for example close to 4 deg incidence at $M_0 = 0{\cdot}85$, and the incidence corresponding to the deviation from the original slope has been called α_{K_1}. Curves for low supersonic stream Mach numbers appear to have two changes in slope and in such cases the earlier kink is labelled α_{K_2}. The possible significance of α_{K_1} and α_{K_2} is suggested in Fig. 33 where it seems clear that α_{K_1} is related to the beginning of leading-edge separation and the accompanying change in the chordwise pressure distribution, particularly the loss of the leading-edge suction peak. It is interesting to note that the rapid growth of the part-span vortex between incidences of say, 6 and 10 deg at $M_0 = 0{\cdot}85$ (*see* Fig. 4a) has little effect on the slope of the curve shown in Fig. 32.

* In the balance tests zero lift was not obtained at zero wing incidence (*see* Fig. 5a), even though the local section lifts were almost zero. The reasons for this discrepancy are unknown at present. There is therefore some difficulty in determining the magnitude of the lift-dependent drag at very low lift. In general terms then it must correlate with the slope changes near 4 and 5 deg incidence shown in Figs. 7c and 7d respectively; these correspond to an establishment of supersonic-type flow around the leading edge, with a consequent loss of leading-edge suction.

The connection between the wing flow and α_{K_2} is less obvious. It seems likely however that the slope change represents some stage in the development of the flow around the leading edge and the establishment of a forward shock, though not apparently its first appearance or detection. A change in the slope of the lift-dependent drag curve might be expected when an appreciable region of the wing surface near the leading edge is ahead of the forward shock* and the rate of pressure decrease with incidence in the leading-edge region is reduced. The greater delay between the appearance of the forward shock and the slope change at supersonic speeds may be because the shock is a much less pronounced feature of the chordwise pressure distribution as the Mach number increases and hence the resultant pressure change at any point as the shock moves past it is much smaller. It is perhaps appropriate that α_{K_1} can only be clearly defined at stream Mach numbers where the forward shock is present.

The slopes of the lift-dependent drag curves are shown in the two parts of Fig. 34. In the former, the slopes have been measured at constant values of C_L and the changes in value with stream Mach number are influenced by a transition between the regions labelled A, B and C in the inset to Fig. 32. For example at $C_L = 0{\cdot}1$ there is a change from region B to region A as the Mach number increases from $1{\cdot}00$ to $1{\cdot}05$†, and this is accompanied by a fall in slope. The actual slopes within the three regions are shown in Fig. 34b. As some stream speed is approached there is a marked reduction in the change of slope between regions B and C and at low supersonic speeds the slopes are constant even though the incidences at which changes occur (α_{K_1} and α_{K_2}) may alter. By $M_0 = 1{\cdot}41$ however the slopes on regions A and B have increased markedly.

The slopes presented in Fig. 34 can of course be related to an effective lift-dependent drag factor K', where

$$K' = \pi A \frac{d(\Delta C_D)}{d(C_L^2)}.$$

At $C_L = 0{\cdot}1$ this corresponds closely to the more usual factor K'' where

$$K'' = \pi A \frac{\Delta C_D}{C_L^2}$$

because the lift-dependent drag curve may be regarded as linear up to that value of C_L. Once there has been a change in slope, this correspondence is lost. K' is consequently of less value in estimating wing performance, but gives more insight into the effect of the wing flow on the overall forces. For example if the resultant force on the wing becomes normal to the chord plane as the incidence is increased, then K' becomes equal to the reciprocal of the lift-curve slope. The latter quantity varies with Mach number and for $C_L = 0{\cdot}5$ is drawn in Fig. 34a. Its trend is similar to that of K' at this lift coefficient, which implies that the reduction in K' with M_0 is due primarily to a rise in lift-curve slope. A comparison of the relative magnitudes of the two curves suggests that the resultant force is almost normal to the chord plane and hence that the leading-edge suction associated with the velocity peaks near the nose of the wing have been lost over most of the span. This is consistent with known flow pattern and pressure distribution.

---

* Or perhaps more specifically, when the forward shock nears the crest of the wing section. Again the effect will be averaged along the span.

† It is convenient to regard region A as absent below $M_0 = 1{\cdot}05$ since it is defined as lying between the origin and α_{K_2}.

At $M_0 = 0{\cdot}9$ and $C_L = 0{\cdot}1$, K' is comparatively low about $1{\cdot}1$, and hence little more than the theoretical value of K' for elliptic spanwise loading. The closeness to which the experimental loading on the wing approaches the elliptic form is indicated in Fig. 29a for $\alpha = 2$ deg. When the Mach number is increased the spanwise loading is farther from the elliptic form and K' is increased.

There are several alternative methods of performing the lift-dependent drag analysis, each of which can be used to illustrate some particular aspect. For example, the direction of the resultant force on the wing and its variation with incidence or Mach number is sometimes obtained most easily by considering the axial force which is measured directly on the tunnel balance. Another approach is shown in Fig. 35, where for three typical Mach numbers ΔC_D is plotted against $C_L \tan\alpha$. When these quantities are equal, as in the broken lines with 45 deg slope, the resultant force is normal to the chord-plane. More usually the slope of the experimental line increases with incidence until it approaches 45 deg, as at $M_0 = 0{\cdot}85$. At $M_0 = 1{\cdot}41$, this condition is not achieved within the range of the balance tests ($\alpha \leqslant 9$ deg). The changes in slope in this diagram resemble those in Fig. 22 and all but one of the kinks have a close counterpart to the conditions represented by α_{K_1} and α_{K_2}. The exception is at $M_0 = 0{\cdot}85$ at an incidence of about $6{\cdot}5$ deg where the slope change is indicative of the developing vortex over the wing and the closer approach to the complete loss of leading-edge suction. This effect does not show up in Fig. 32. The slopes of corresponding curves in the two methods of plotting are related by the lift-curve slope, and the change in this quantity balances out the variation of the resultant-force direction.

5. *Some Effects of Cropping the Wing Tip.* As was mentioned in the Introduction, some preliminary observations were made with the wing before the tip was cropped to form the planform shown in Fig. 1a. In this state the tip chord was $0{\cdot}1$ in. (Fig. 1b). The true delta planform was thus approached very closely and the model will be referred to as 'uncropped'.

These tests with the uncropped wing were limited in extent, being restricted to measurements of the pressure distribution on the upper surface at station D for incidences between 0 and 10 deg for a Mach number range of $0{\cdot}70$ to $1{\cdot}22$. These were supplemented by some oil-flow patterns. No balance measurements were made.

Comparisons between results from the wing in the cropped and uncropped states are included as Figs. 36 and 37.

At $M_0 = 0{\cdot}80$ and moderate incidences the pressures at station D are lower towards the rear of the chord in the uncropped state, probably because the tip influence is less marked in this case. The suction peak near the leading edge is almost unchanged. Leading-edge separation, however, occurs at a somewhat lower incidence on the uncropped wing due to the higher velocities developed very close to the tip. When a part-span vortex is present on the wing in both tip states, its position is very similar except close to the tip itself, where the vortex sweep is increased by the tip chord (Fig. 37a). This tip effect on vortex position is responsible for the dissimilarity in the pressures at station D (Fig. 36) at $\alpha = 6$ and 8 deg.

When the stream Mach number is increased to $0{\cdot}90$, the pressure distribution at $\alpha = 0$ deg for the uncropped wing does not show the small shock which lies across the station when the tip is cropped; the shock is also absent at 2 deg incidence. As at the lower stream Mach number the vortex development is similar on both wings.

By $M_0 = 1{\cdot}00$, the flow over the forward part of the chord is similar in both states at incidences below 6 deg, and the chief effect of the cropping is to move the rear shock slightly forward. One

interesting feature of Fig. 37b (i) is the appearance of a forward shock on the uncropped wing; for the cropped wing, leading-edge separation has developed by 6 deg incidence. The two vortices, one associated primarily with the shock-induced separation and the other with the leading-edge separation are similarly situated on the wing surface however. Once again as the incidence is increased (Fig. 37b (ii)) the vortex development is similar, although the mean pressure level at station D is lower in the uncropped state.

The agreement between the two sets of pressure distributions is very marked at $M_0 = 1{\cdot}11$, the main differences being due to the rather lower pressures developed over the rear of the chord when the wing is uncropped. The forward shock tends to be more aft as the incidence increases though the difference is very small at $\alpha = 6$ deg (Fig. 37c). This figure shows a small region of outboard shock between the tip and the intersection of the forward shock with the trailing edge. At 10 deg incidence for this stream Mach number, the leading-edge flow is completely separated for the cropped wing, but is attached up to station C for the uncropped state. This follows the trend first noticed at $M_0 = 1{\cdot}00$. For a given spanwise station, just before separation, the pressure distribution in the leading-edge region is probably similar in the two states. This suggests that the local flow conditions required for the beginning of the inboard spread of tip separation are not the same for the two planforms, though from Fig. 8b it seems likely that the rate at which the inboard movement takes place is controlled by the attainment of a simple pressure condition. This condition is most probably determined initially by the flow conditions at the tip, which would be different for the cropped and uncropped wings.

This brief comparison suggests therefore that the effect of modifying the tip shape becomes much less marked, in terms of pressure-distribution changes at a given spanwise station, as the Mach number increases. At low supersonic speeds it seems that the flow over most of the upper surface will be unaffected by such modifications, except near the trailing edge, though there may be some change in the incidences at which tip separation spreads inboard along the leading edge.

6. *Wave Reflection from the Tunnel Walls.* It was stated in Section 2.3 above that no corrections have been applied to the present results to allow for the constraining effects of the tunnel walls at subsonic and transonic speeds. Though theoretical methods of estimating corrections to model forces and flow velocity are at present rather uncertain, it is probable that the magnitude of such corrections is small and that their absence does not greatly affect the overall flow description contained in the present paper.

The problem of wave reflection from the tunnel walls is somewhat different; it is virtually impossible to allow for this effect either on the overall wing forces or on the detailed pressure distributions, but nevertheless the distortion involved may be considerable. It is convenient to distinguish two different types of wave reflection, one of diffuse compressive systems (or of expansion zones), and the other of finite-strength shock waves. The former type usually impose an overall but gradual change of pressure on the wing surface; the latter is usually made apparent by a sudden pressure rise.

It is not appropriate to discuss wave-reflection problems in detail in the present text. This has been done adequately elsewhere (*see*, for example, Refs. 7 to 9). It should however be pointed out that the transonic results obtained with the delta half-wing in both cropped and uncropped forms are subject to this type of interference. That associated with a reflected shock wave is frequently clearly detectable, particularly if it is the bow wave which is being reflected from the tunnel wall.

An example is indicated in Fig. 2a at $M_0 = 1{\cdot}16$. The reflection of the bow wave from the far sidewall strikes station D at about $0{\cdot}6$ chord (event denoted by ringed I). Pressures to the rear of this position are higher than would be the case in interference-free flow. At station C there is no evidence of this shock, which confirms that the wave reflects from the far solid sidewall and not from the slotted top and bottom liners.

Several examples of bow-wave reflection from both sets of walls can be seen in the pressure distributions contained in the various parts of Fig. 2. In many cases the effect is most pronounced on the lower surface when the wing is at incidence, presumably because the flow velocity between the wall and the wing is lower than for the upper surface, and the bow wave when reflected does not clear the model. This must be true on both surfaces at stream speeds just above the sonic value, but the bow wave is then comparatively weak and has less effect than at slightly higher speeds. The most noticeable distortions of the chordwise pressure distributions occur in fact at stream Mach numbers of $1{\cdot}11$ and $1{\cdot}16$.

In some cases wave-reflection interference seems to appear as slow compression followed by an expansion, so that the local pressures near the trailing edge of the pressure-plotting station are near (or even slightly below) the value expected in the absence of interference. An example can be seen in Fig. 2c, for $M_0 = 1{\cdot}11$ on the lower surfaces at stations A, B and C.

A complete discussion of the characteristics of wave-reflection interference in the present tests requires rather more exact knowledge of the bow-wave shape than was in fact obtained. Moreover, it would be necessary to distinguish bow-wave reflection effects from the rather similar distortions caused by stray shocks within the working section. These are known to originate from some of the many junctions in the sidewalls and, in addition, there is a serious disturbance from a junction* on both the slotted liners. The purpose of this section then is merely to draw attention to the presence of this form of interference.

When the wing is at incidence and the incoming disturbance causes a rise in pressure over the aft portion of the lower surface at some particular station, the upper surface usually escapes this form of interference because of the higher local velocities. Thus the local lift is increased and the section pitching moment becomes more negative. At the same time the chordwise force acting on the section will generally be smaller; in most cases this should lead to a slight reduction in section drag. The contribution of these changes in lift and pitching moment to the overall wing coefficients will probably be small however, since the majority of the interference effects occur over the outer part of the wing. Certainly, it is not easy to detect evidence of wave-reflection interference in the curves of Fig. 5a, for example. The changes in wing drag due to the same cause are not readily apparent, and only in Fig. 30, where the section drag is plotted against stream Mach number at zero incidence does there appear to be an appreciable effect. This occurs at $M_0 = 1{\cdot}16$, where the pressure-drag coefficient is low; the value is, of course, obtained from an integration of the corresponding distribution shown in Fig. 2a, a curve which has already been commented upon above.

Though the effects of wave-reflection may sometimes be serious and inevitably complicate attempts to use local section data, their influence on the analysis presented in the earlier sections of the report may be less severe. Partly this is because these have been concerned primarily with flow development over the upper surface of the wing (which seems to be less subject to clear-cut

* Between the upstream section where the slots are tapered and the downstream section where the slots are of constant width.

interference effects) and partly because most use of detailed pressure distributions has fortunately been made in regions which are not obviously subject to this type of interference. In addition much of the analysis has been concerned with broad, or general, effects so that local increases in interference are less misleading.

7. *Concluding Remarks.* The results obtained from the series of tests made on the cropped-delta half-wing have been used primarily to obtain a fuller understanding of the flow about sweptback wings at transonic and supersonic speeds. The contents of the present paper have been limited to a presentation of a representative selection of the results obtained together with some discussion of their interpretation and the manner in which they fit into the existing framework of knowledge. No comparison has been made with the tapered wing of Warren 12 planform, which has the same leading-edge sweep and profile and which has been the subject of an earlier intensive study at the N.P.L. A report making such a comparison will be issued later, and will illustrate for example the significant changes in wing characteristics which result from the elimination of the outboard shock in the present delta planform.

The flow development with incidence and stream Mach number does not contain any novel features, but follows the now well-established pattern of events. The growth and movement of the part-span vortex arising from the leading-edge separation is gradually replaced by a region of attached leading-edge flow and a forward shock as the stream Mach number is increased. The rear shock which develops initially near the wing tip moves rearward and spreads inboard, losing sweep at the same time until the trailing edge is reached. With the cropped planform the strong outboard shock does not occur since the forward and rear shocks do not intersect ahead of the trailing edge. This must be attributed primarily to the absence of trailing-edge sweep.

The chief interest in the present results lies perhaps more in the details of the flow development. The conditions for the aft movement of the forward shock from the leading edge seem to agree with those predicted from a simple model of the local flow, and it has once more been demonstrated that the pressures between the leading edge and the forward shock are largely independent of Mach number at low supersonic stream speeds. The condition for flow separation through the forward shock, in terms of a critical Mach number component normal to the shock, is very similar to that found for other wings having a similar leading-edge sweep. In the present text, an alternative criterion, based on the relative positions of the shock and the reattachment line appropriate to the particular incidence, has been suggested though it is difficult at present to see how these two approaches may be related.

The conditions for the first appearance of the rear shock have not been established in a completely satisfactory manner due to absence of chordwise pressure distributions outboard of $0{\cdot}9$ semi-span, and a consequent lack of knowledge of local isobar sweep. On the other hand, separation through the rear shock occurs in very similar circumstances to those deduced for two-dimensional flow and the rear shock on this wing has little sweep when separation takes place and hence agreement with aerofoil data should be expected. Nevertheless the result is gratifying.

The region between the forward and rear shocks seems in certain cases at transonic speeds to have cone-like-flow characteristics and this results in local pressures which are almost a constant fraction of the stream static pressure so that p/p_0 does not change with Mach number.

The apparent complexity of the flow and its variation with incidence and Mach number, appear to have little effect on the wing lift and moment. The most noticeable feature is the increase in lift

at high incidence and rearward movement of the centre-of-pressure position associated with the aft movement of the rear shock. The wing drag increases of course as the Mach number approaches unity but the significant part of the drag rise occurs about 0·05 in Mach number after the initial appearance of the first shock wave. The drag itself is not noticeably affected by the transition from leading-edge separation to attached flow as the Mach number is increased at constant incidence but there is strong evidence that the onset of leading-edge separation itself is responsible for a sharp increase in lift-dependent drag.

Though there has been a considerable advance in our understanding of swept-wing flow in recent years, it represents little more than a beginning to the solution of the complex problems involved in designing efficient wings for operational use at transonic and low supersonic speeds. With a plane wing similar to that used in the present tests many of the difficulties occur in an acute form and hence are amenable to study and perhaps ultimate elimination by more sophisticated designs. The analysis of the flow development is therefore felt to be of more value than a simple presentation of the result obtained and it is this belief that has influenced the structure of the present report.

Acknowledgements. The authors wish to acknowledge the assistance of Mr. J. E. G. Townsend, Miss B. M. Davis and Miss R. Buckthorpe in obtaining and analysing the original data.

REFERENCES

No.	*Author*	*Title, etc.*
1	I. M. Hall and E. W. E. Rogers ..	The flow pattern on a tapered sweptback wing at Mach numbers between 0·6 and 1·6. A.R.C. R. & M. 3271. Part I. July, 1960.
2	I. M. Hall and E. W. E. Rogers ..	Experiments with a tapered sweptback wing of Warren 12 planform at Mach numbers between 0·6 and 1·6. A.R.C. R. & M. 3271. Part II. July, 1960.
3	I. M. Hall	The operation of the N.P.L. 18 in. × 14 in. Wind Tunnel in the transonic speed range. A.R.C. C.P. 338. January, 1957.
4	E. W. E. Rogers and I. M. Hall ..	An investigation at transonic speeds of the performance of various distributed roughness bands used to cause boundary-layer transition near the leading edge of a cropped delta half-wing.
	C. J. Berry and J. E. G. Townsend	Appendix. A roughness band technique and materials. A.R.C. C.P. 481. May, 1959.
5	E. W. E. Rogers, J. E. G. Townsend and C. J. Berry	A study of the effect of leading-edge modifications on the flow over a 50 deg sweptback wing at transonic speeds. A.R.C. R. & M. 3270. May, 1960.
6	D. W. Holder, H. H. Pearcey and G. E. Gadd	The interaction between shock waves and boundary layers. With a note on the effects of the interaction on the performance of supersonic intakes: by J. Seddon. A.R.C. C.P. 180. February, 1954.
7	H. H. Pearcey, C. S. Sinnott and J. Osborne	Some effects of wind-tunnel interference observed in tests on two-dimensional aerofoils at high subsonic and transonic speeds. N.P.L./Aero/373. February, 1959.
8	E. W. E. Rogers and I. M. Hall ..	Wall interference at transonic speeds on a hemisphere-cylinder model. A.R.C. C.P. 510. September, 1959.
9	F. O'Hara, L. C. Squire (R.A.E.) and A. B. Haines (A.R.A.)	An investigation of interference effects on similar models of different size in various transonic tunnels in the U.K. A.R.C. 21,094. February, 1959.
10	W. A. Page	Experimental study of the equivalence of transonic flow about slender cone-cylinders of circular and elliptic cross section. N.A.C.A. Tech. Note 4233. April, 1958.

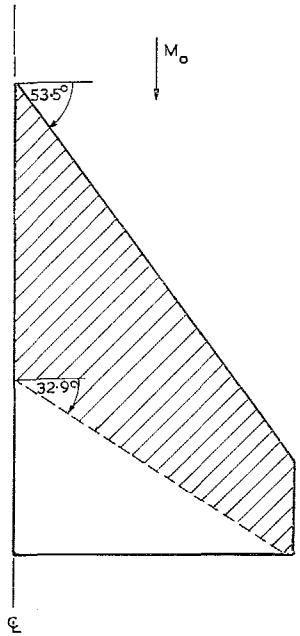

FIG. 1a. Comparison between cropped-delta planform and that for tapered half-wing of Reference 1 and 2 (shown shaded). Comparison made at same semi-span dimension. Both wings have 6 per cent thick RAE 102 section in stream direction.

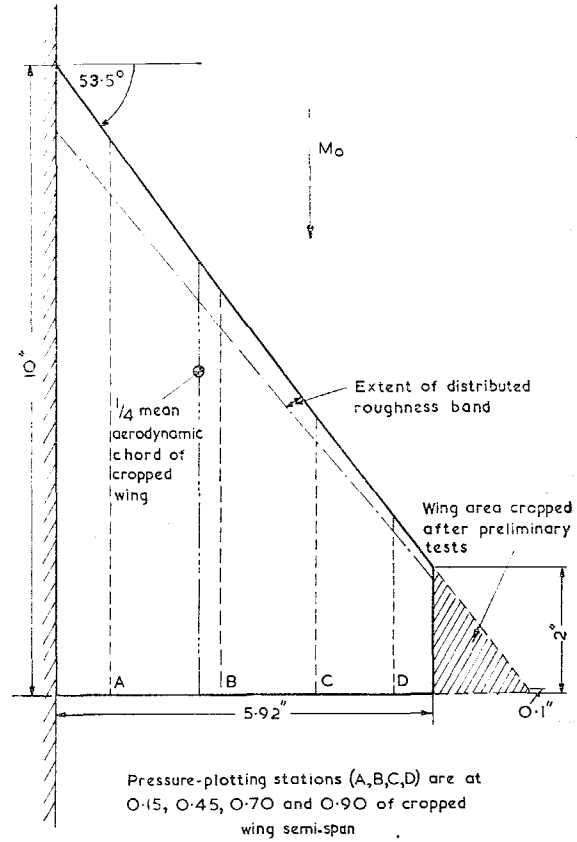

Pressure-plotting stations (A,B,C,D) are at 0·15, 0·45, 0·70 and 0·90 of cropped wing semi-span

Streamwise section: 6% RAE 102
Aspect Ratio: 1·97 (cropped) 2·90 (original state)
Mean aerodynamic chord of cropped wing: 6·89in.

FIG. 1b. Details of delta half-wing model.

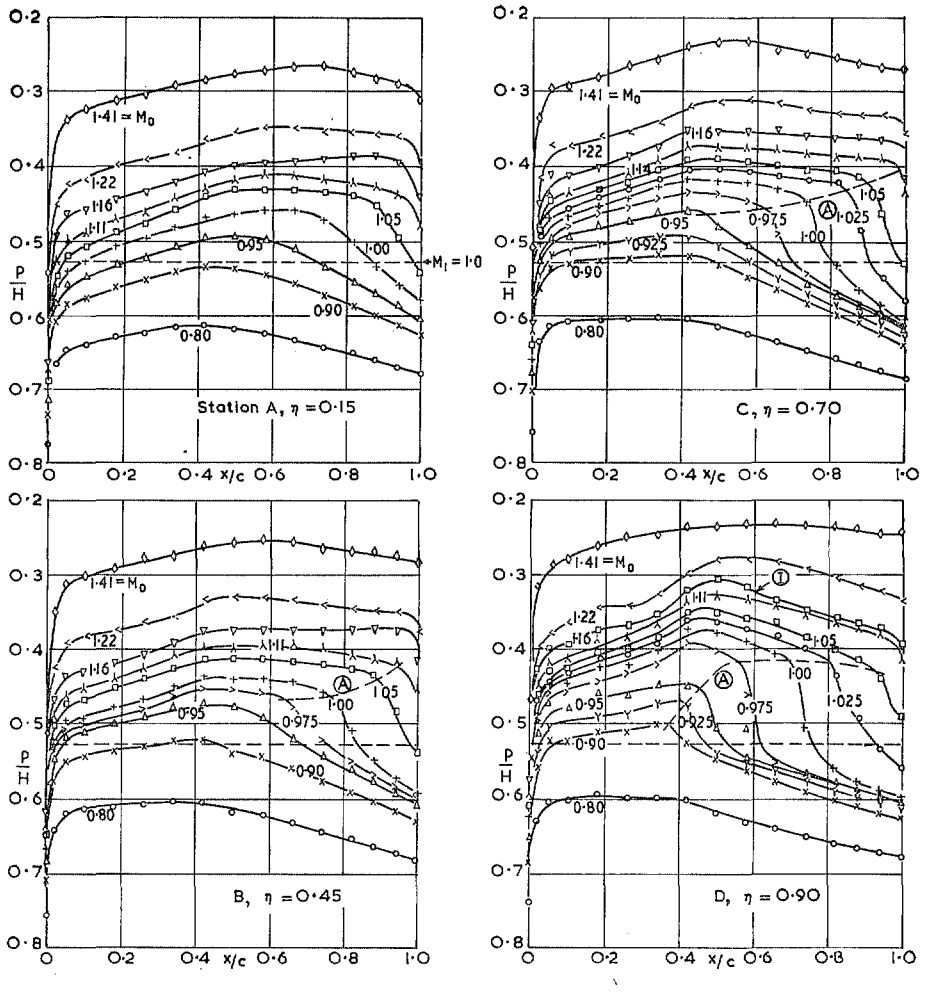

FIG. 2a. Chordwise pressure distributions at $\alpha = 0$ deg.

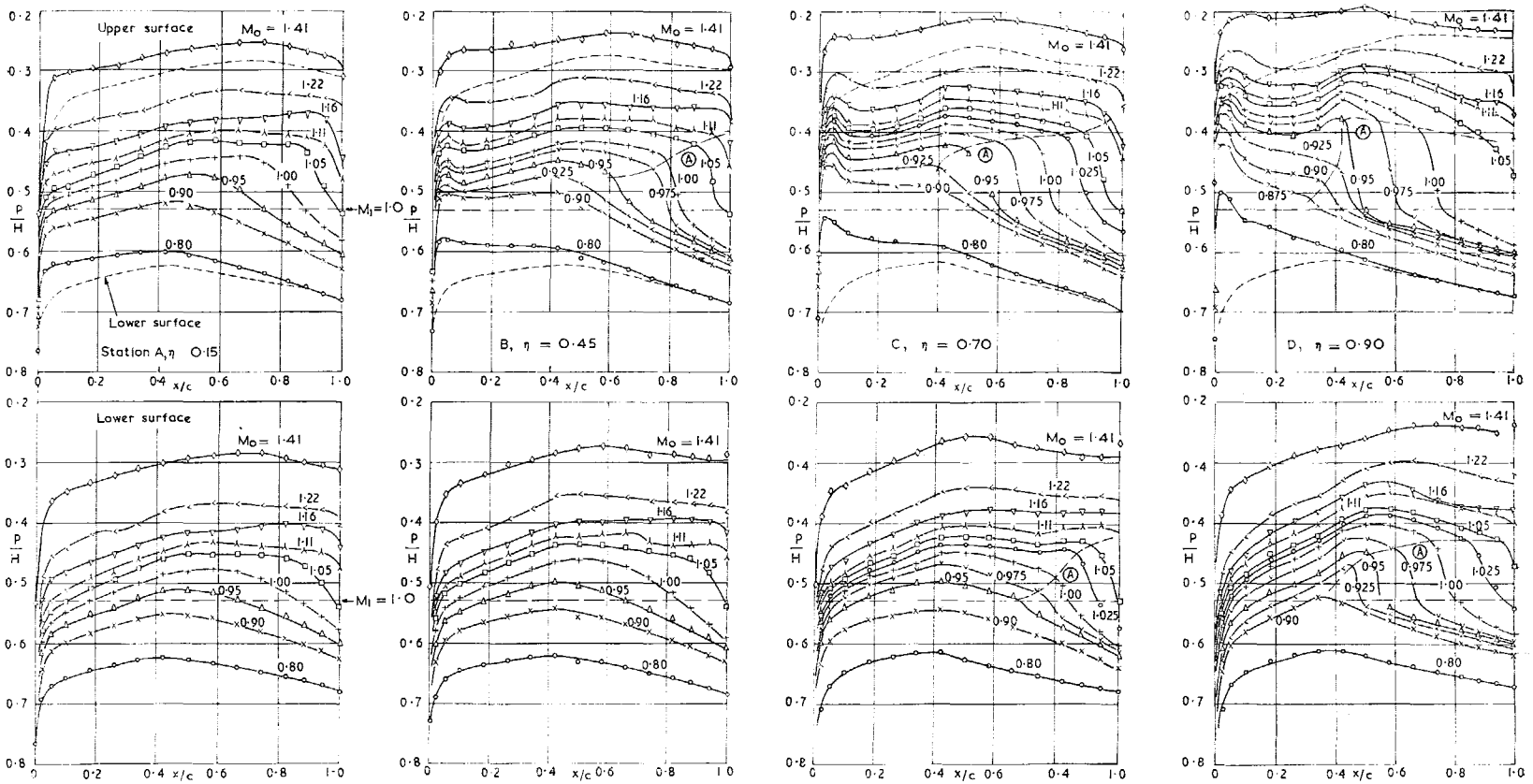

FIG. 2b. Chordwise pressure distributions at $\alpha = 2$ deg.

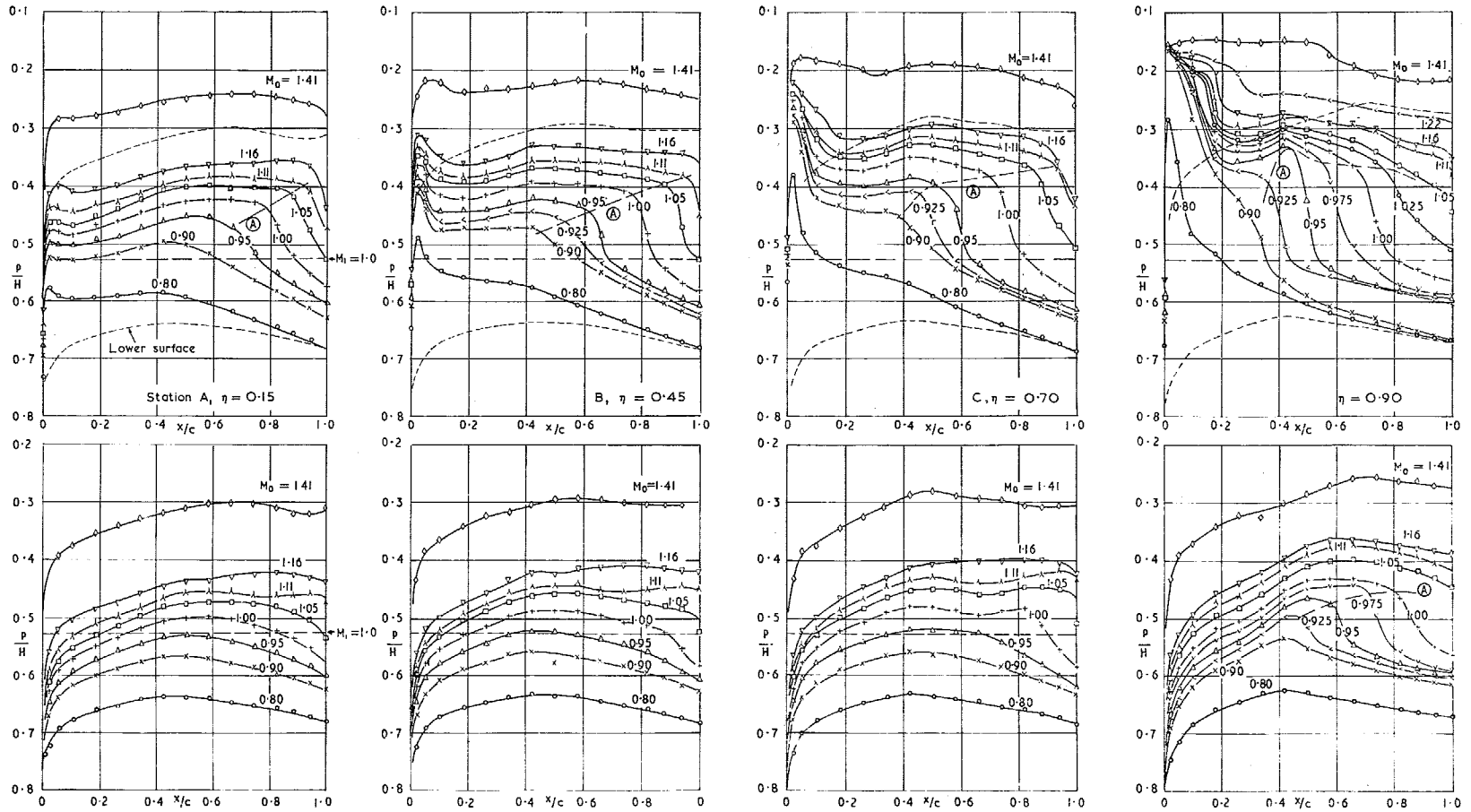

FIG. 2c. Chordwise pressure distributions at $\alpha = 4$ deg.

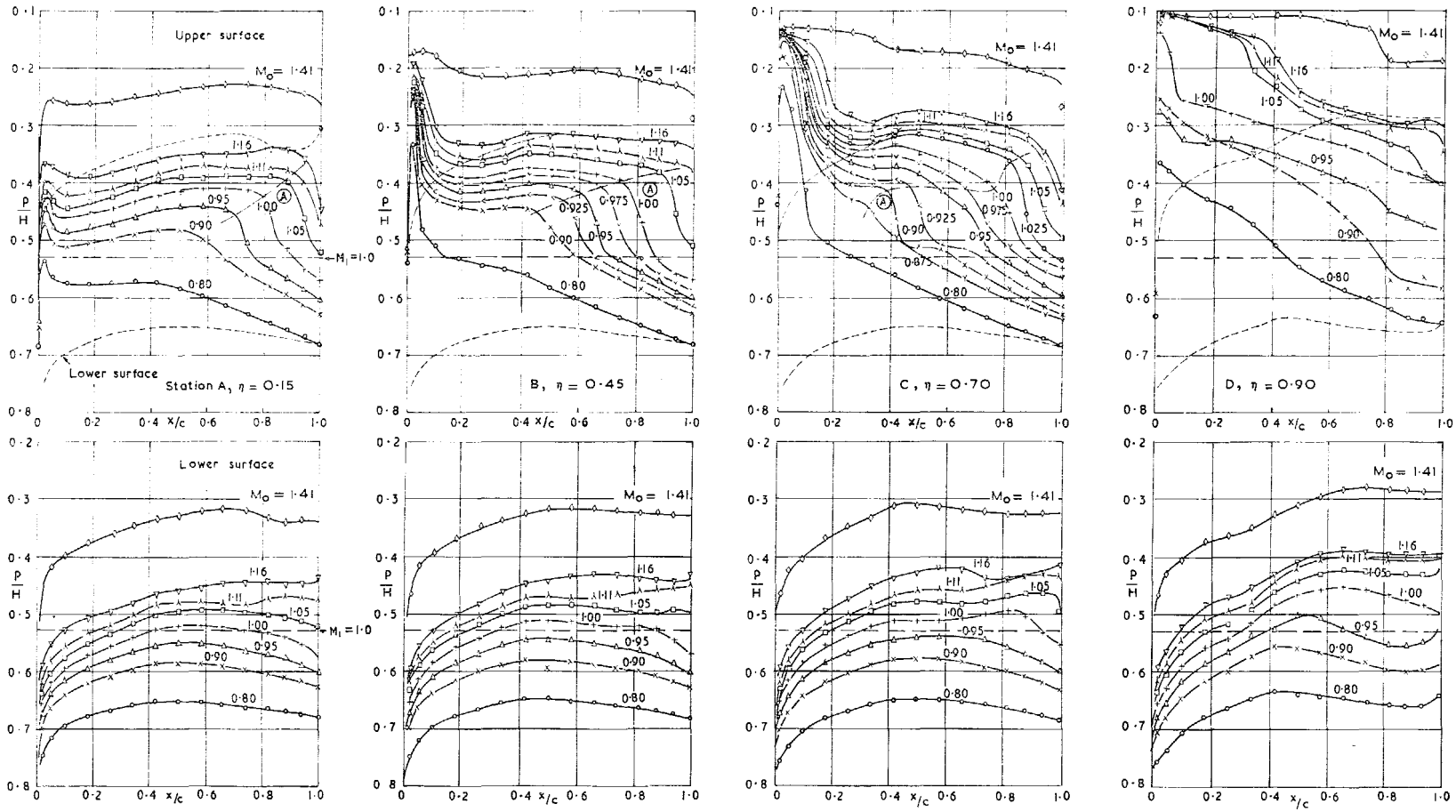

FIG. 2d. Chordwise pressure distributions at $\alpha = 6$ deg.

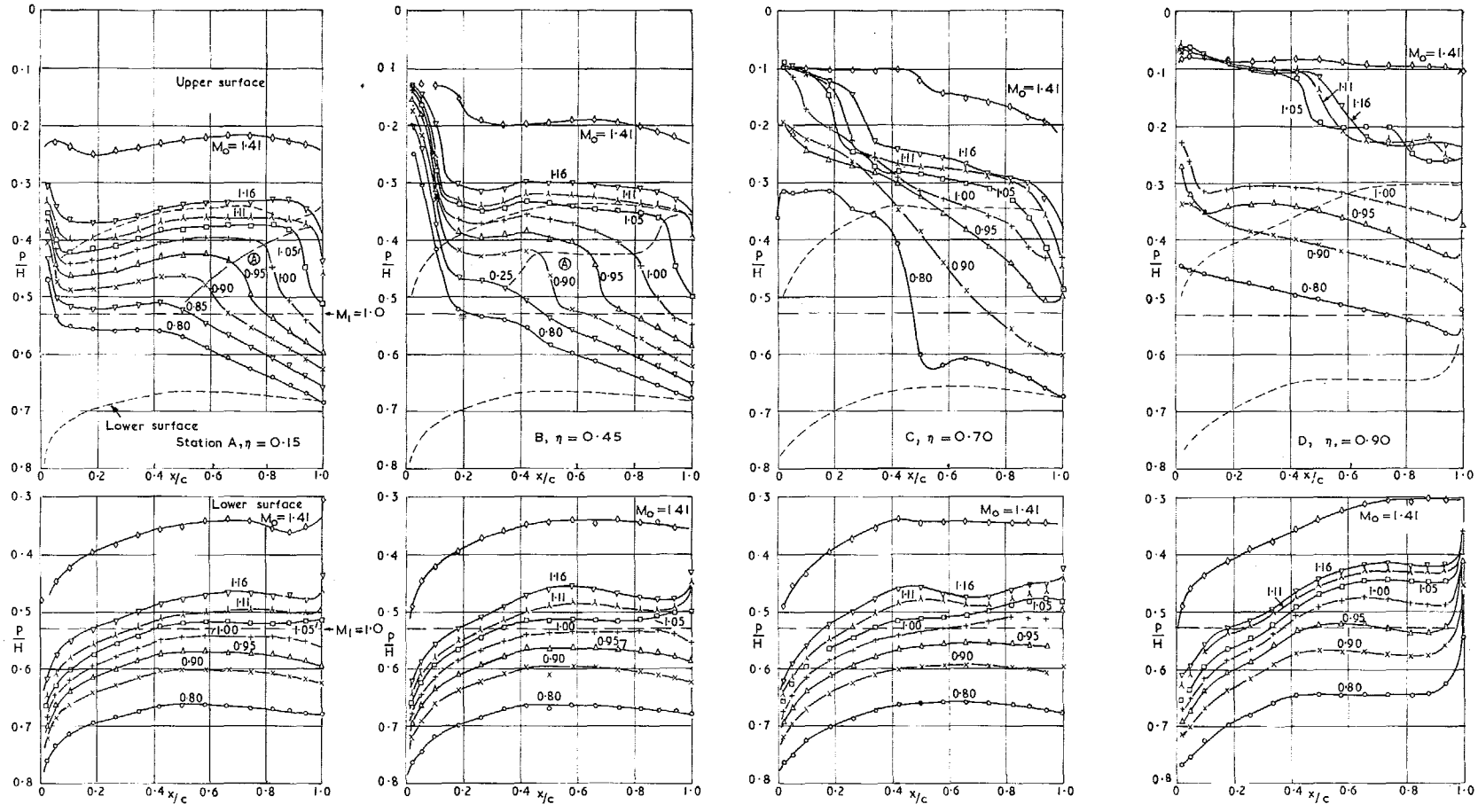

FIG. 2e. Chordwise pressure distributions at $\alpha = 8$ deg.

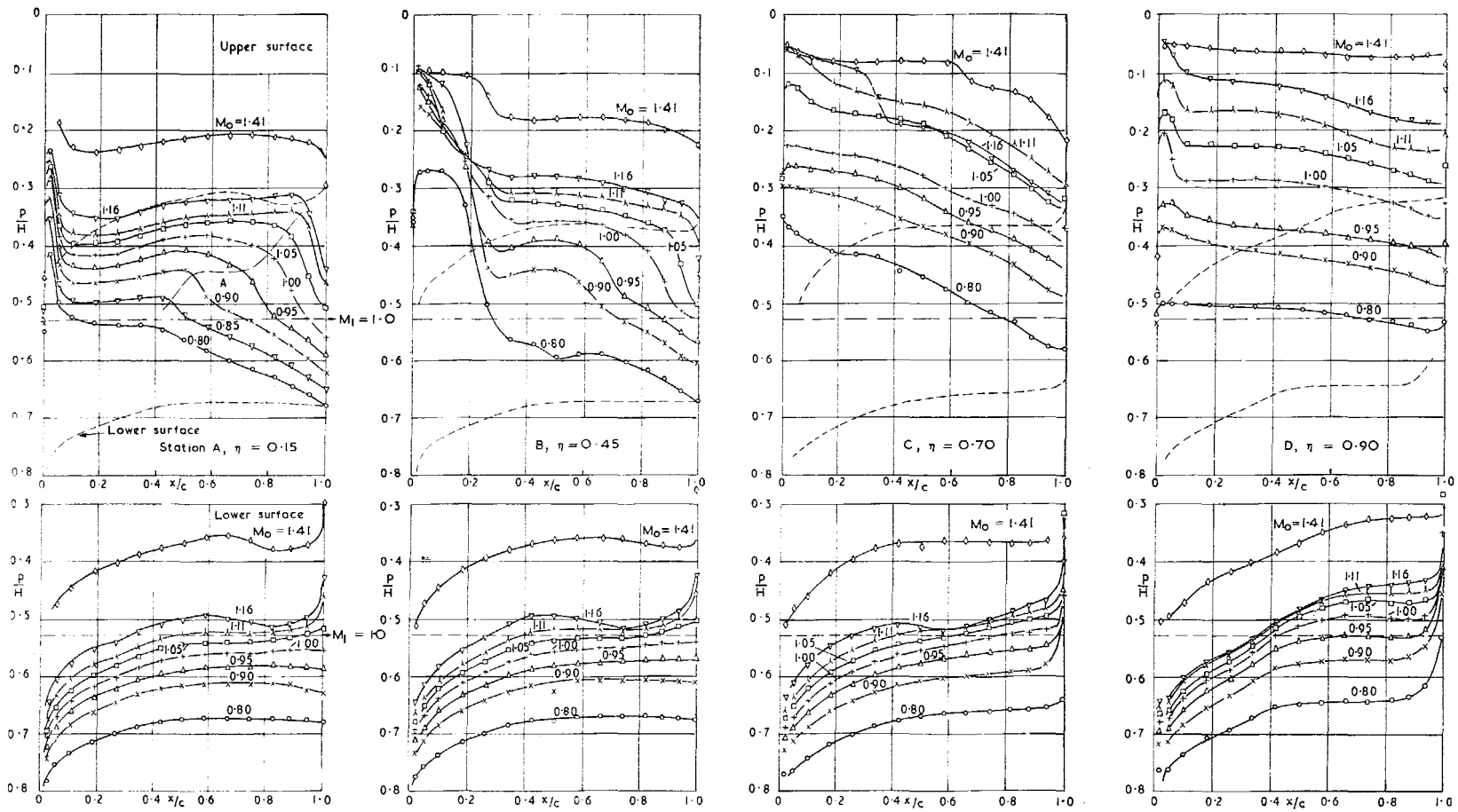

FIG. 2f. Chordwise pressure distributions at $\alpha = 10$ deg.

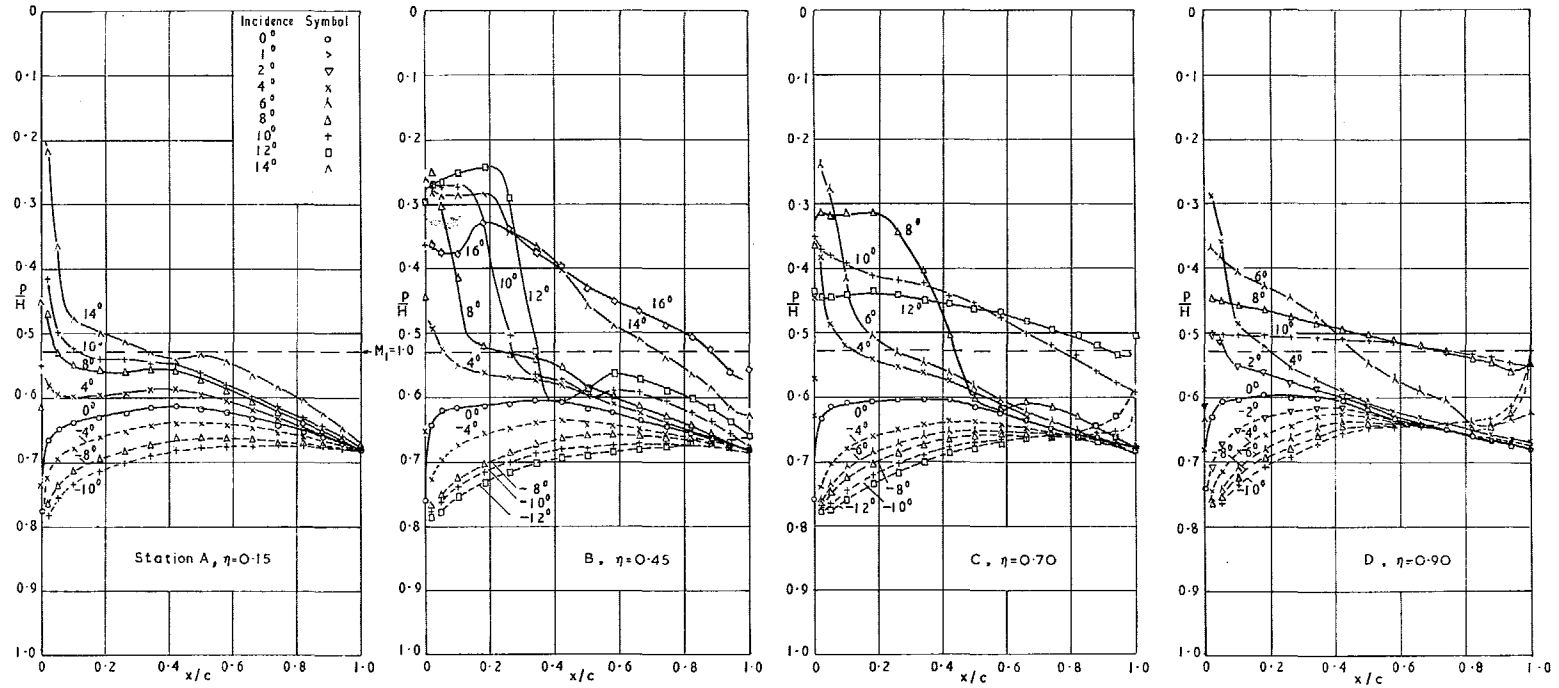

FIG. 3a. Chordwise pressure distributions at $M_0 = 0{\cdot}80$.

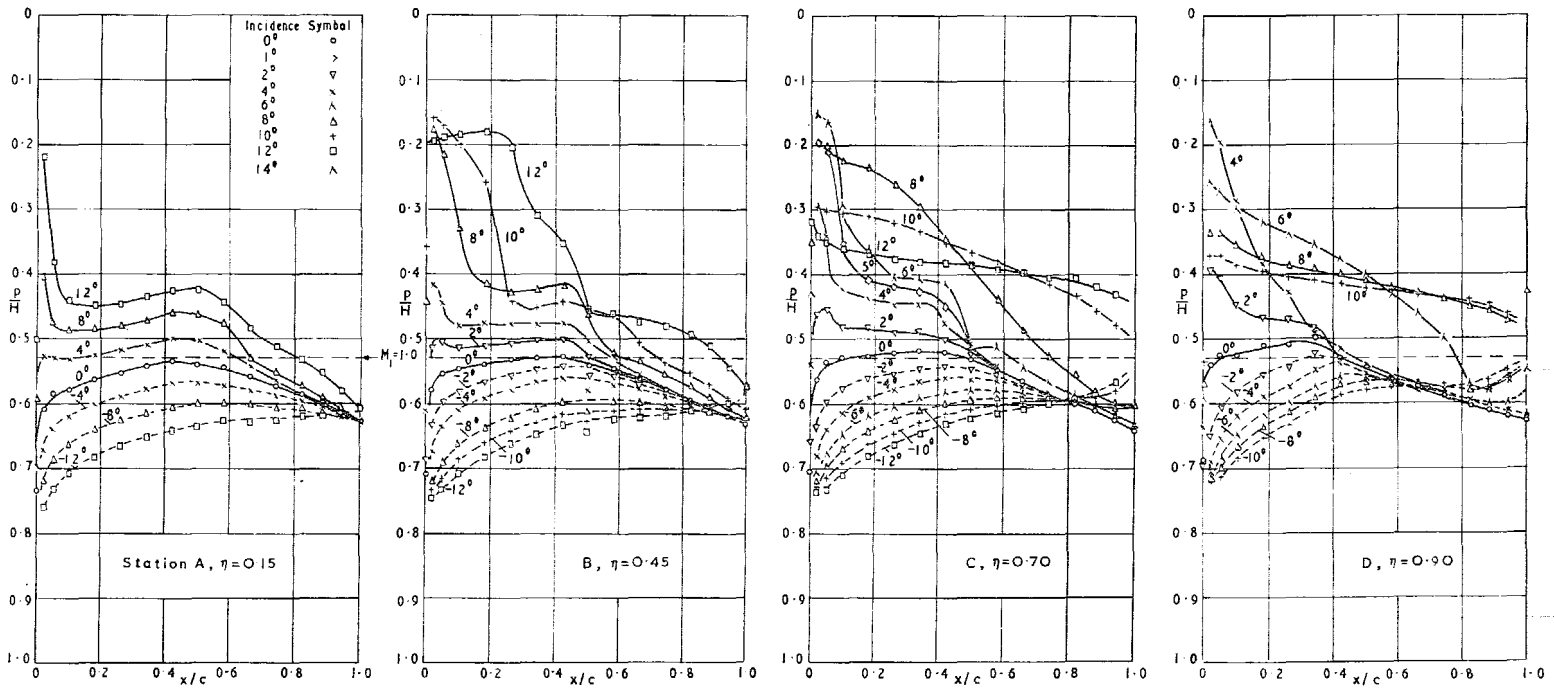

FIG. 3b. Chordwise pressure distributions at $M_0 = 0{\cdot}90$.

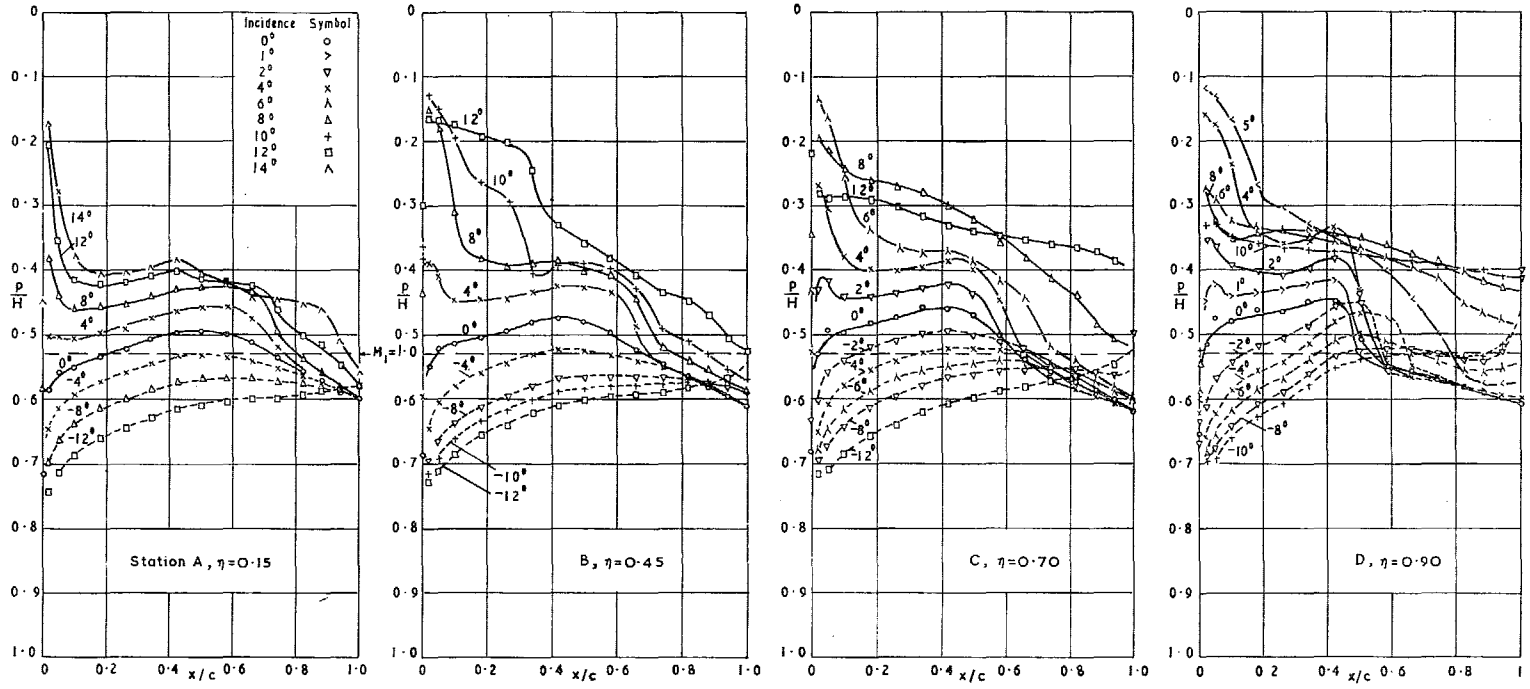

FIG. 3c. Chordwise pressure distributions at $M_0 = 0{\cdot}95$.

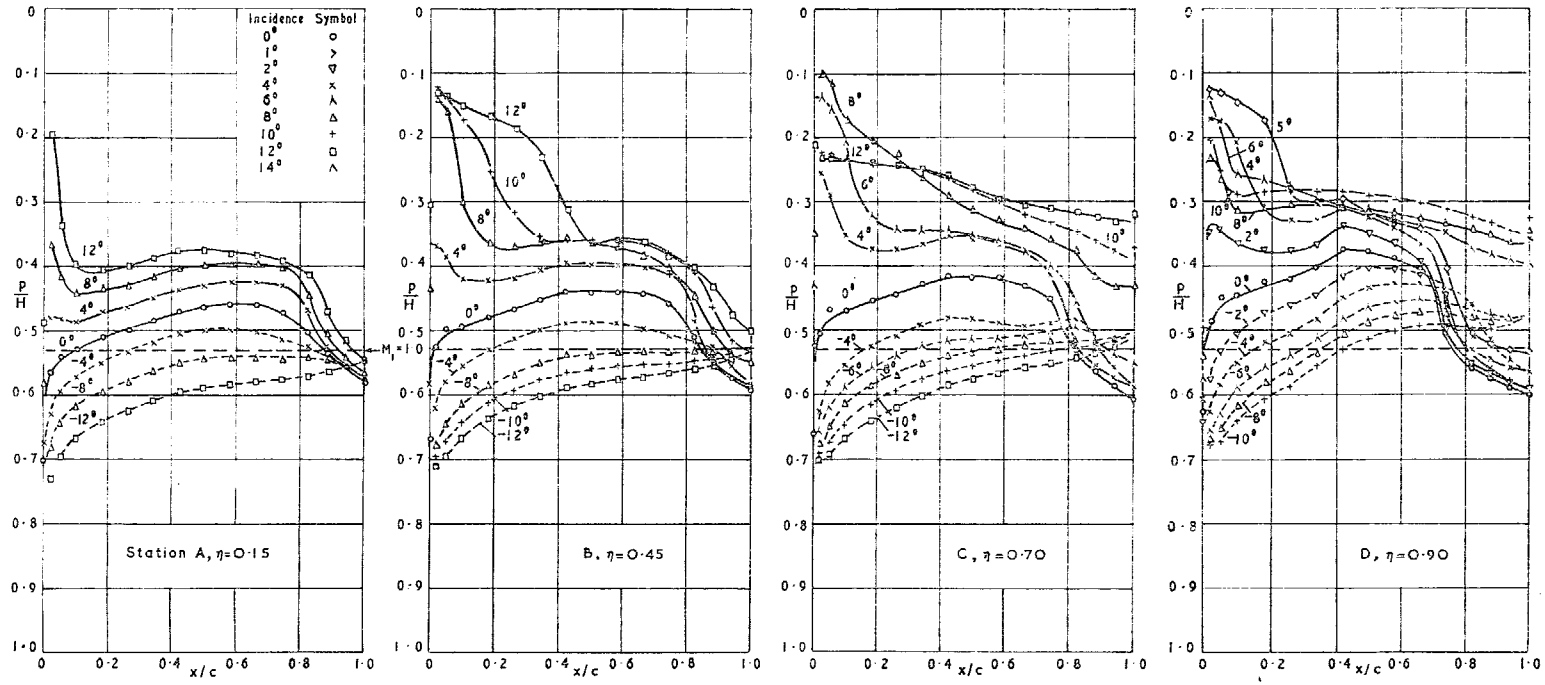

FIG. 3d. Chordwise pressure distributions at $M_0 = 1{\cdot}00$.

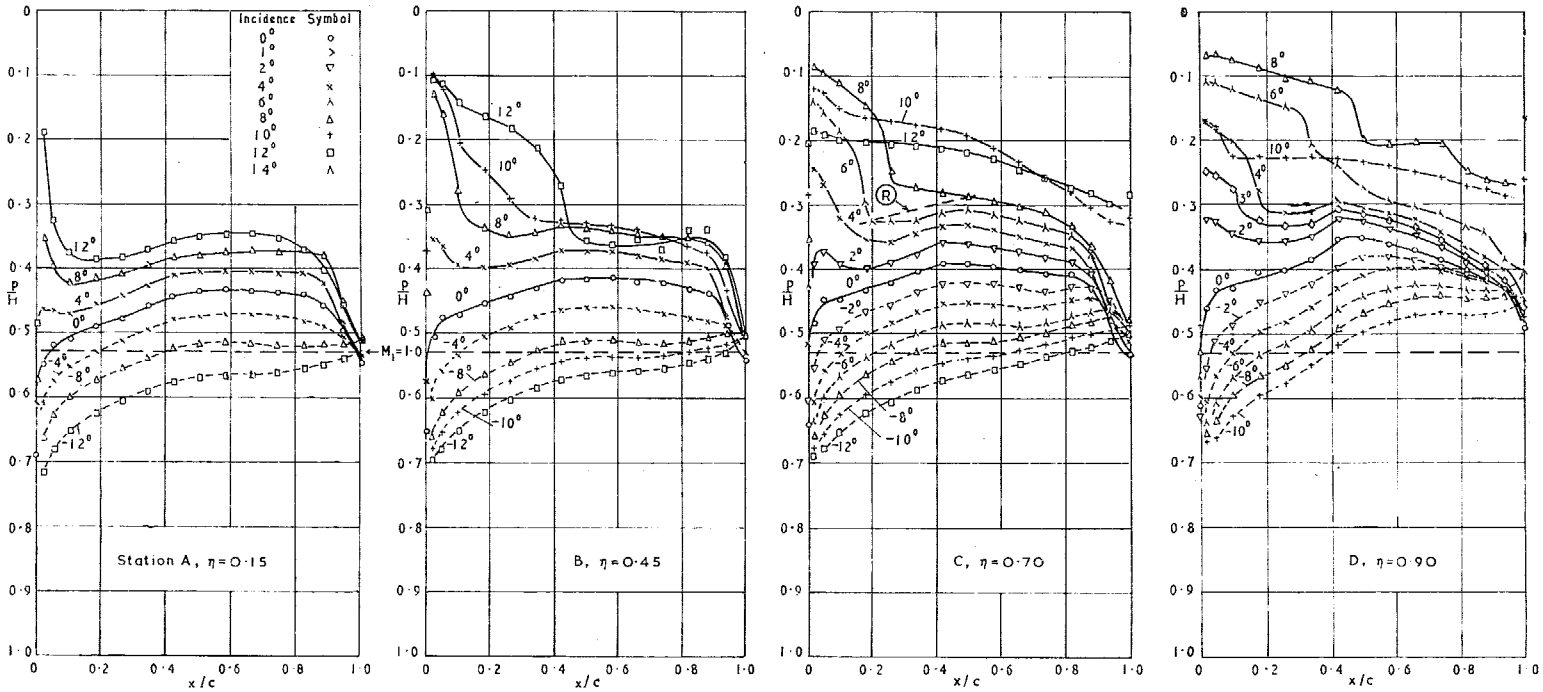

FIG. 3e. Chordwise pressure distributions at $M_0 = 1{\cdot}05$.

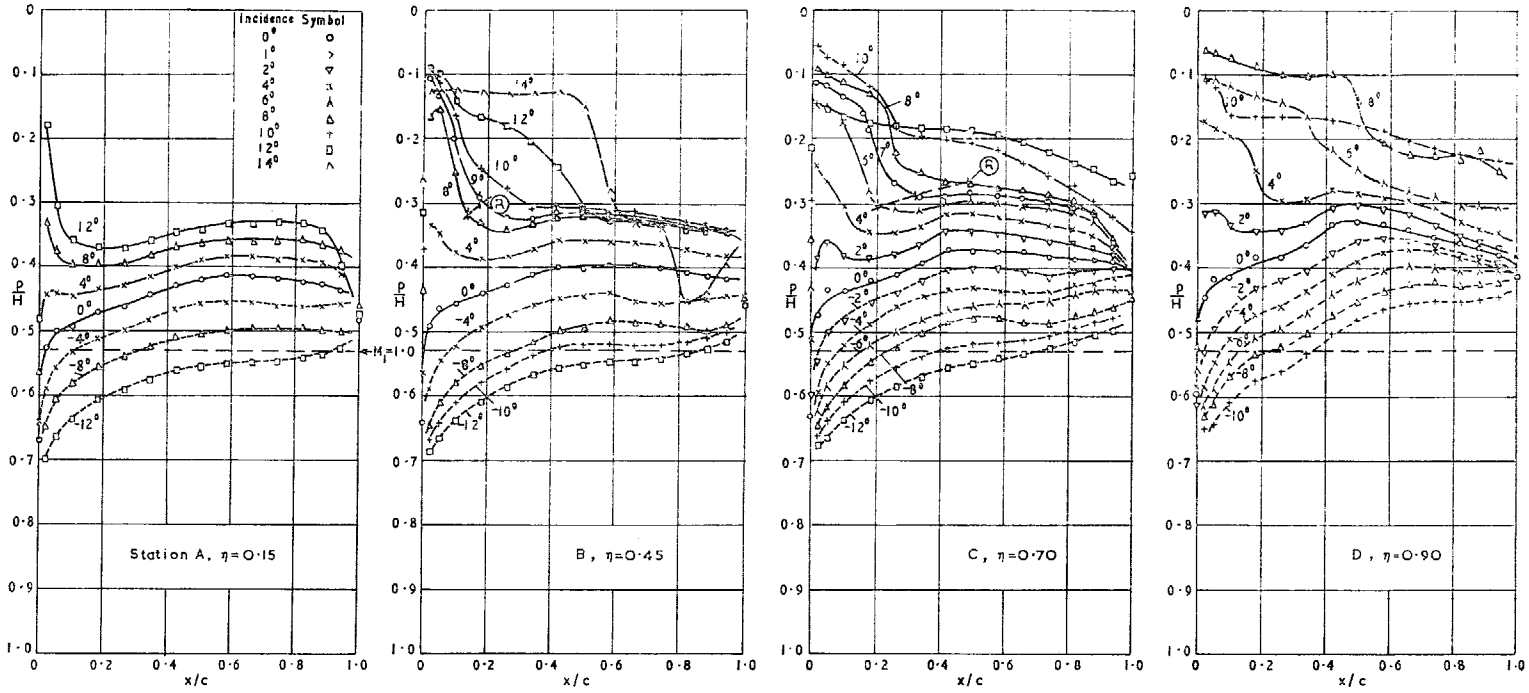

FIG. 3f. Chordwise pressure distributions at $M_0 = 1{\cdot}11$.

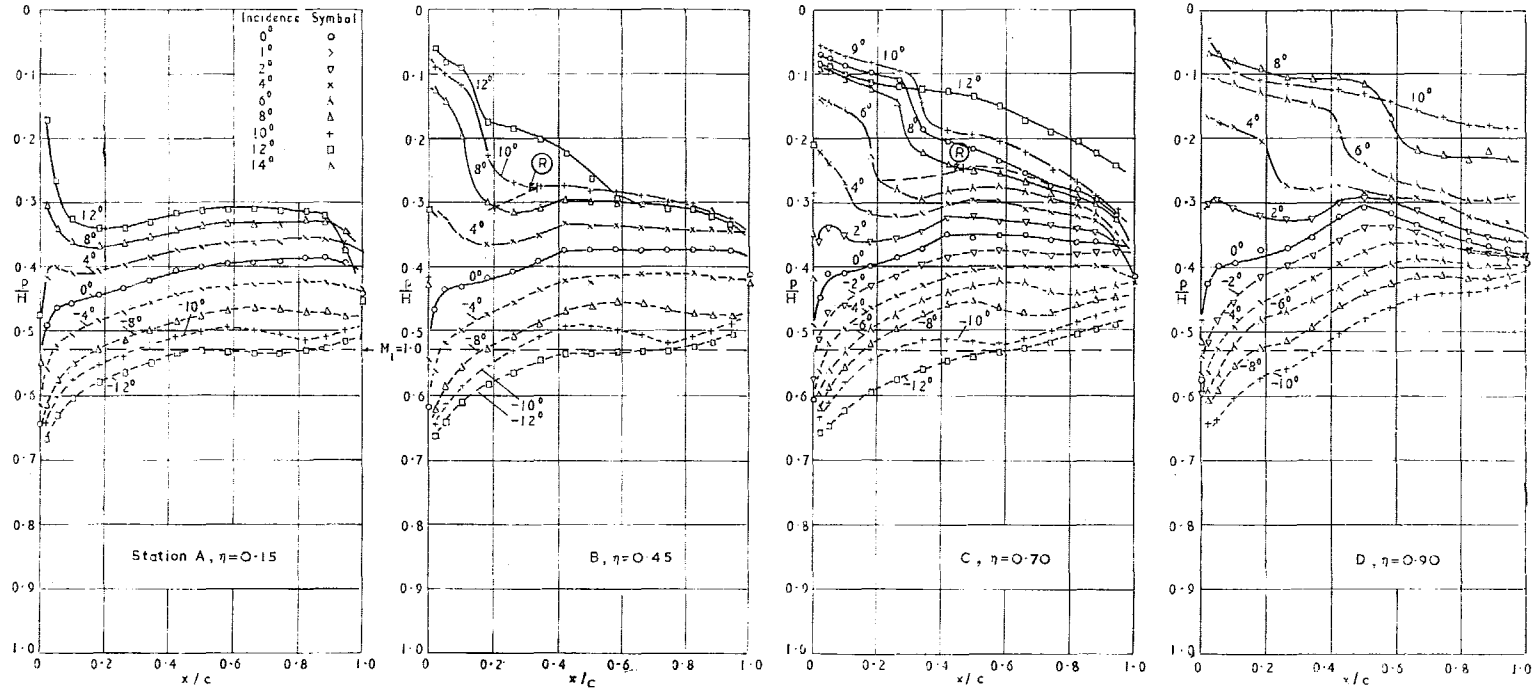

FIG. 3g. Chordwise pressure distributions at $M_0 = 1{\cdot}16$.

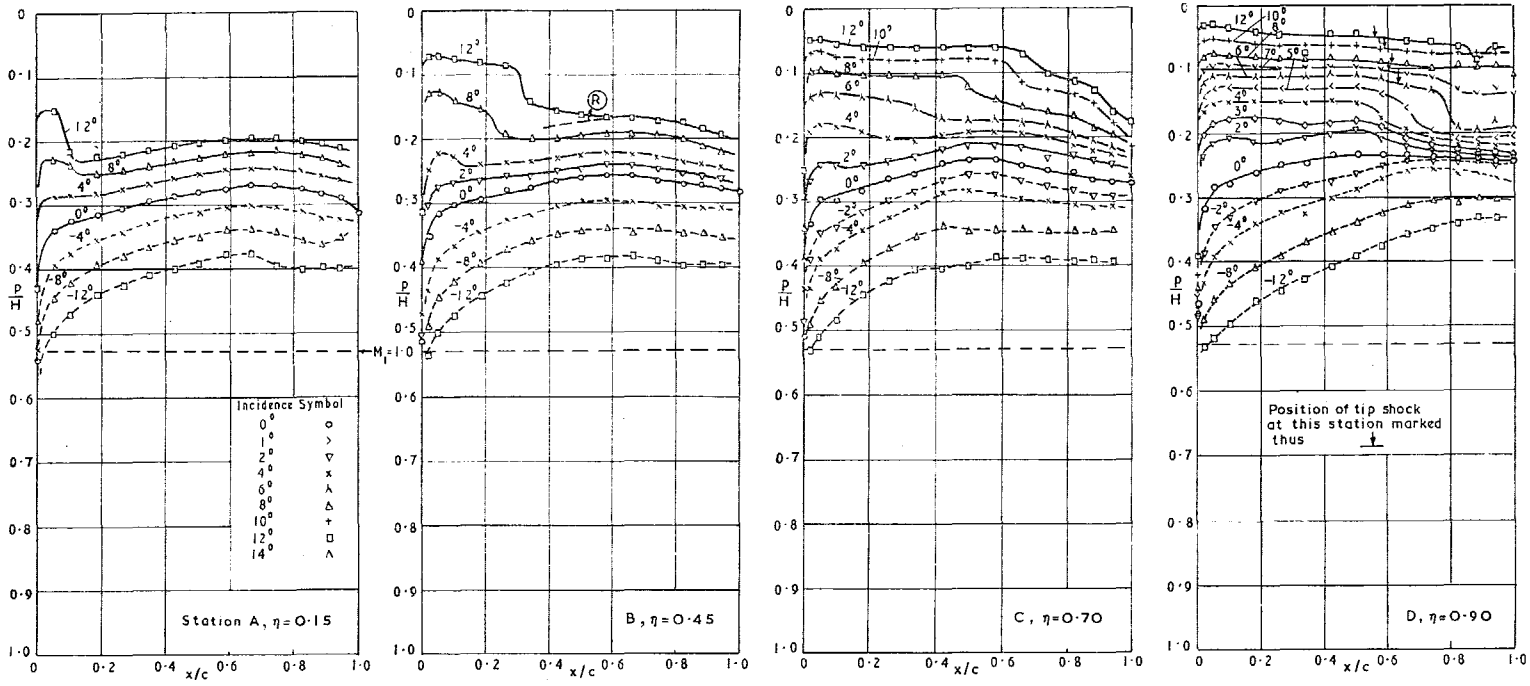

FIG. 3h. Chordwise pressure distributions at $M_0 = 1{\cdot}41$.

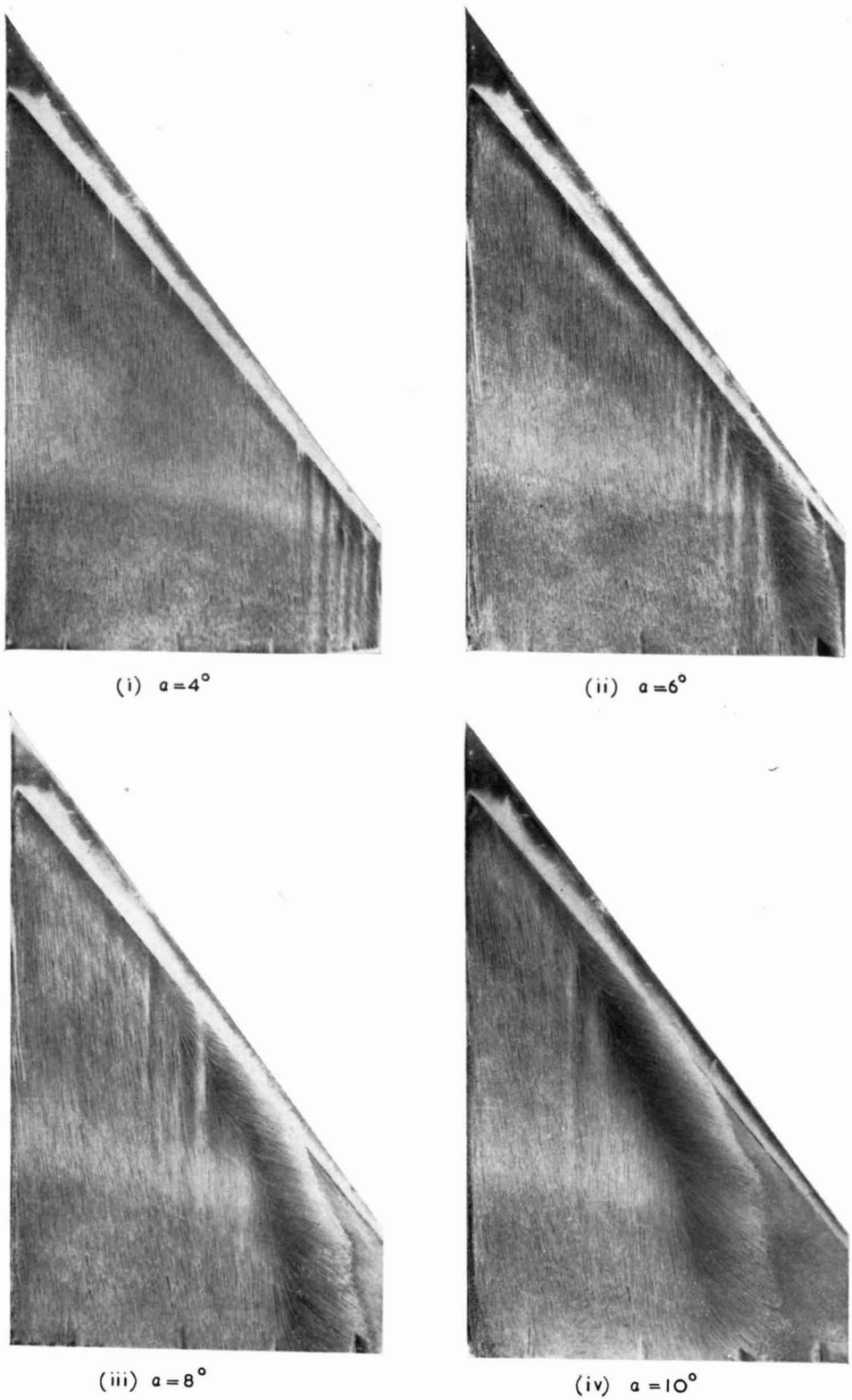

FIG. 4a. Oil-flow patterns on wing upper surface at $M_0 = 0{\cdot}80$.

(85536)

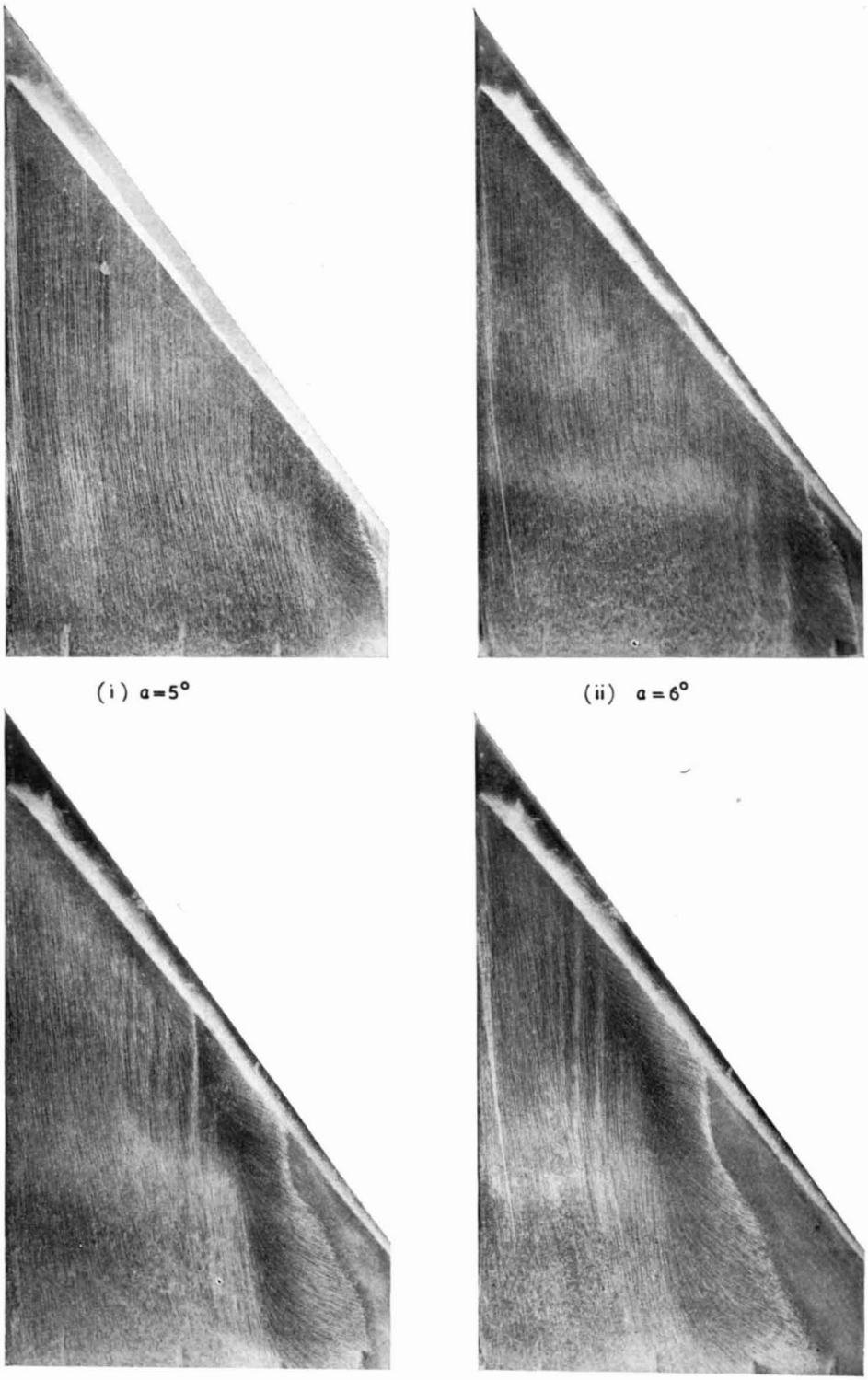

FIG. 4b. Oil-flow patterns on wing upper surface at $M_0 = 0{\cdot}90$.

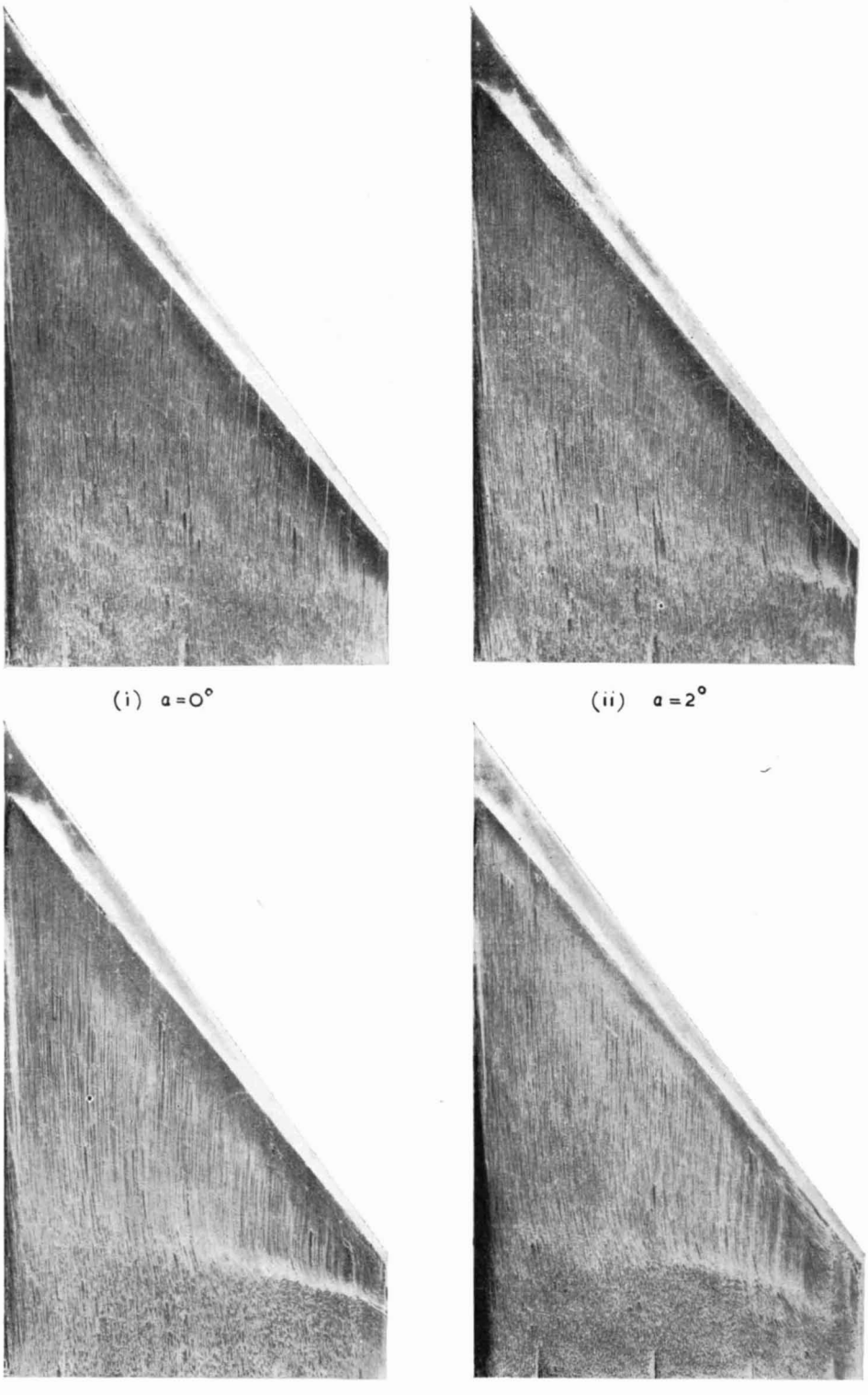

FIG. 4c. Oil-flow patterns on wing upper surface at $M_0 = 0{\cdot}95$.

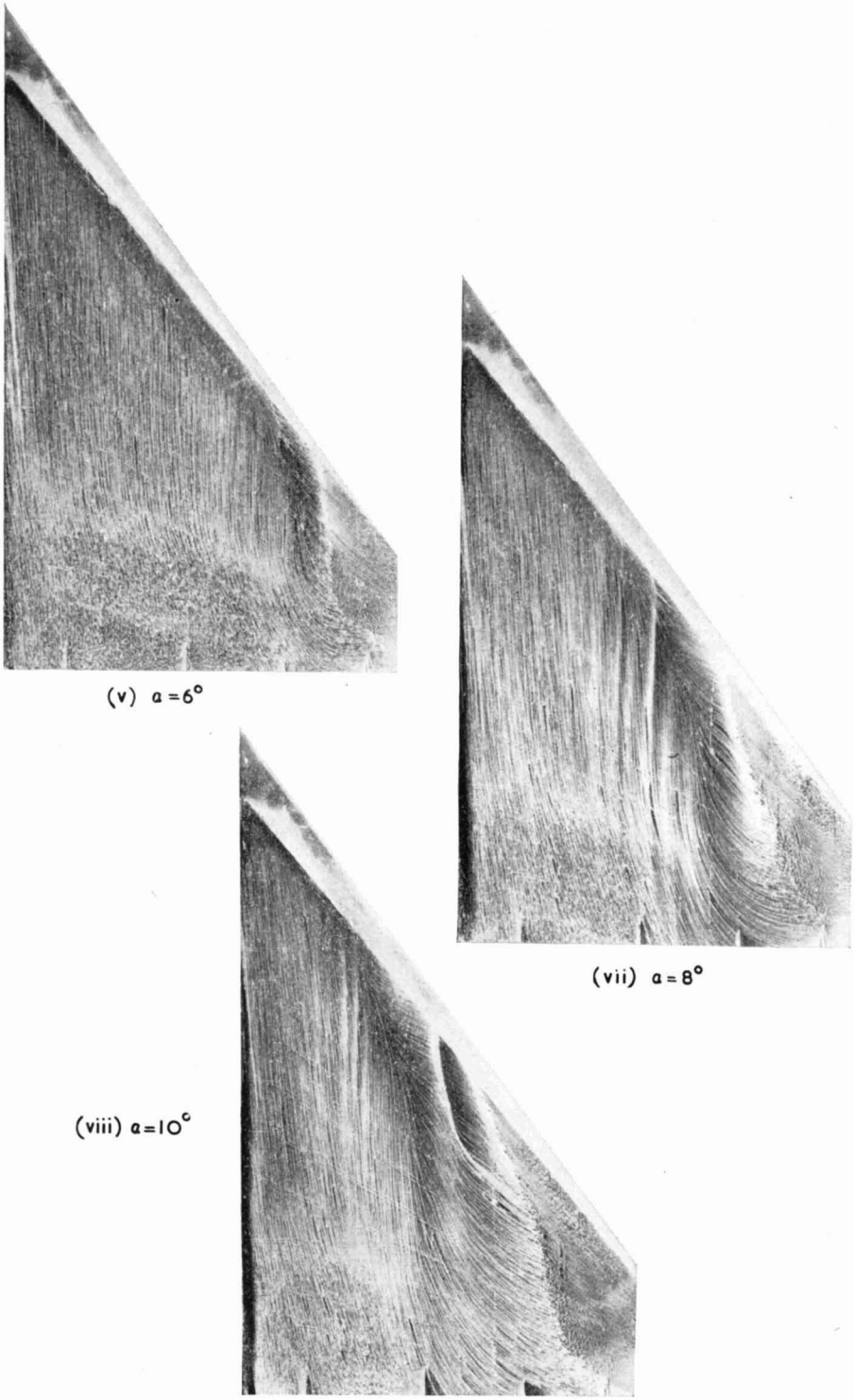

FIG. 4c (*cont.*). Oil-flow patterns on wing upper surface at $M_0 = 0{\cdot}95$.

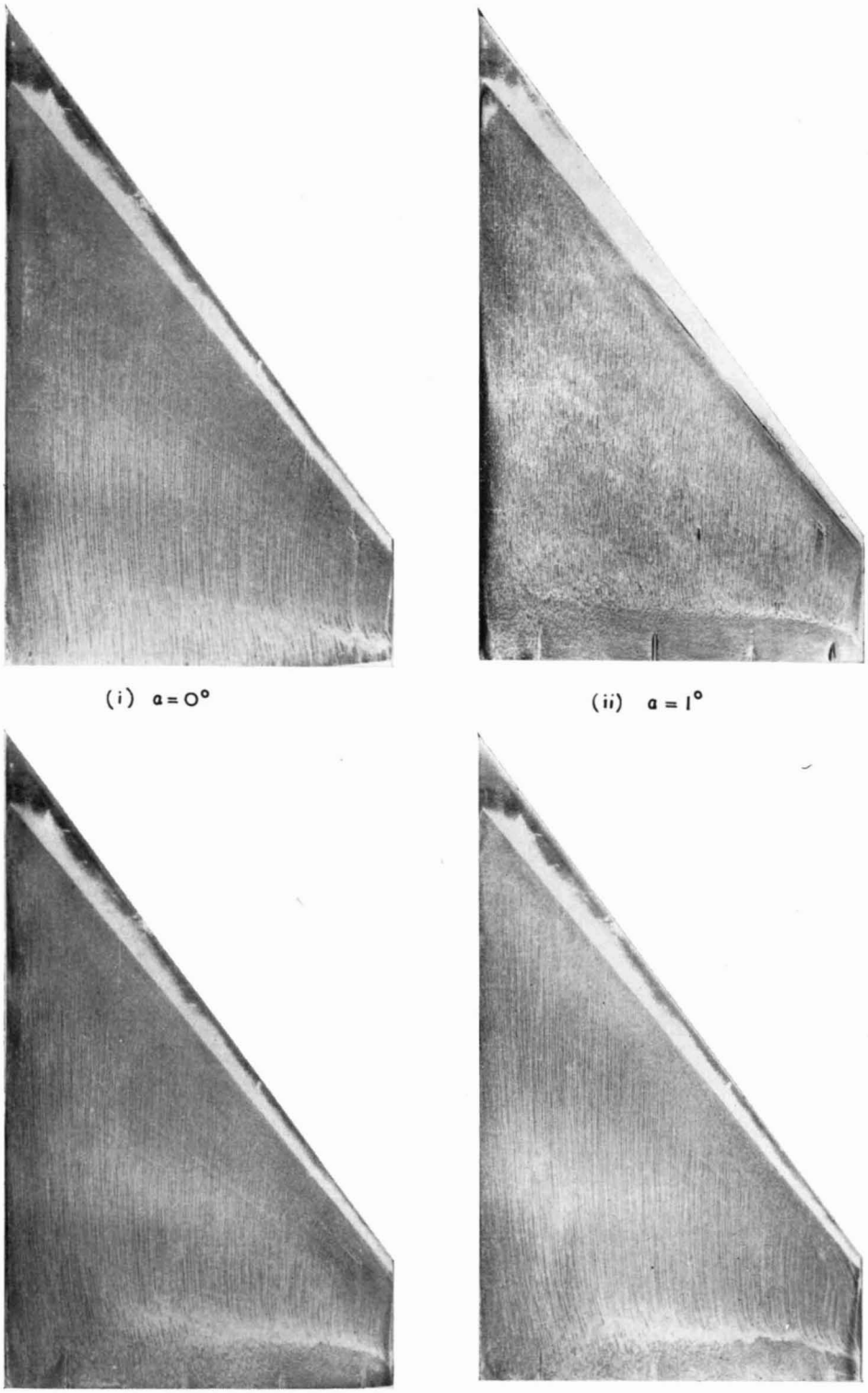

FIG. 4d. Oil-flow patterns on wing upper surface at $M_0 = 1{\cdot}00$.

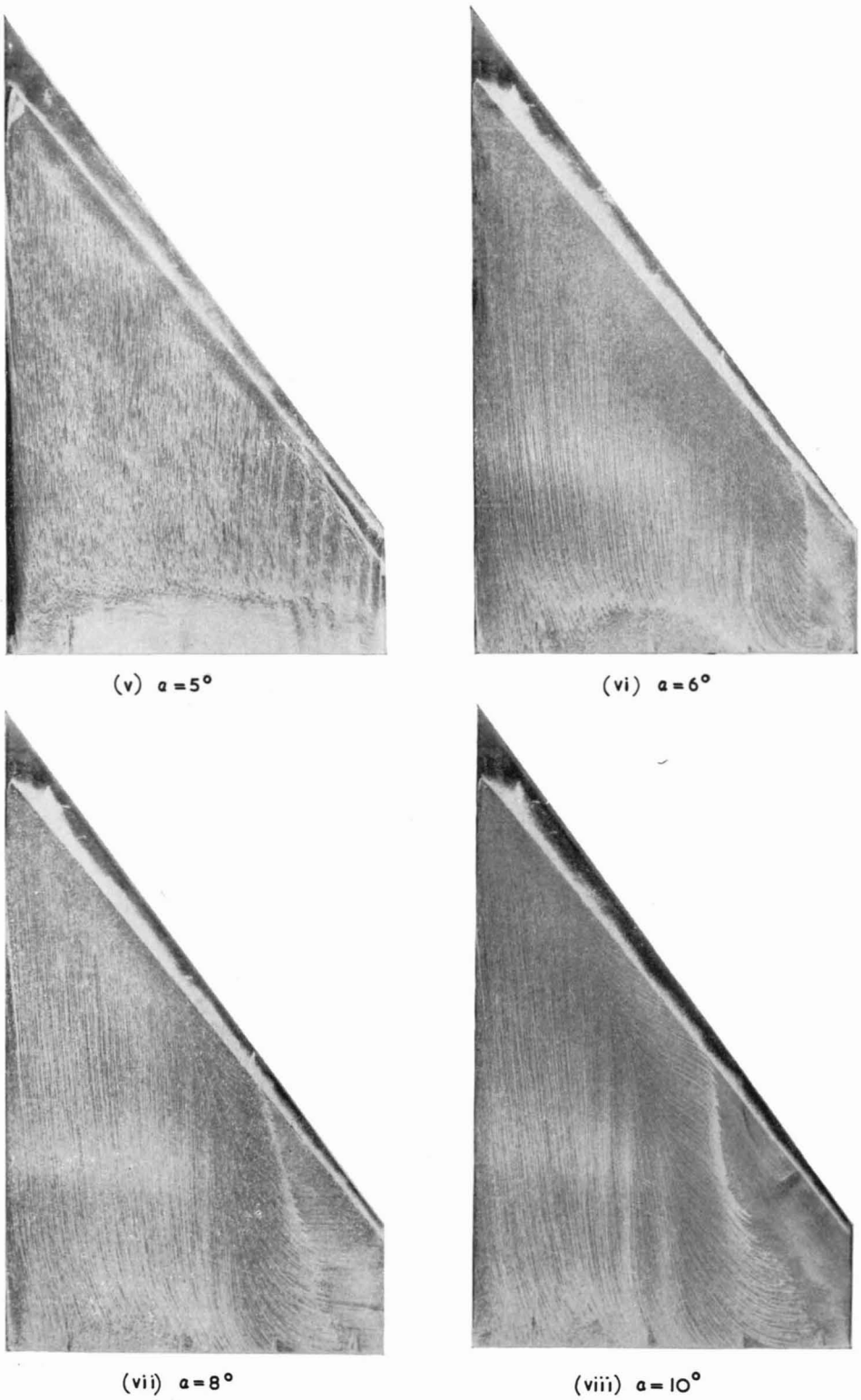

FIG. 4d (*cont.*). Oil-flow patterns on wing upper surface at $M_0 = 1{\cdot}00$.

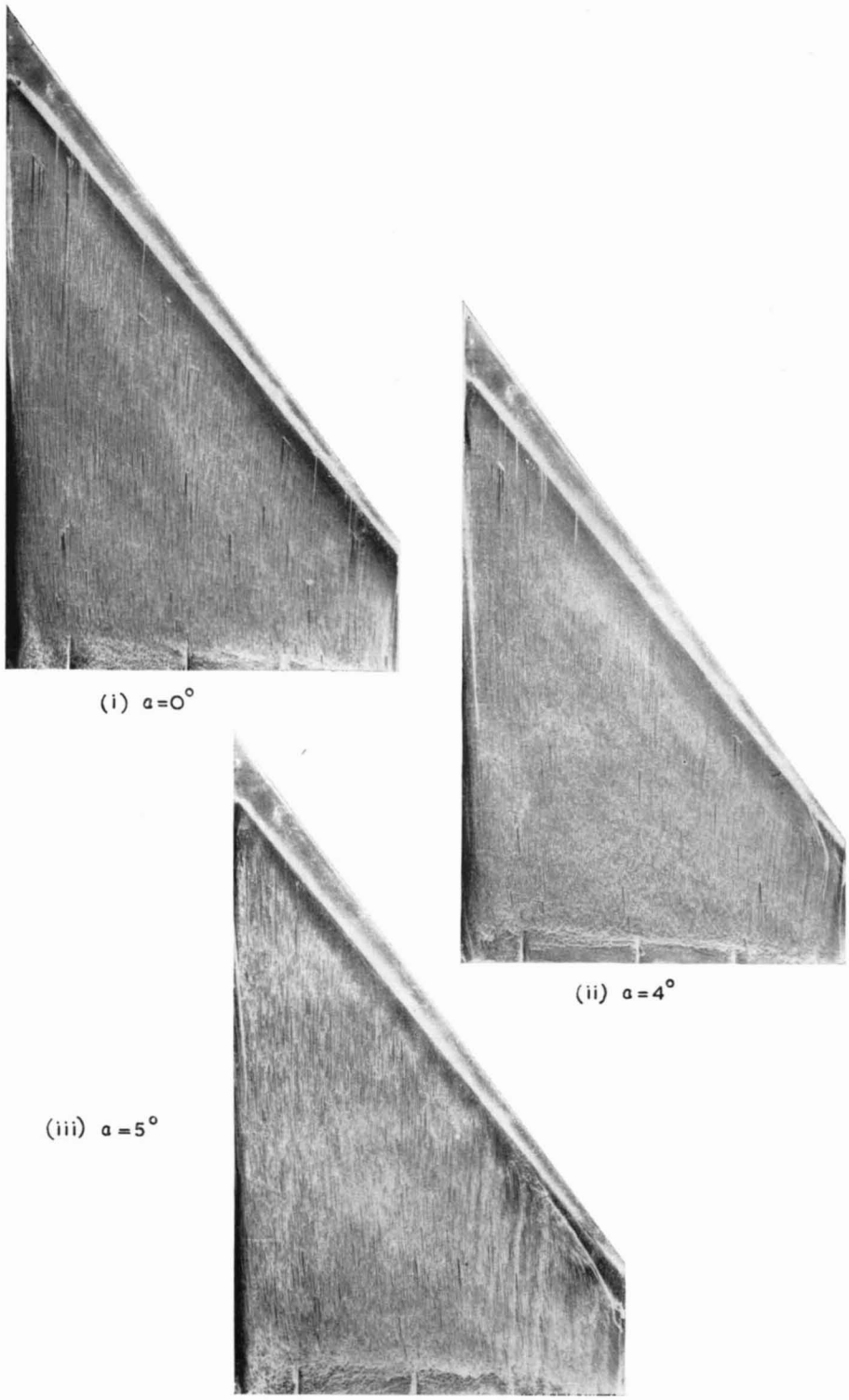

FIG. 4e. Oil-flow patterns on wing upper surface at $M_0 = 1{\cdot}05$.

(85536) C***

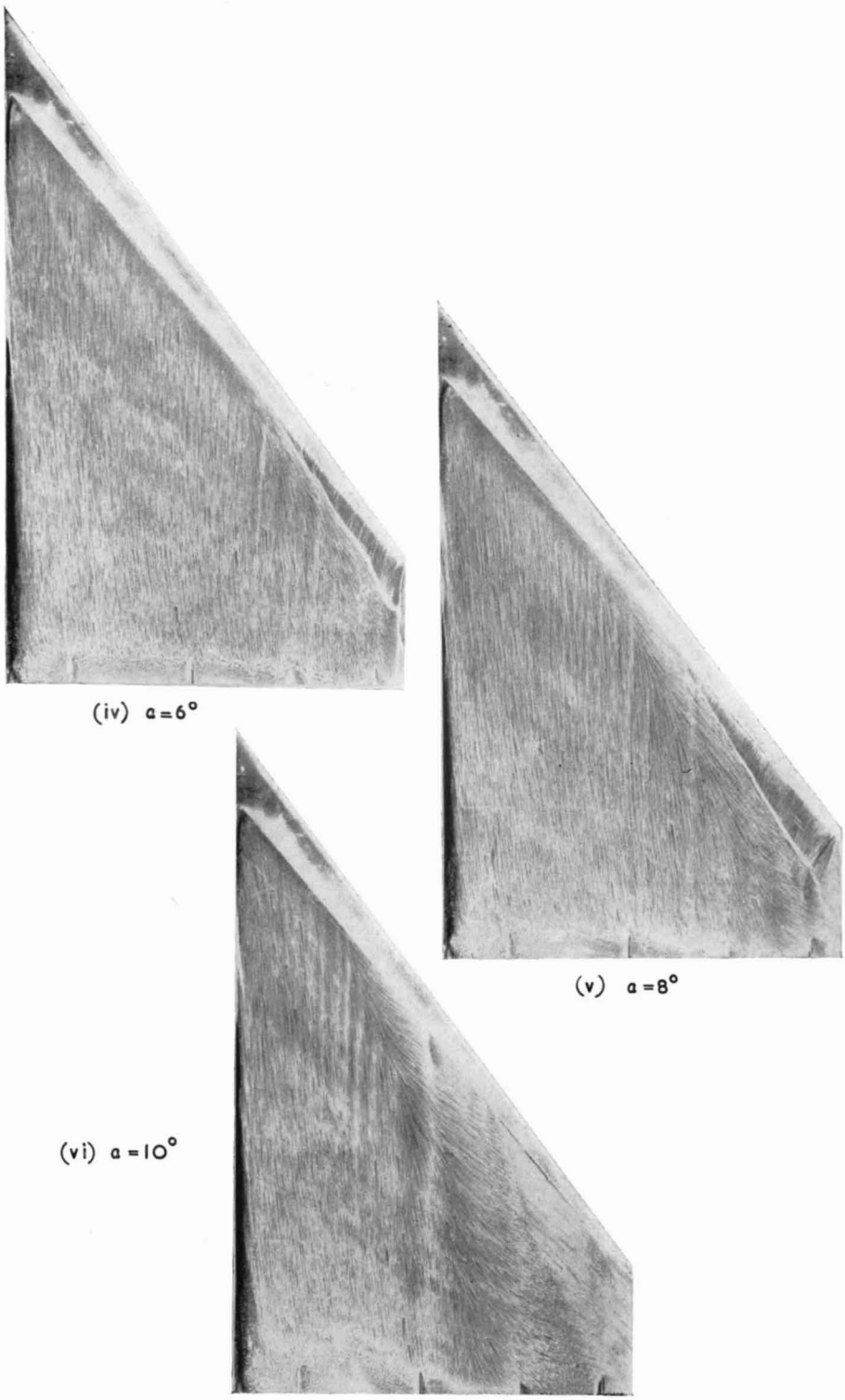

FIG. 4e (*cont.*). Oil-flow patterns on wing upper surface at $M_0 = 1{\cdot}05$.

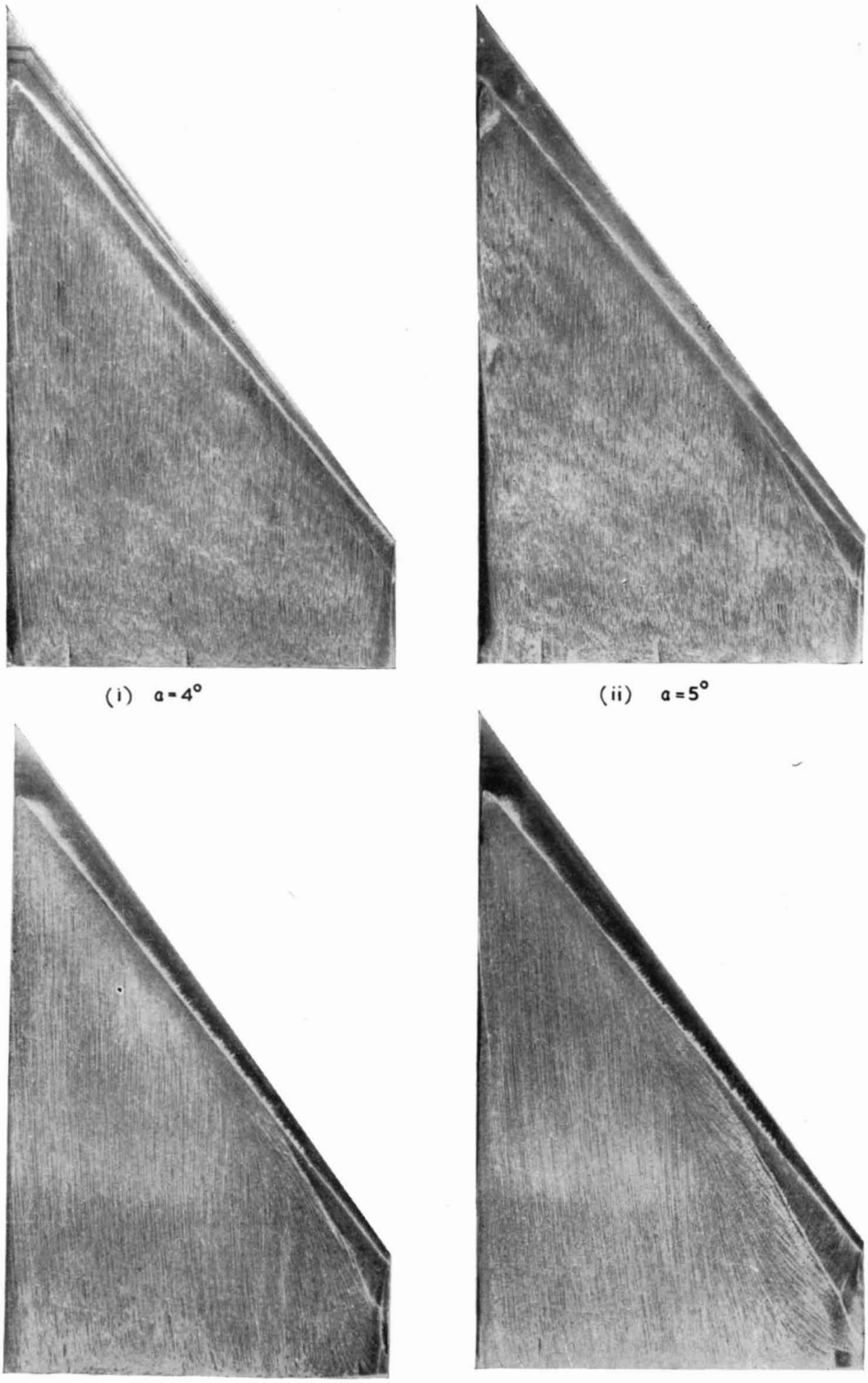

FIG. 4f. Oil-flow patterns on wing upper surface at $M_0 = 1{\cdot}11$.

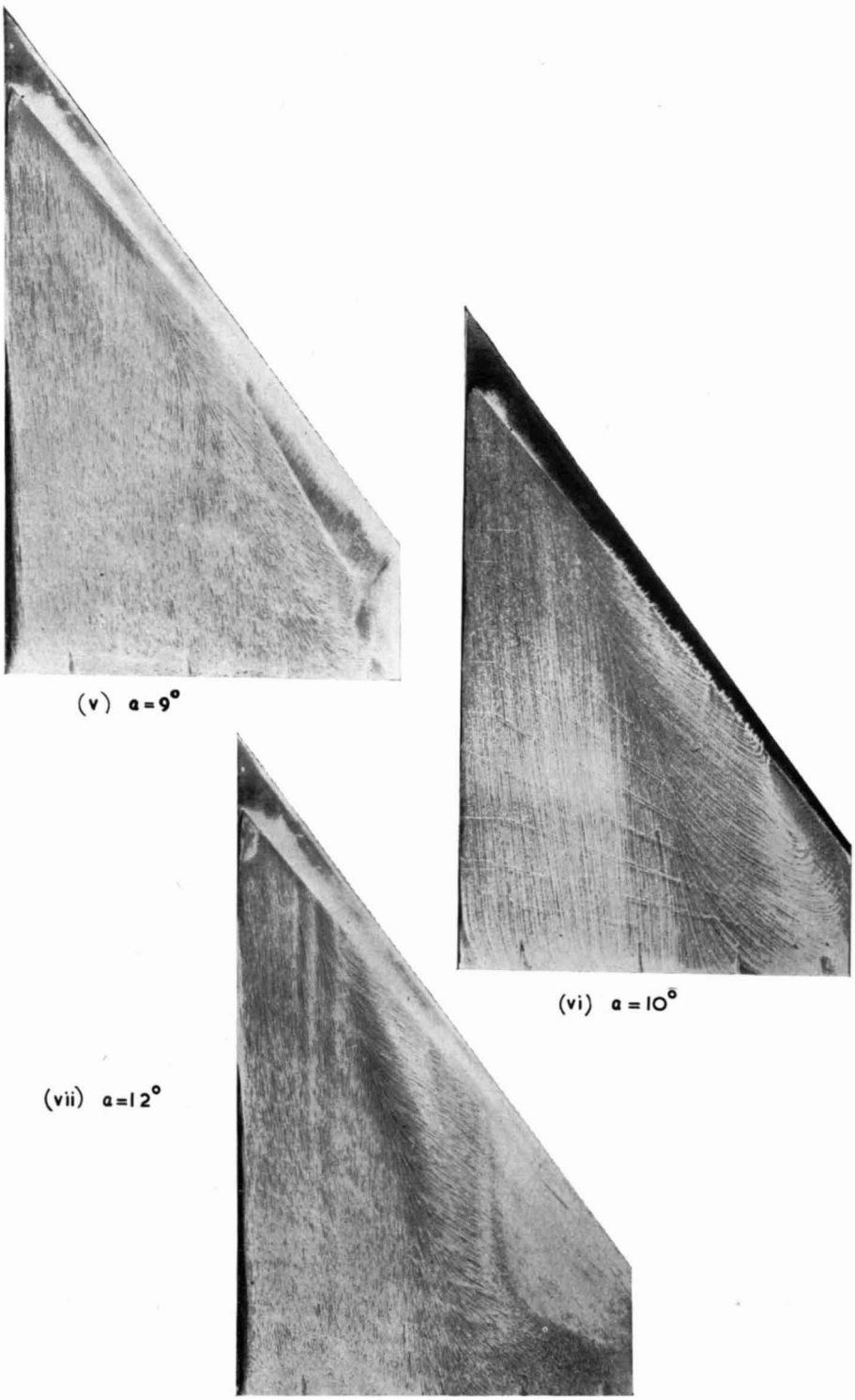

FIG. 4f (*cont.*). Oil-flow patterns on wing upper surface at $M_0 = 1{\cdot}11$.

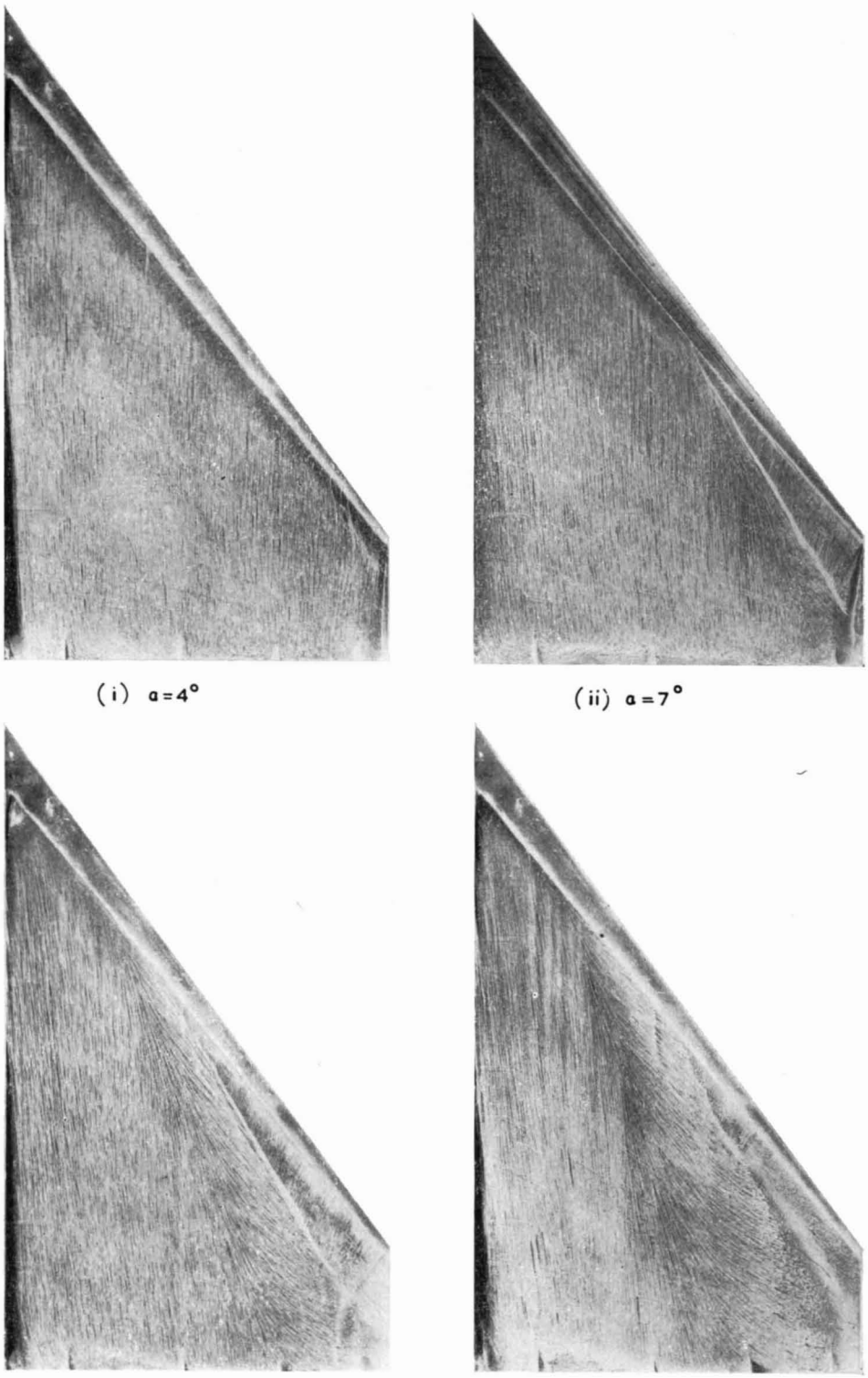

FIG. 4g. Oil-flow patterns on wing upper surface at $M_0 = 1{\cdot}16$.

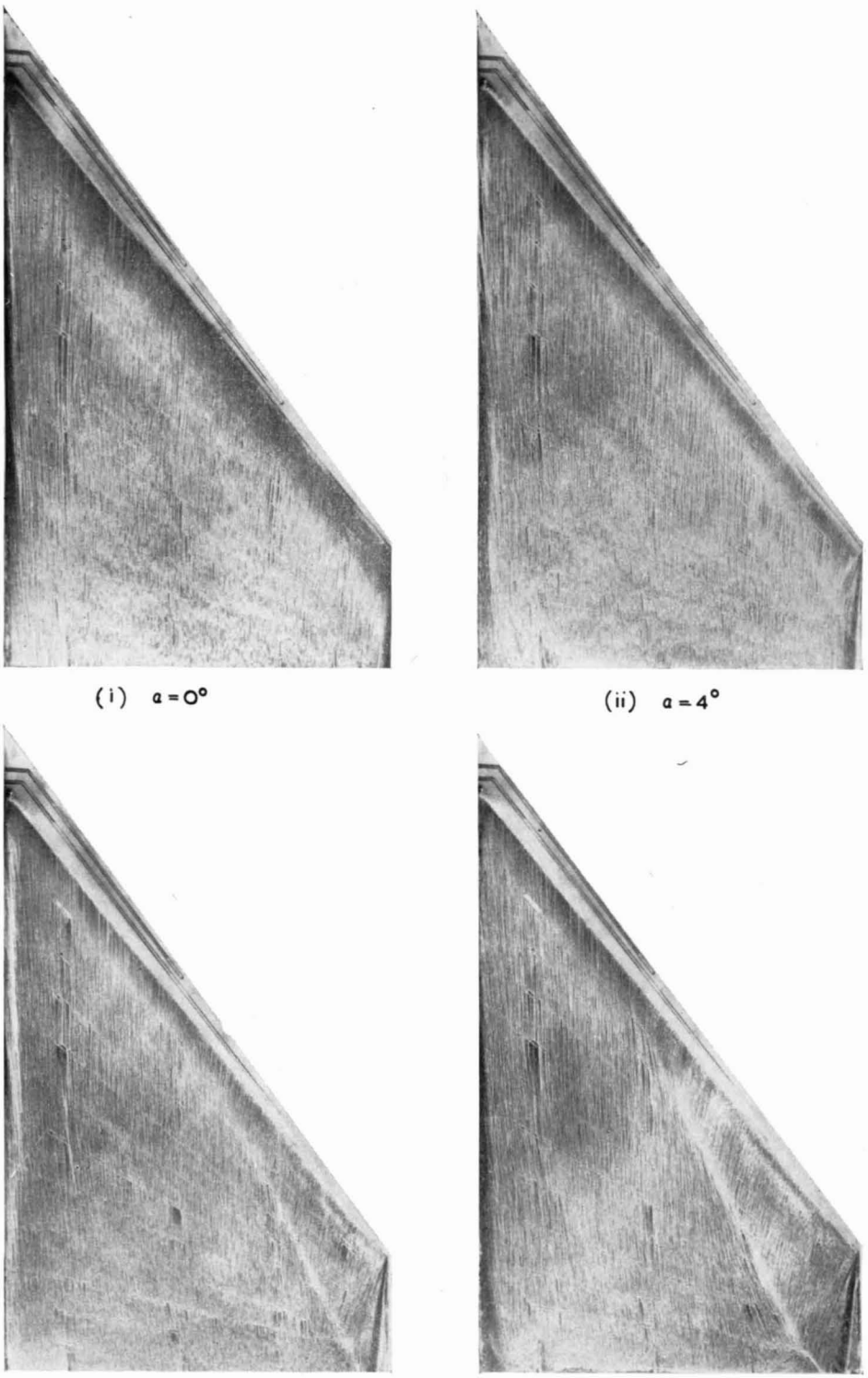

FIG. 4h. Oil-flow patterns on wing upper surface at $M_0 = 1{\cdot}41$.

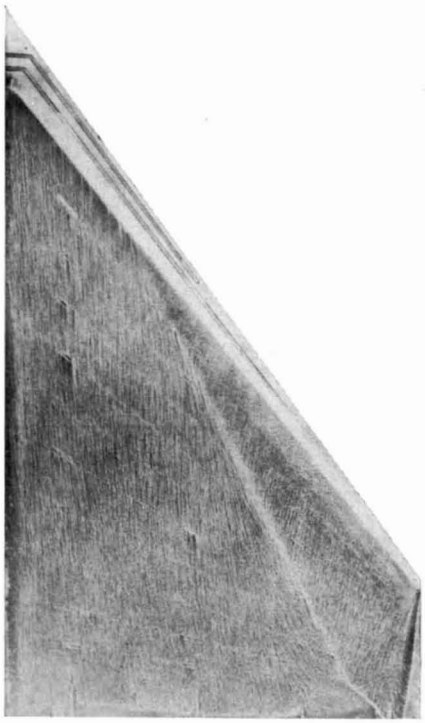

(v) $\alpha = 9°$

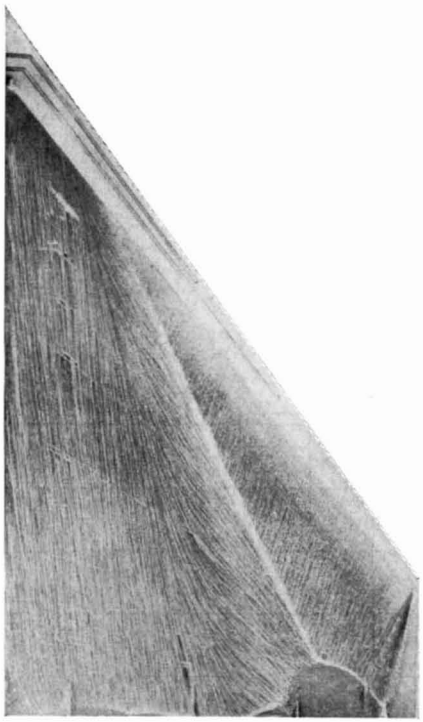

(vi) $\alpha = 13°$

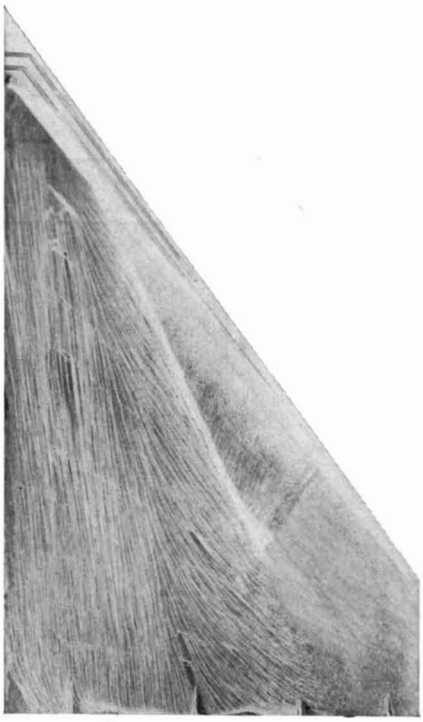

(vii) $\alpha = 14°$

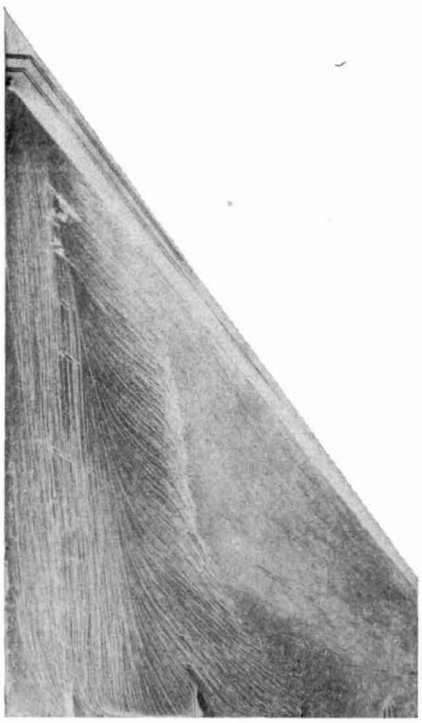

(viii) $\alpha = 16°$

FIG. 4h (*cont.*). Oil-flow patterns on wing upper surface at $M_0 = 1{\cdot}41$.

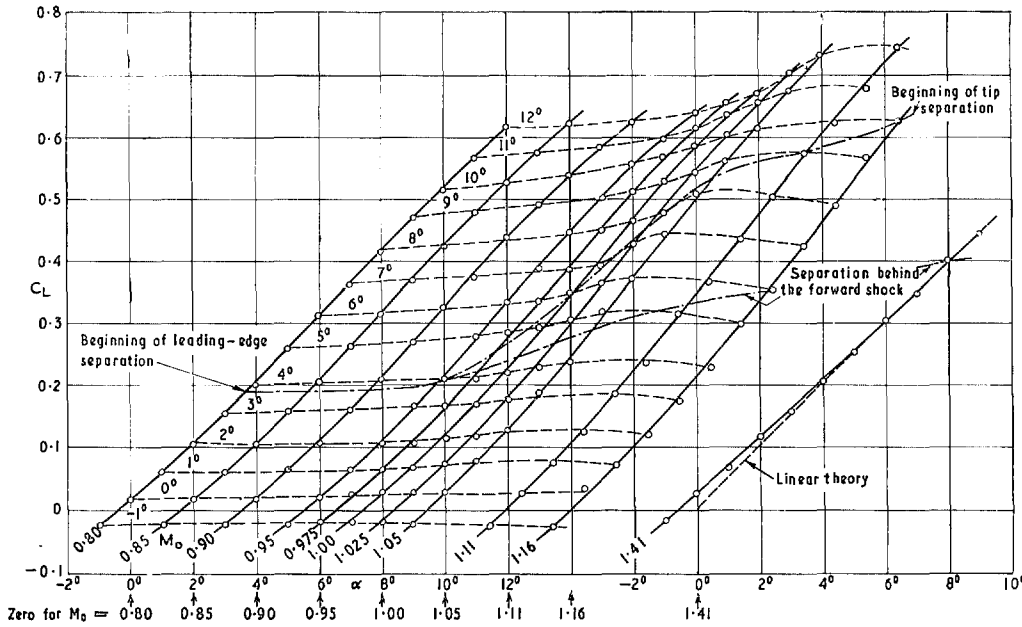

FIG. 5a. Lift results for cropped-delta half-wing (from balance tests).

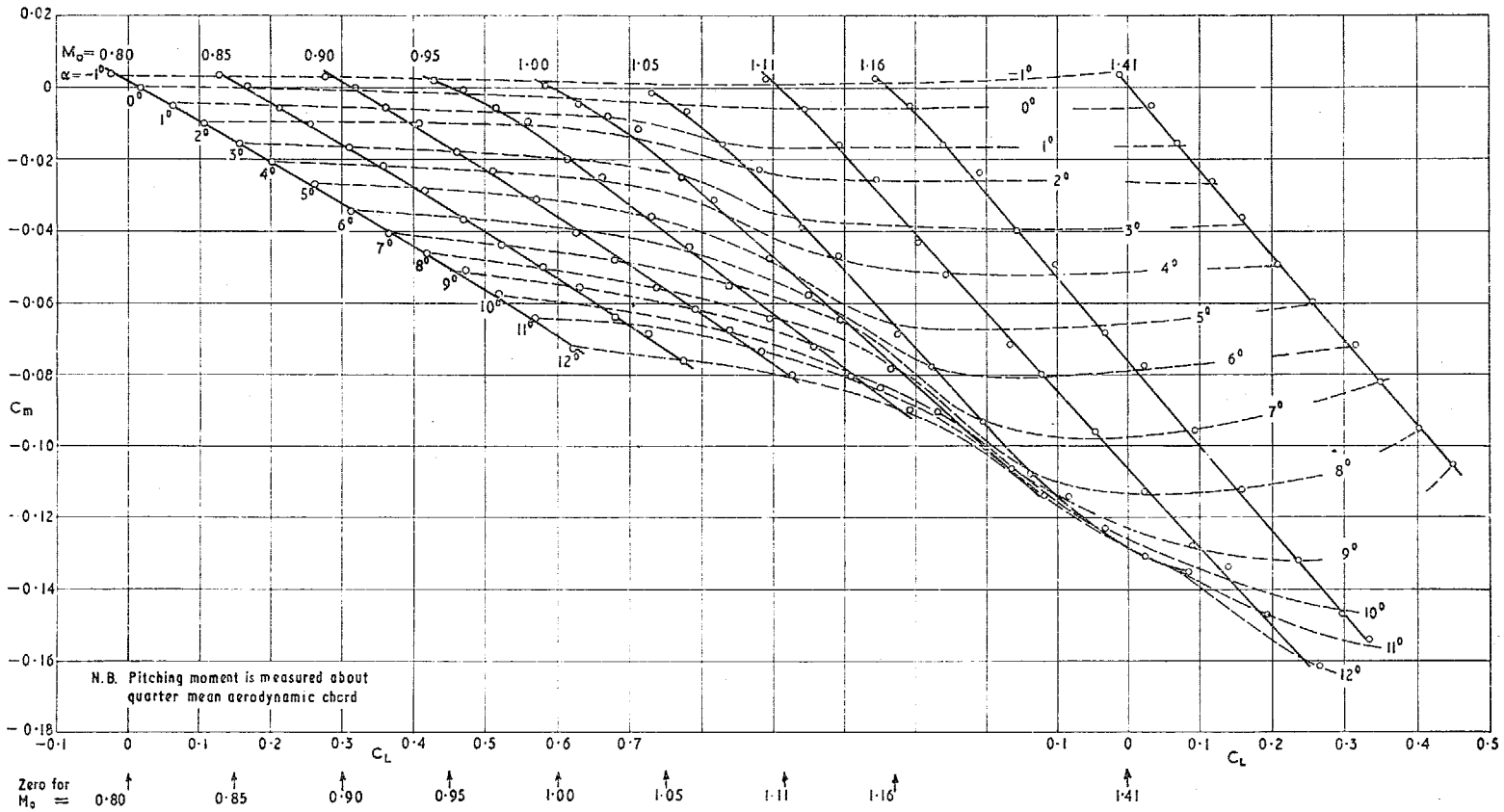

FIG. 5b. Pitching-moment results for cropped-delta half-wing (from balance tests).

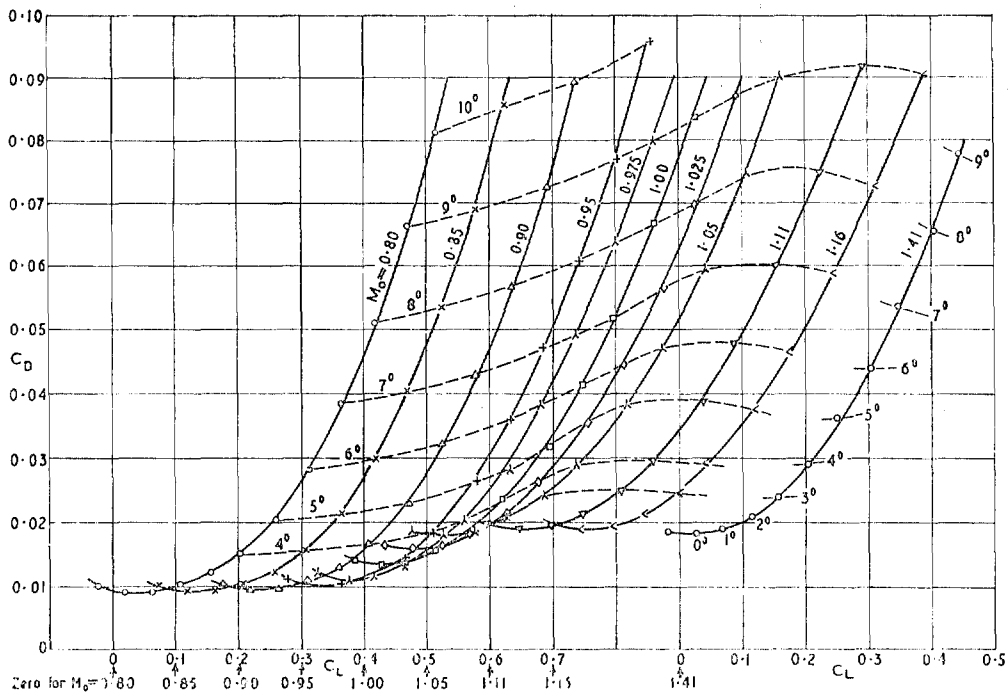

FIG. 5c. Drag polars for cropped-delta half-wing (from balance tests).

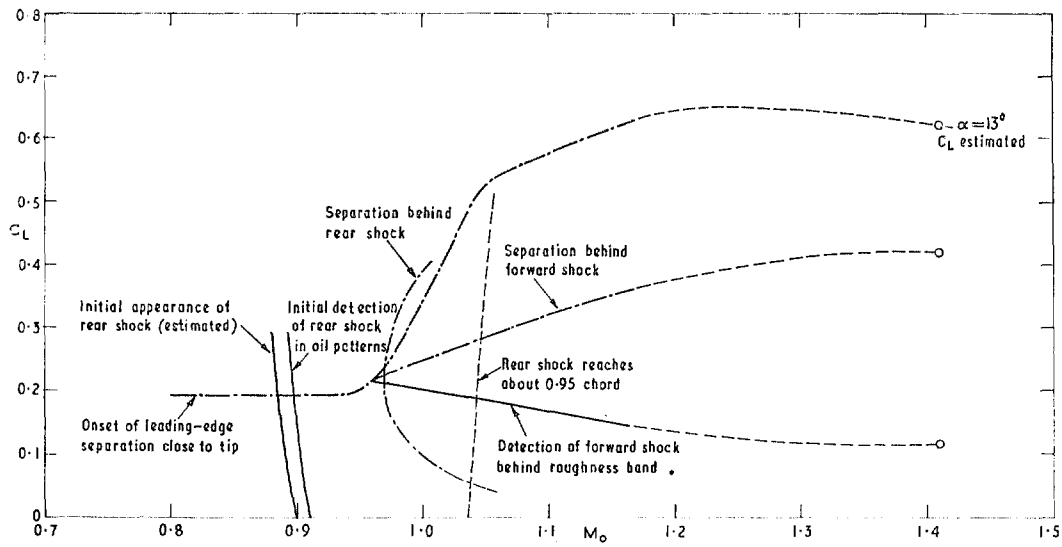

FIG. 5d. Approximate flow boundaries obtained from oil patterns.

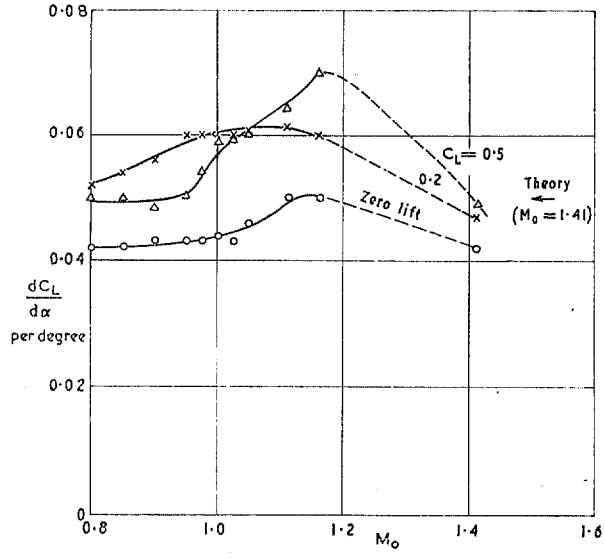

FIG. 6a. Approximate lift-curve slopes for cropped-delta half-wing.

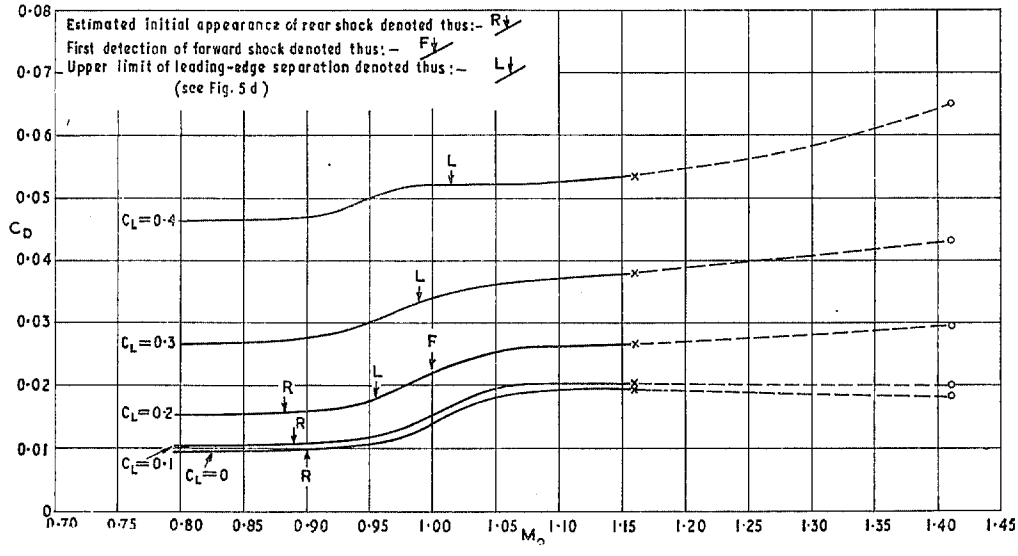

FIG. 6b. Variation of drag at constant lift.

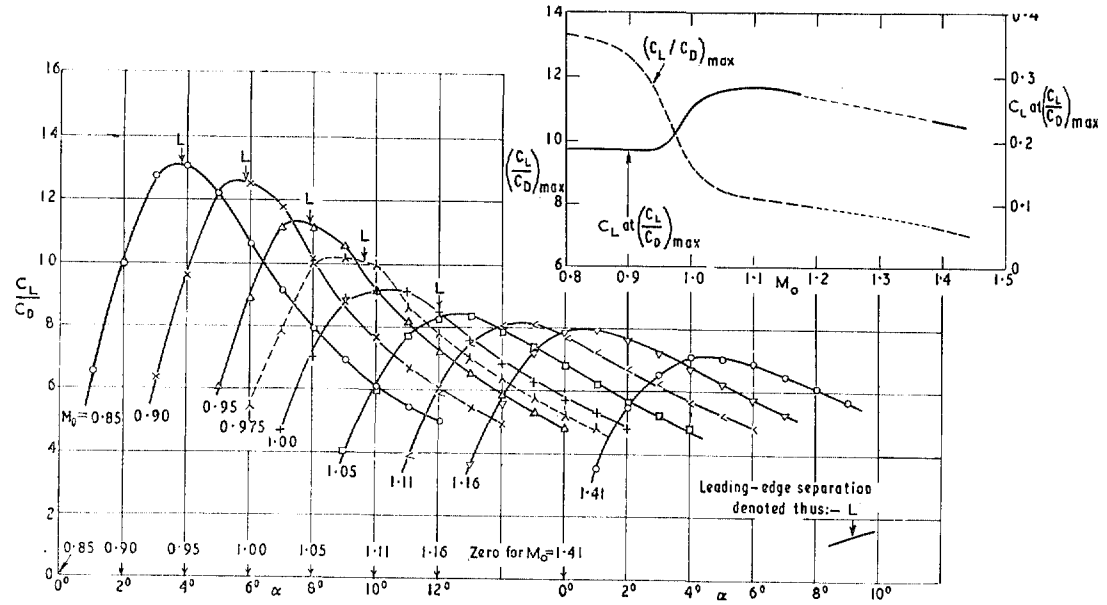

FIG. 6c. Variation of lift/drag ratio with stream Mach number.

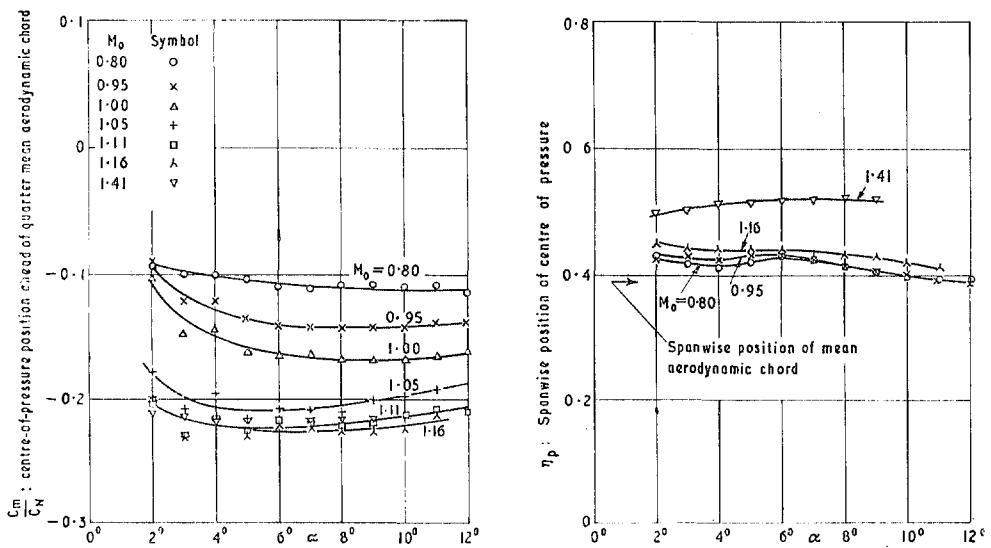

FIG. 6d. Chordwise and spanwise positions of centre of pressure for cropped half-wing.

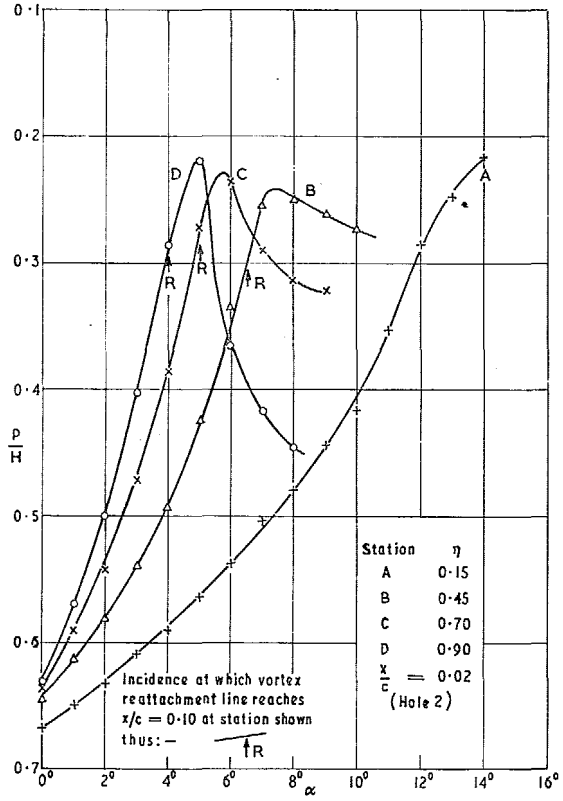

FIG. 7a. Pressure variation with incidence near leading edge at $M_0 = 0{\cdot}80$.

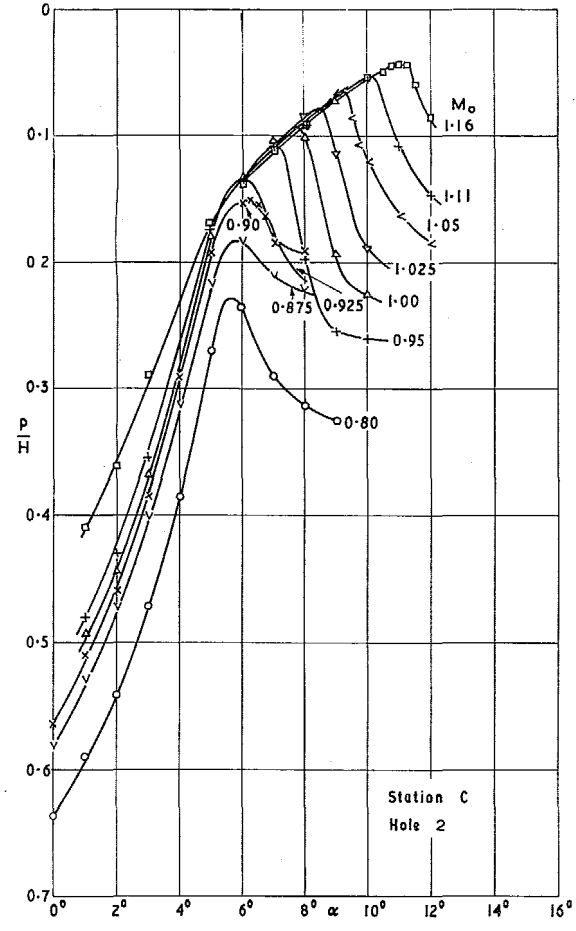

FIG. 7b. Pressure variation with incidence and M_0 at $(x/c) = 0{\cdot}02$, $\eta = 0{\cdot}70$.

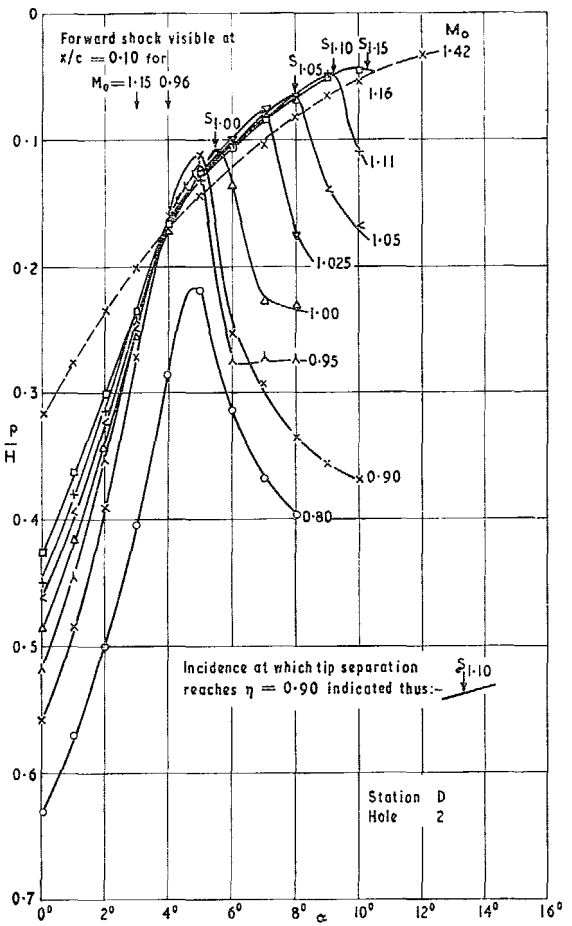

FIG. 7c. Pressure variation with incidence and M_0 at $(x/c) = 0{\cdot}02$, $\eta = 0{\cdot}90$.

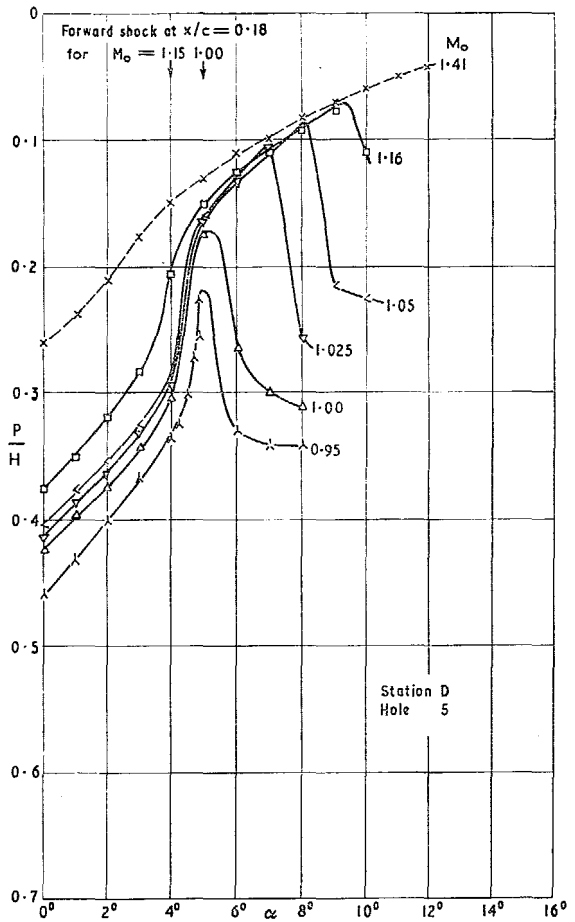

FIG. 7d. Pressure variation with incidence at M_0 at $(x/c) = 0{\cdot}18$, $\eta = 0{\cdot}90$.

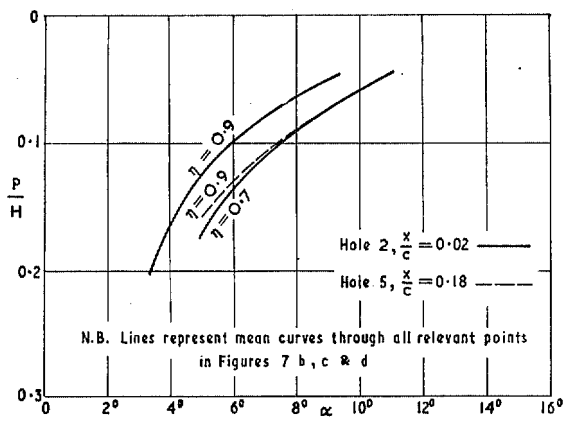

FIG. 8a. Approximate form of transonic pressure freeze curves suggested by Figures 7b, c and d.

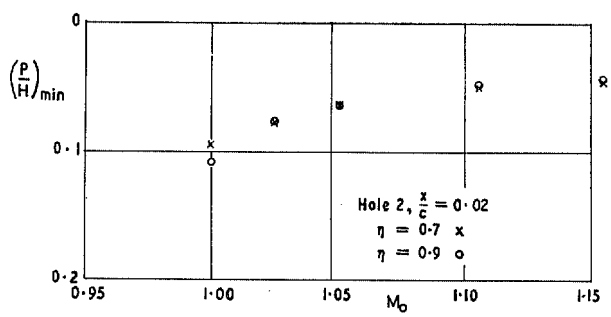

FIG. 8b. Minimum pressure observed at $(x/c) = 0{\cdot}02$ at two spanwise stations (*see* Figures 7b and c).

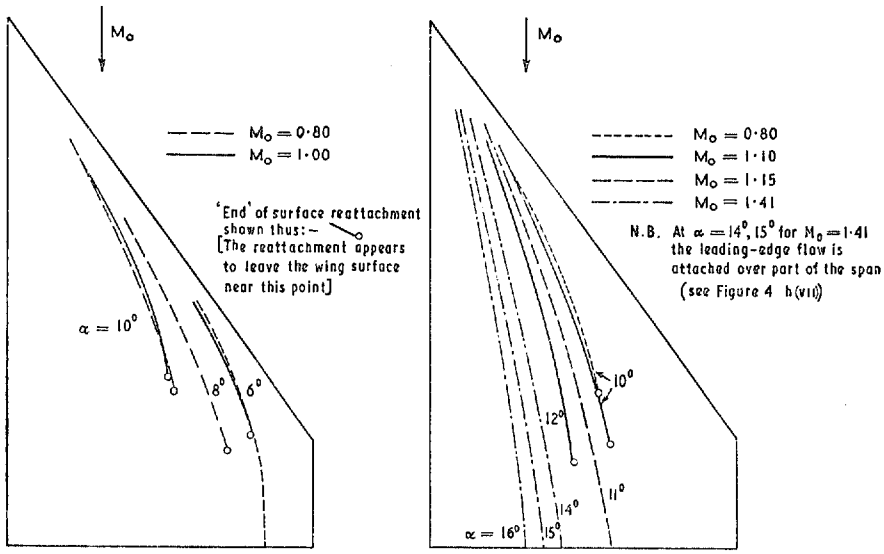

FIG. 9a. Variation of reattachment line with incidence and Mach number.

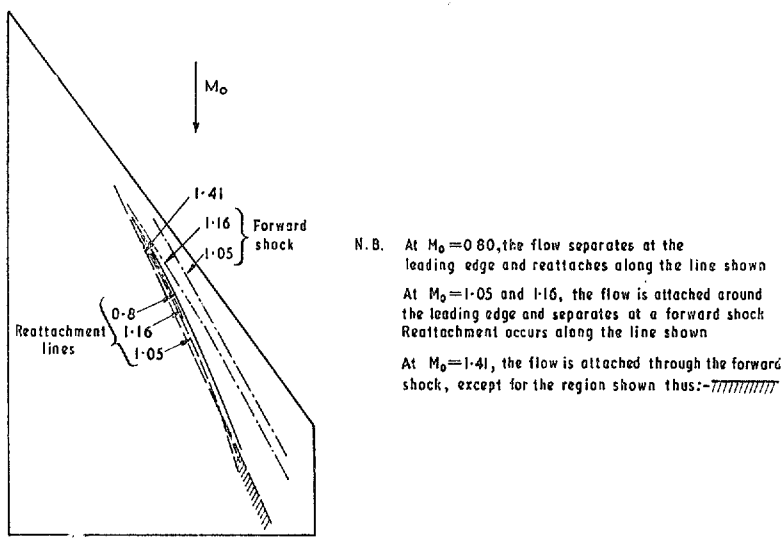

FIG. 9b. Reattachment-line positions at $\alpha = 8$ deg with and without leading-edge separation.

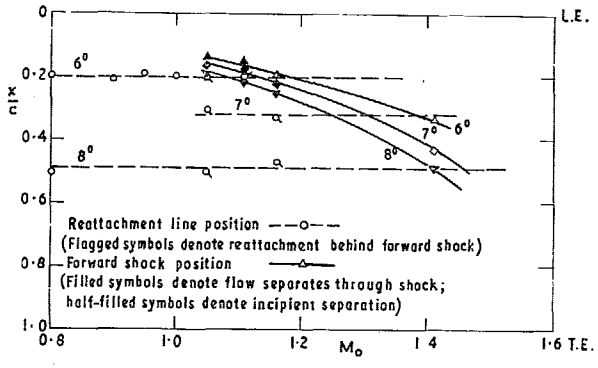

FIG. 10a. Reattachment-line position in relation to forward shock at $\eta = 0{\cdot}7$.

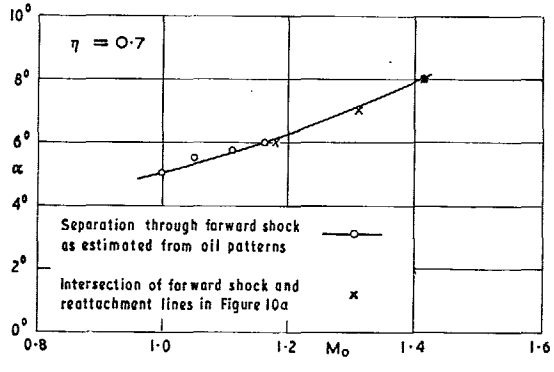

FIG. 10b. Separation through the forward shock and its apparent correlation with relative positions of the shock and the reattachment line.

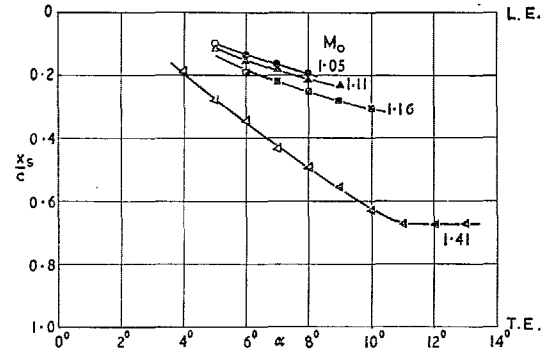

(a) $\eta = 0{\cdot}7$, Station C

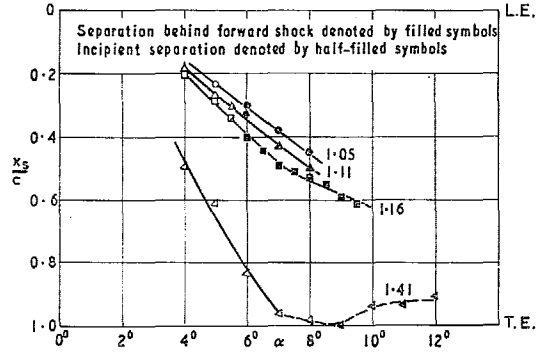

(b) $\eta = 0{\cdot}9$, Station D

FIGS. 11a and b. Chordwise position of forward shock at two spanwise stations.

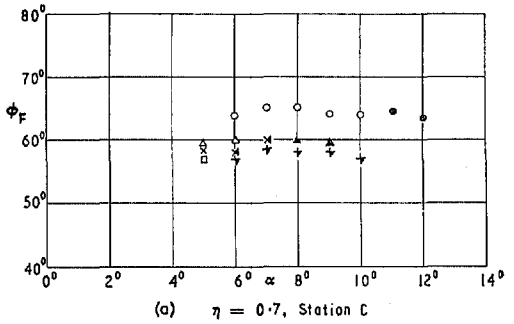

(a) $\eta = 0{\cdot}7$, Station C

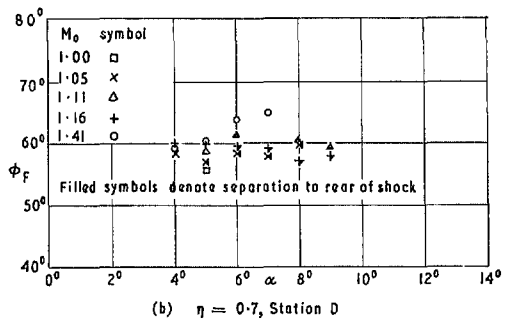

(b) $\eta = 0{\cdot}7$, Station D

FIGS. 12a and b. Geometric sweep of forward shock at two spanwise stations.

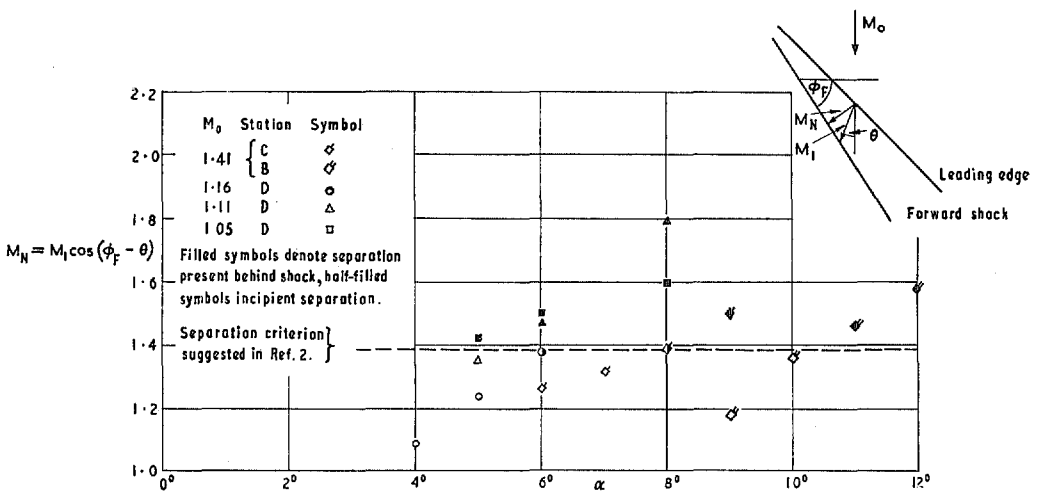

FIG. 13. Separation conditions for forward shock at various spanwise stations.

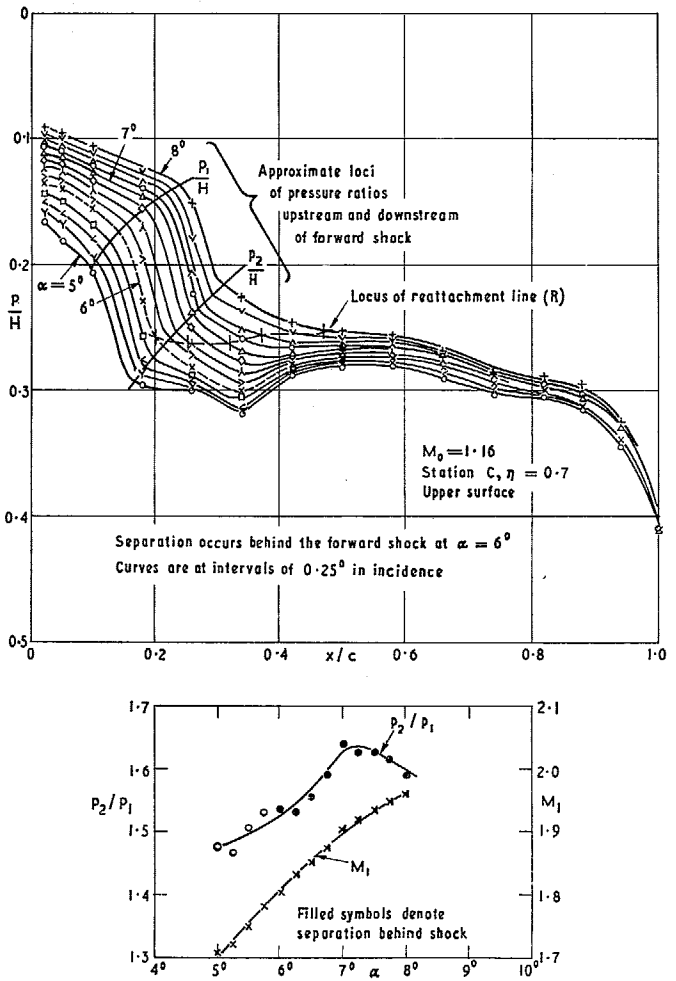

FIG. 14. Chordwise pressure distributions near condition of flow separation at forward shock.

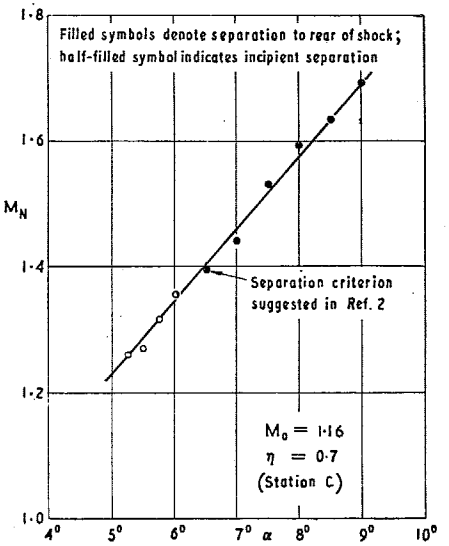

FIG. 15. Mach number normal to forward shock through separation condition.

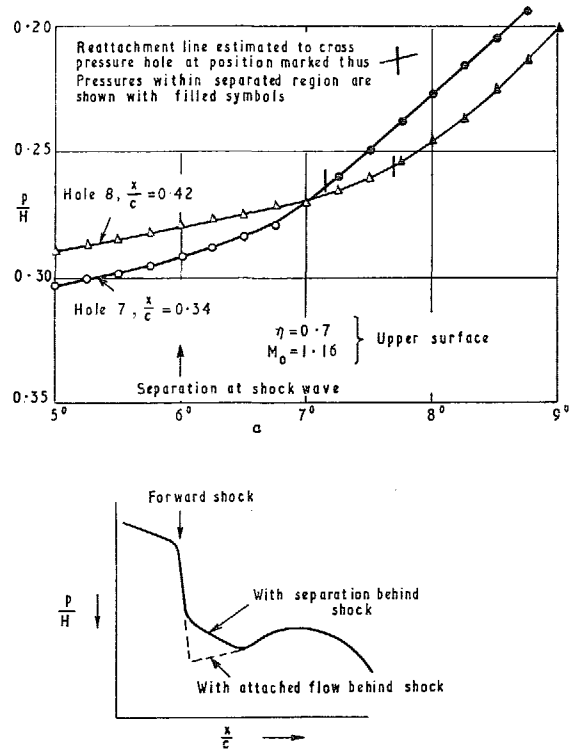

FIG. 16. Surface pressure development in region beneath vortex associated with forward-shock separation.

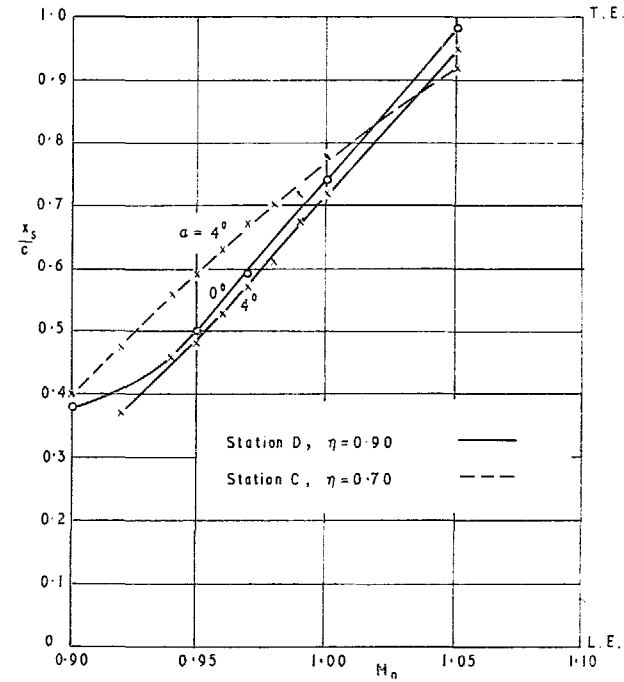

FIG. 17. Position of rear shock at two outboard stations.

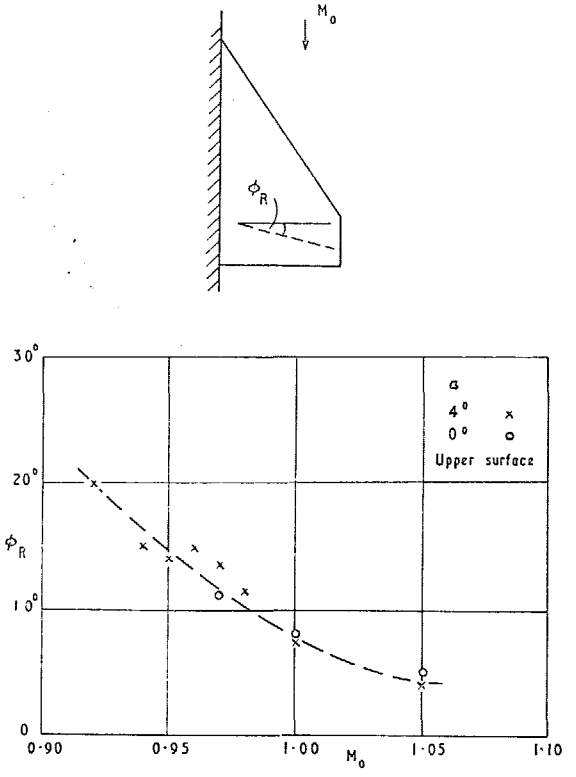

FIG. 18. Geometric sweep of rear shock between 0·7 and 0·9 semi-span.

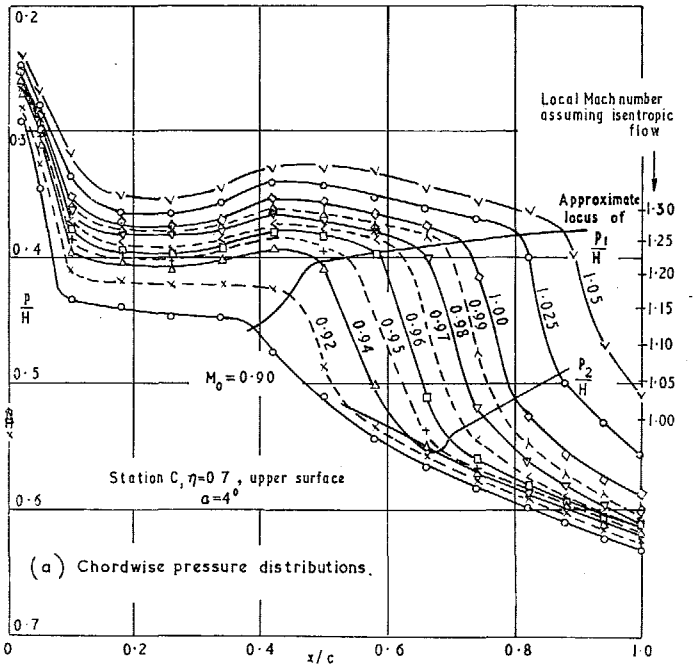

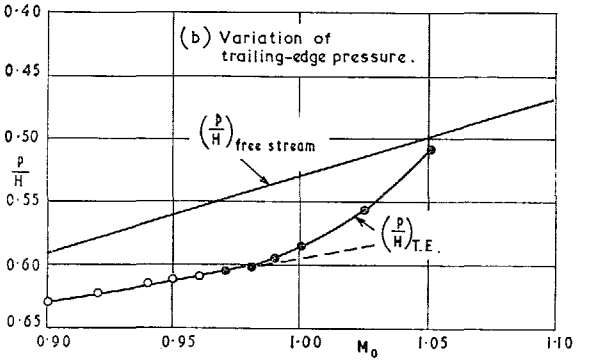

FIGS. 19a and b. Development of separation at rear shock. Filled symbols denote presence of separation.

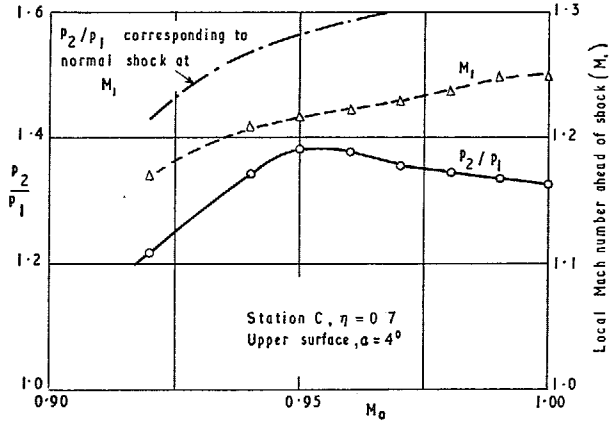

FIG. 19c. Variation of shock pressure ratio and upstream local Mach number with stream Mach number through separation condition. Filled symbols denote separation detected on wing surface.

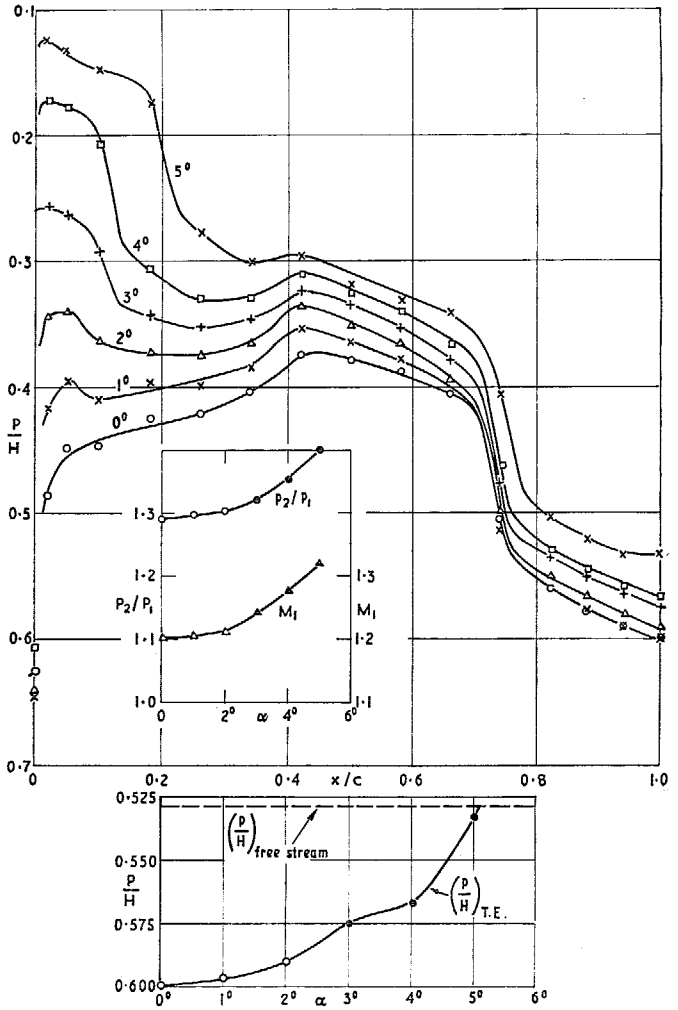

FIG. 20. Development of separation at rear shock (station D, $M_0 = 1{\cdot}00$, upper surface). Filled symbols denote presence of separation.

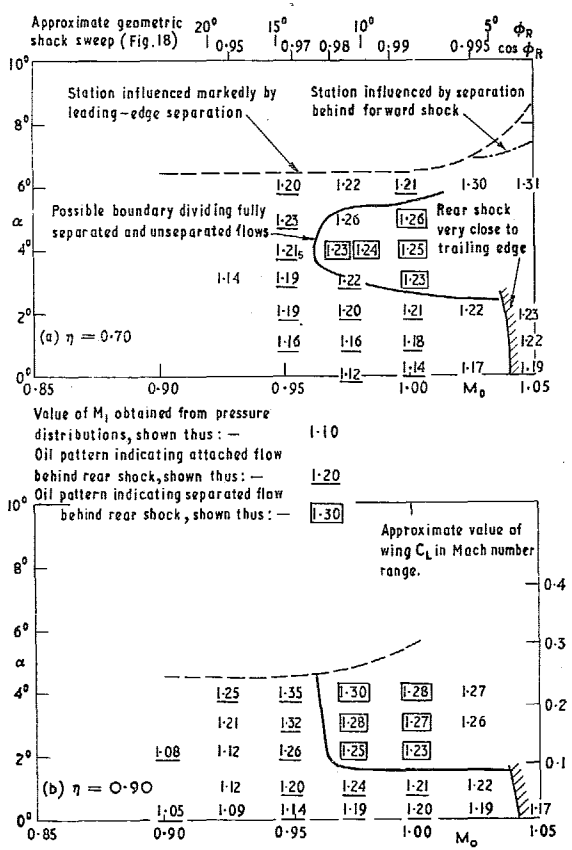

FIG. 21. Diagrams of relationship between Mach number ahead of rear shock and flow separation.

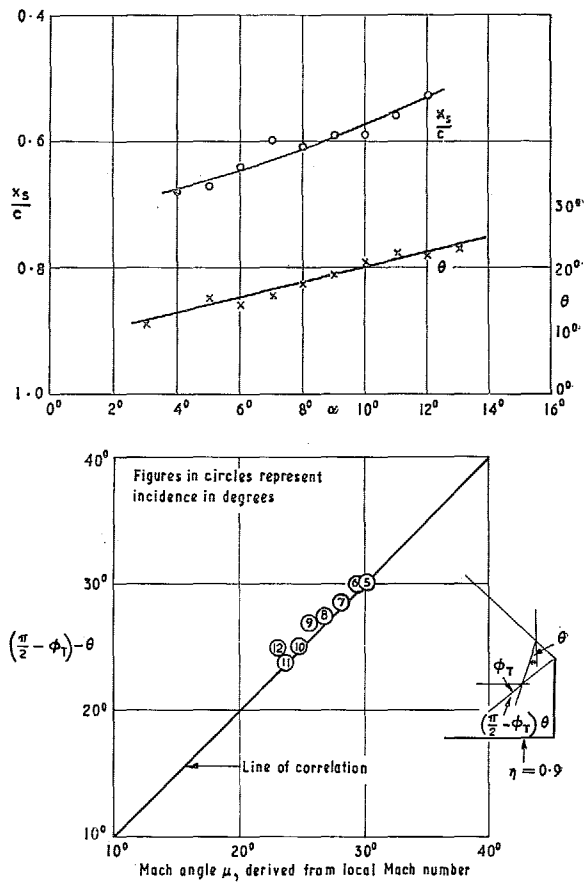

FIG. 22. Tip-shock characteristics at $M_0 = 1{\cdot}41$ for station D ($\eta = 0{\cdot}9$).

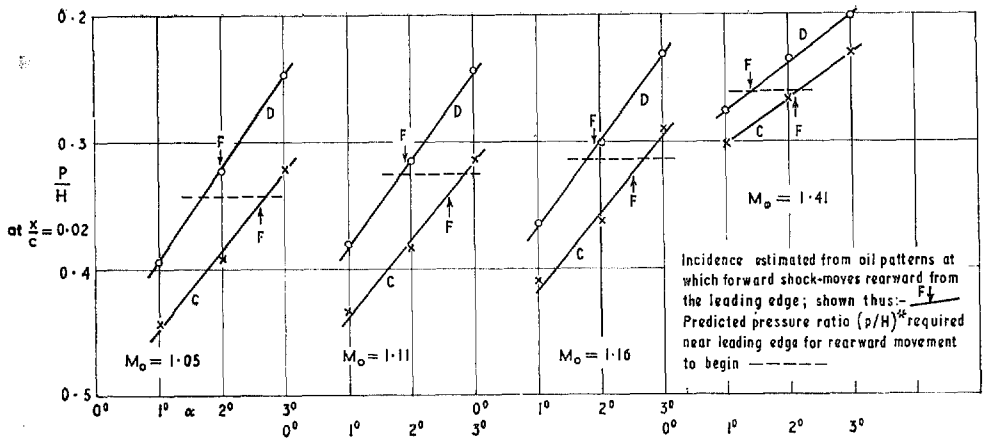

FIG. 23a. Estimation of critical incidence for rearward movement of forward shock.

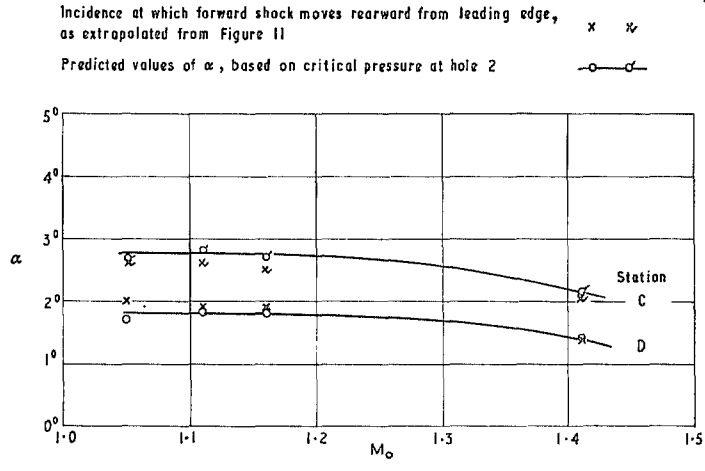

FIG. 23b. Comparison of theoretical and experimental values of critical wing incidence for rearward movement of forward shock.

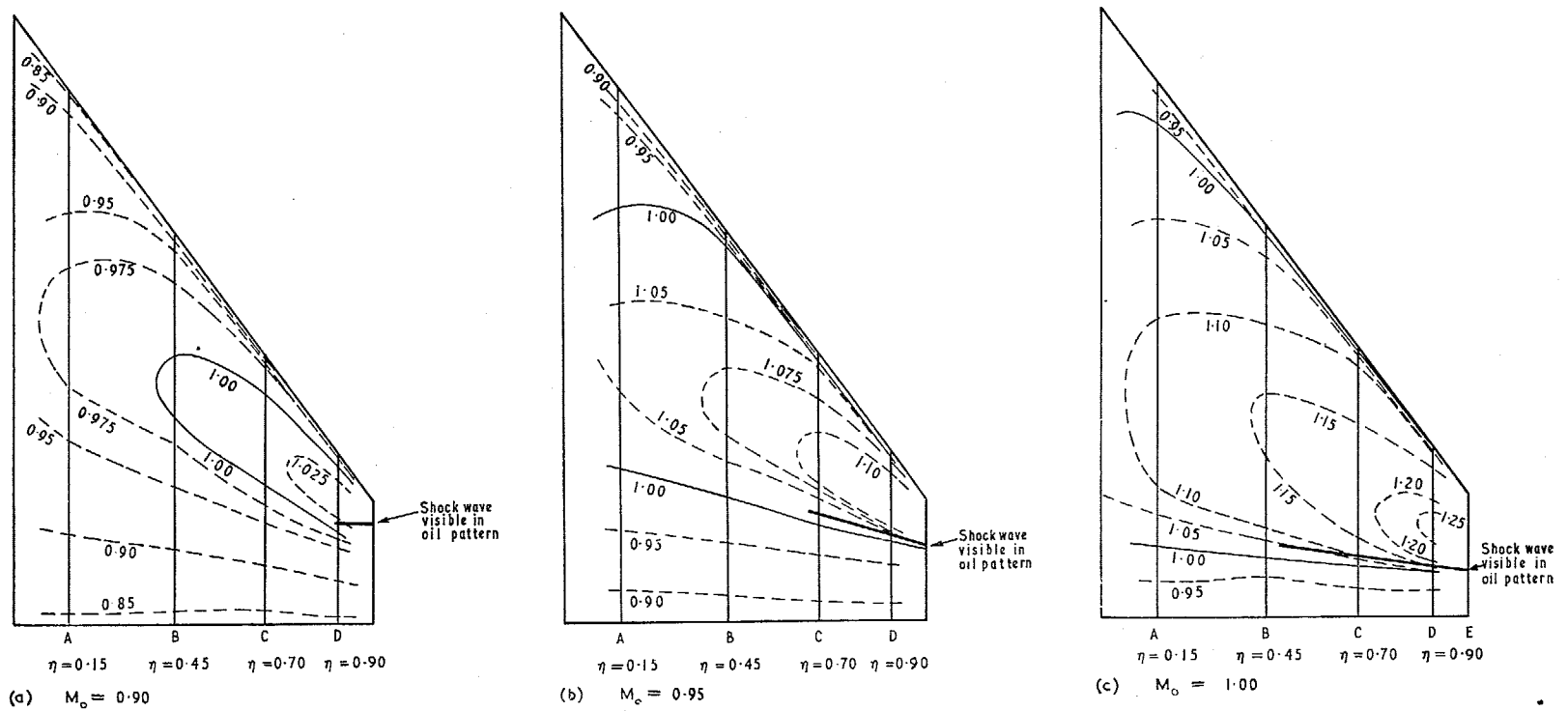

FIG. 24. Isobar patterns at $\alpha = 0$ deg, showing local Mach numbers on wing surface.

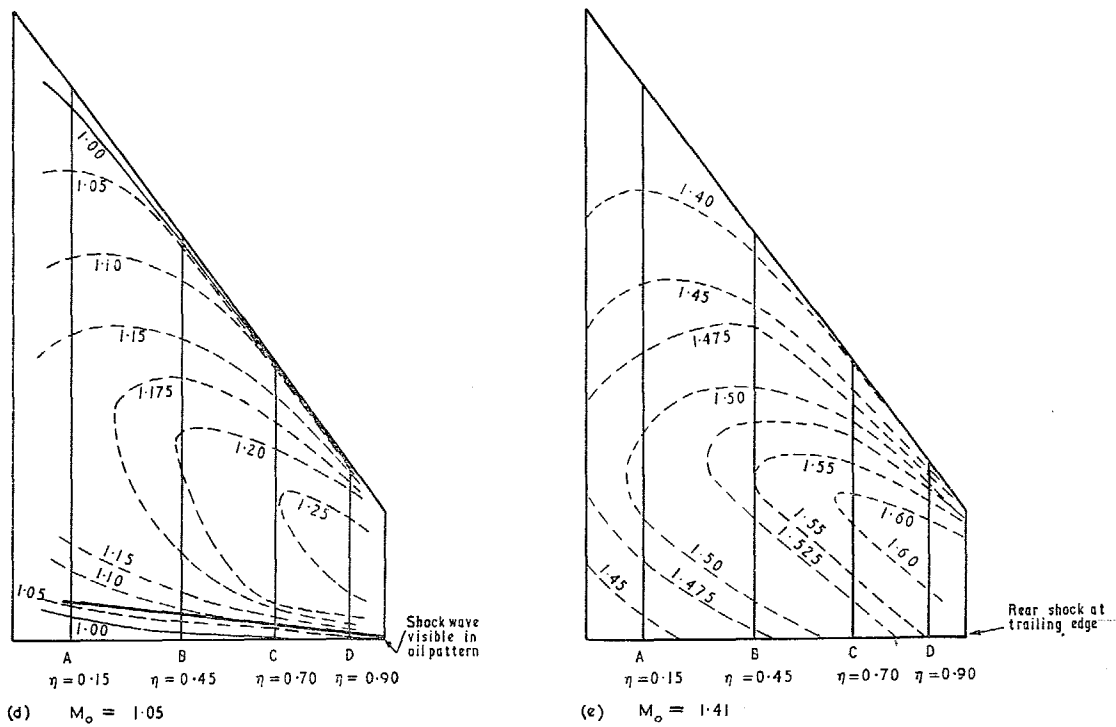

FIG. 24 (*cont.*). Isobar patterns at $\alpha = 0$ deg, showing local Mach numbers on wing surface.

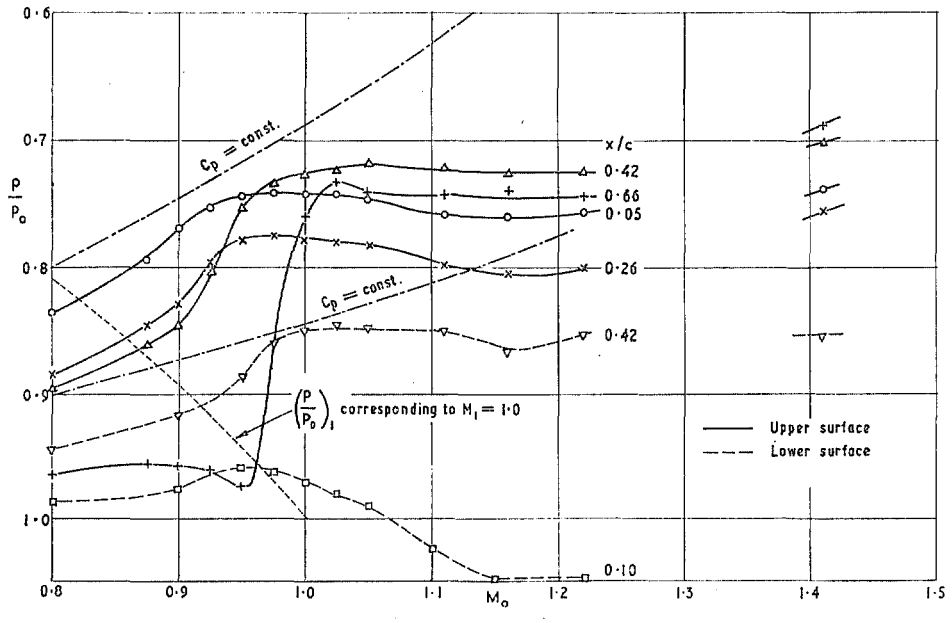

FIG. 25. Variation of pressure ratio p/p_0 with M_0 at various chordwise stations ($\alpha = 2$ deg, $\eta = 0{\cdot}7$).

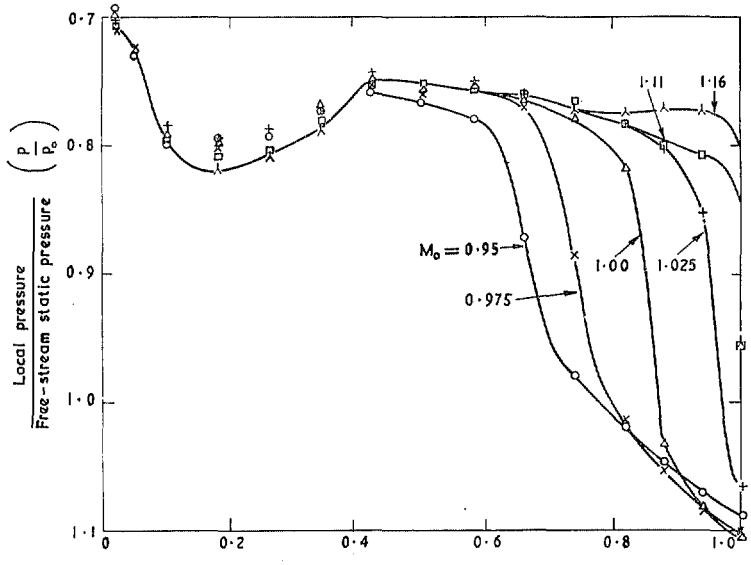

FIG. 26a. Upper-surface pressure distributions at $\alpha = 4$ deg, $\eta = 0{\cdot}70$.

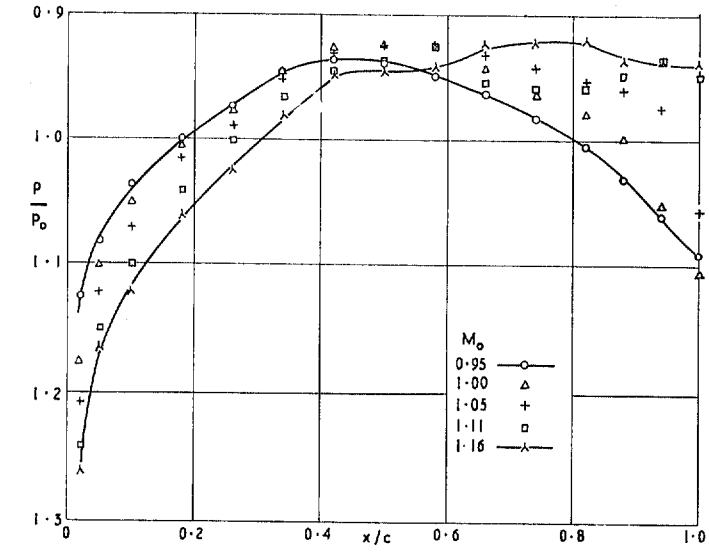

FIG. 26b. Lower-surface pressure distribution at $\alpha = 4$ deg, $\eta = 0{\cdot}70$.

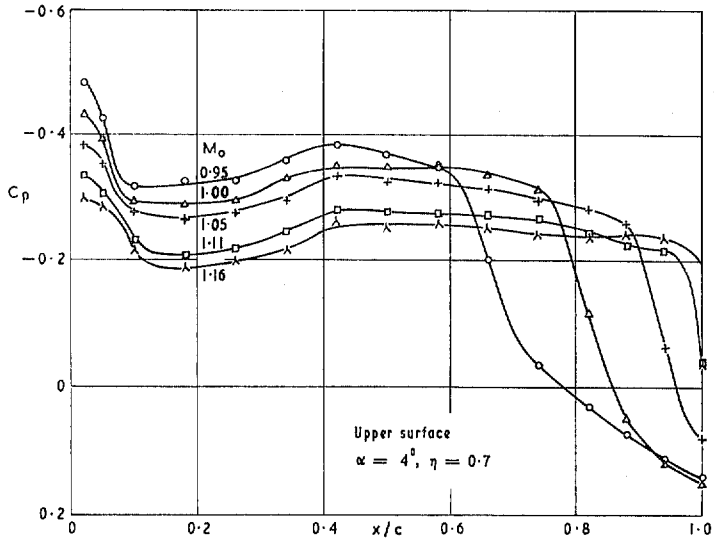

FIG. 26c. Pressure distributions of Figure 24a, plotted in terms of *Cp*.

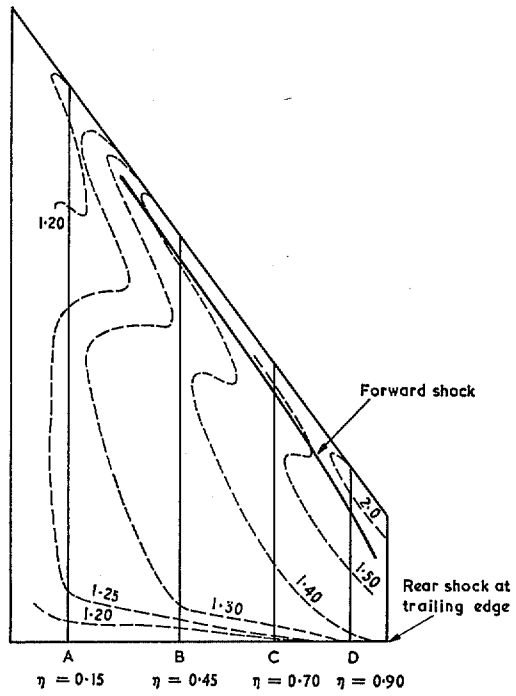

FIG. 27. Isobar pattern on wing upper surface at $M_0 = 1{\cdot}11$, $\alpha = 6$ deg showing local Mach numbers.

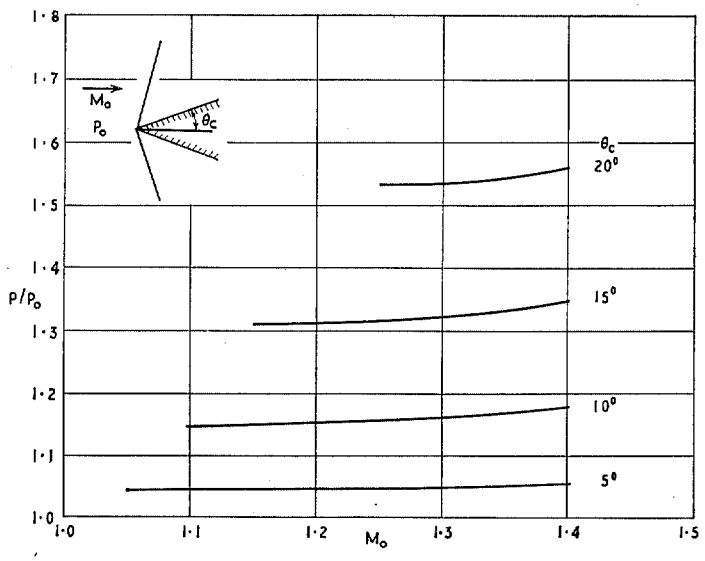

FIG. 28. Variation of parameter p/p_0 in conical flow about slender cones at low supersonic speeds.

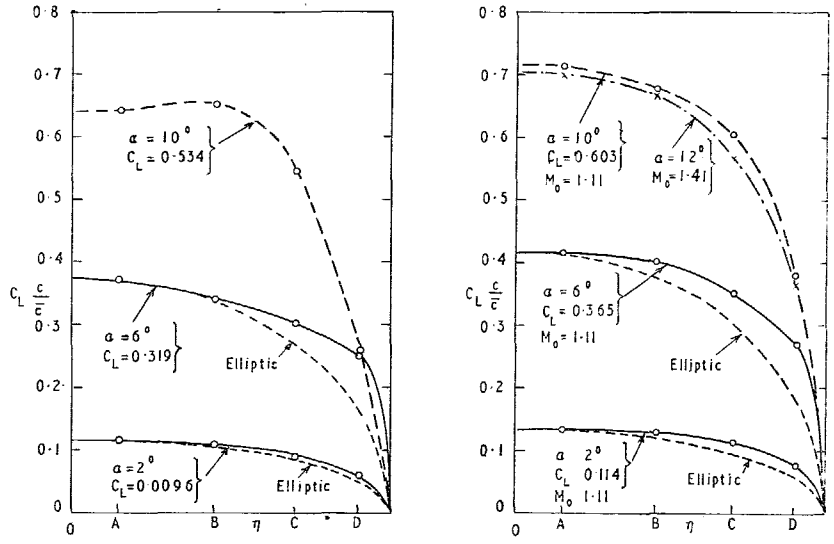

(a) $M_0 = 0·90$ (b) $M_0 = 1·11$ and $1·41$

FIG. 29. Typical spanwise loading curves.

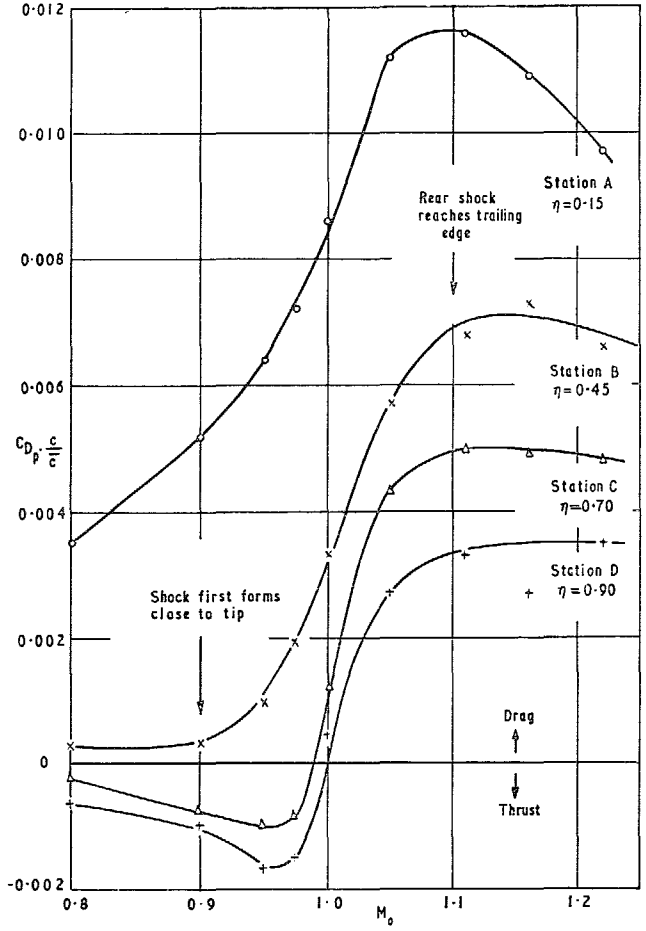

FIG. 30. Local section pressure-drag coefficients at zero incidence.

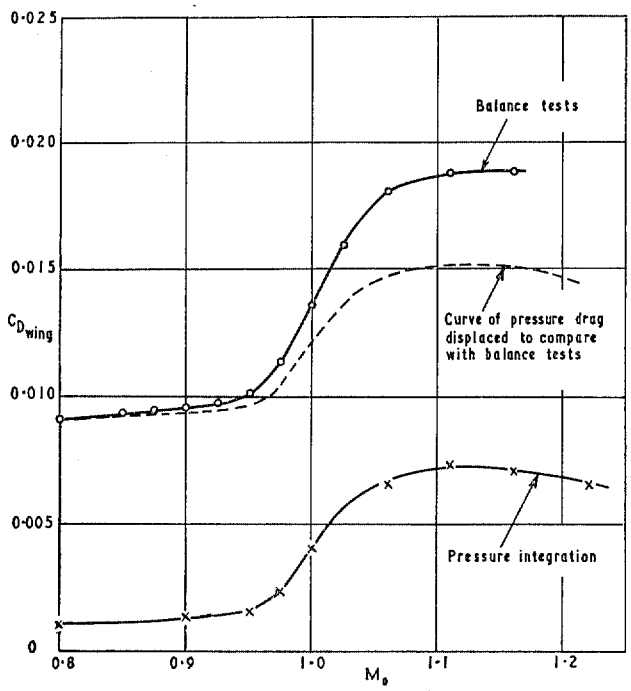

FIG. 31. Comparison of zero-lift drag obtained from balance measurements and by integration of the chordwise pressure distributions.

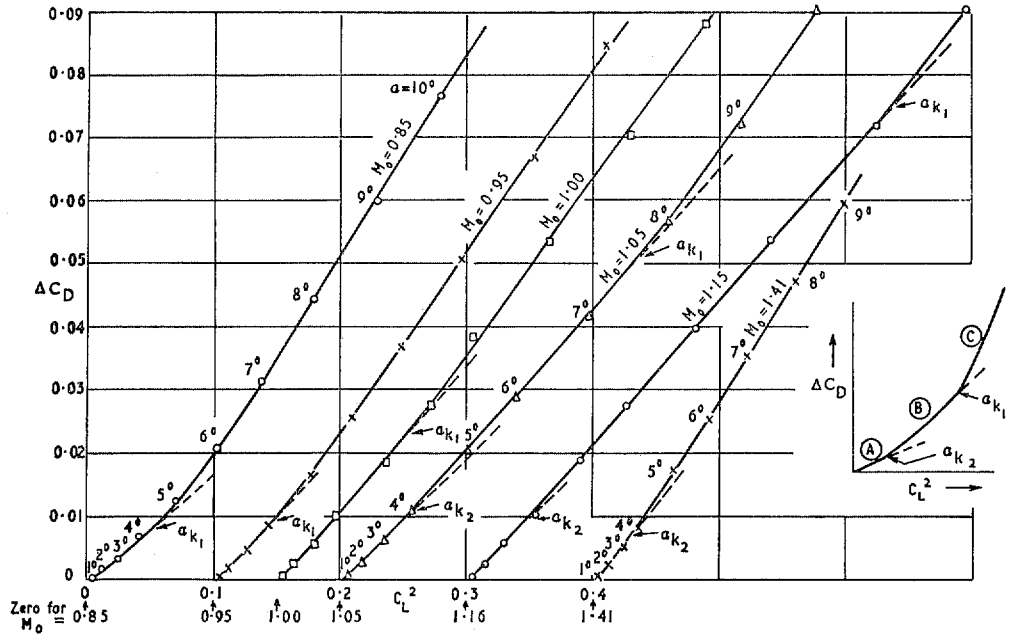

FIG. 32. Lift-dependent drag curves at various stream Mach numbers.

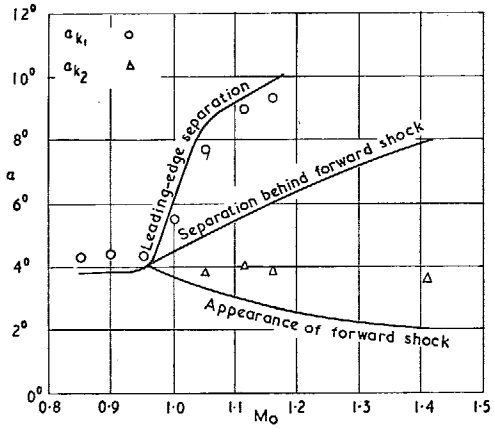

FIG. 33. Relationship between kink incidences and flow-events.

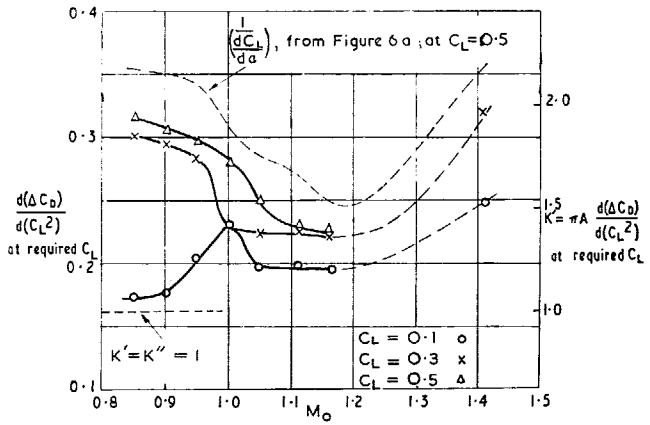

FIG. 34a. Lift-dependent drag-curve slope at specified values of C_L.

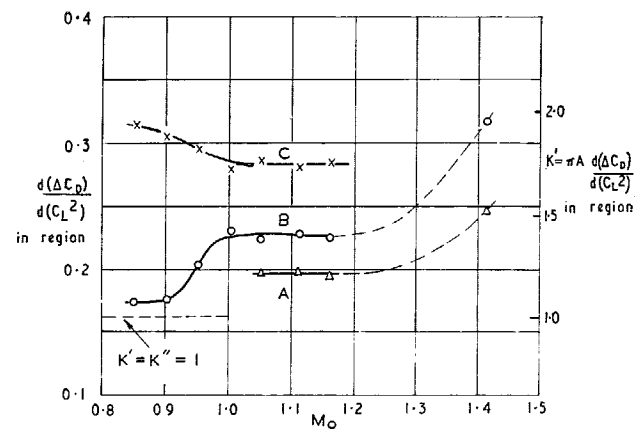

FIG. 34b. Lift-dependent drag-curve slope in the three regions of Figure 32.

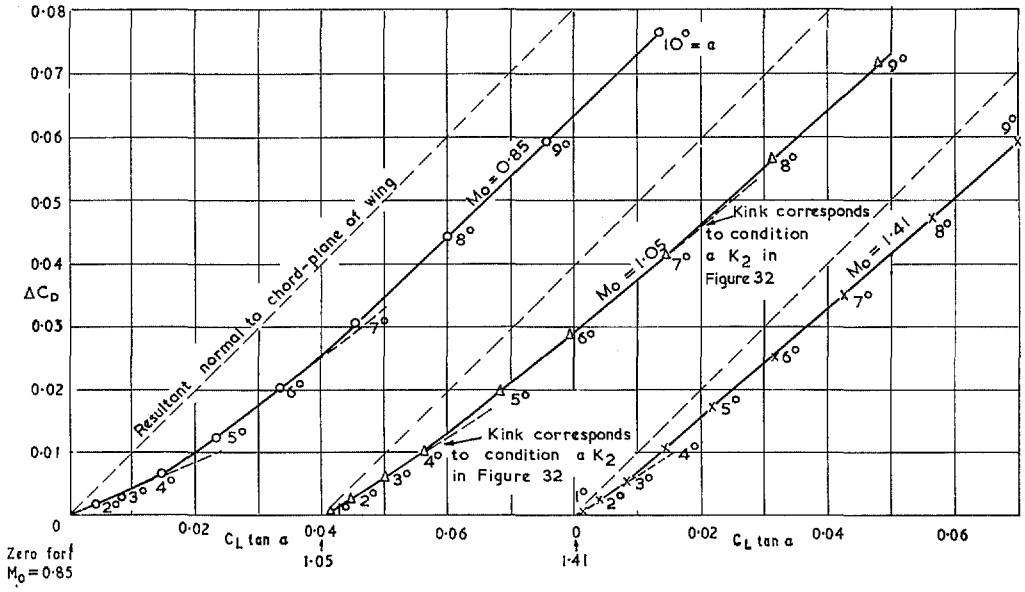

FIG. 35. Alternative analysis of lift-dependent drag.

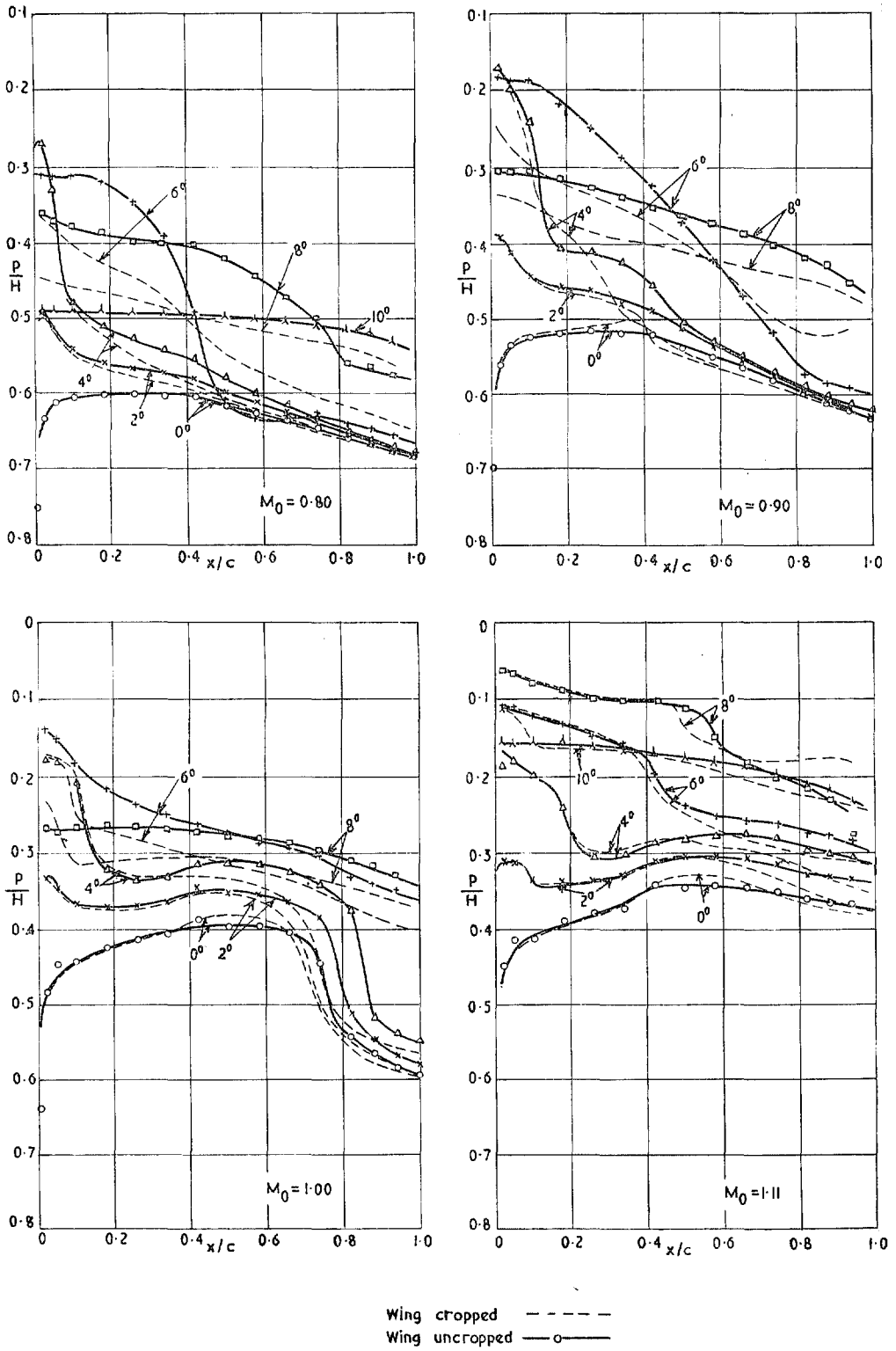

FIG. 36. Comparison of pressures at station D in cropped and uncropped states.

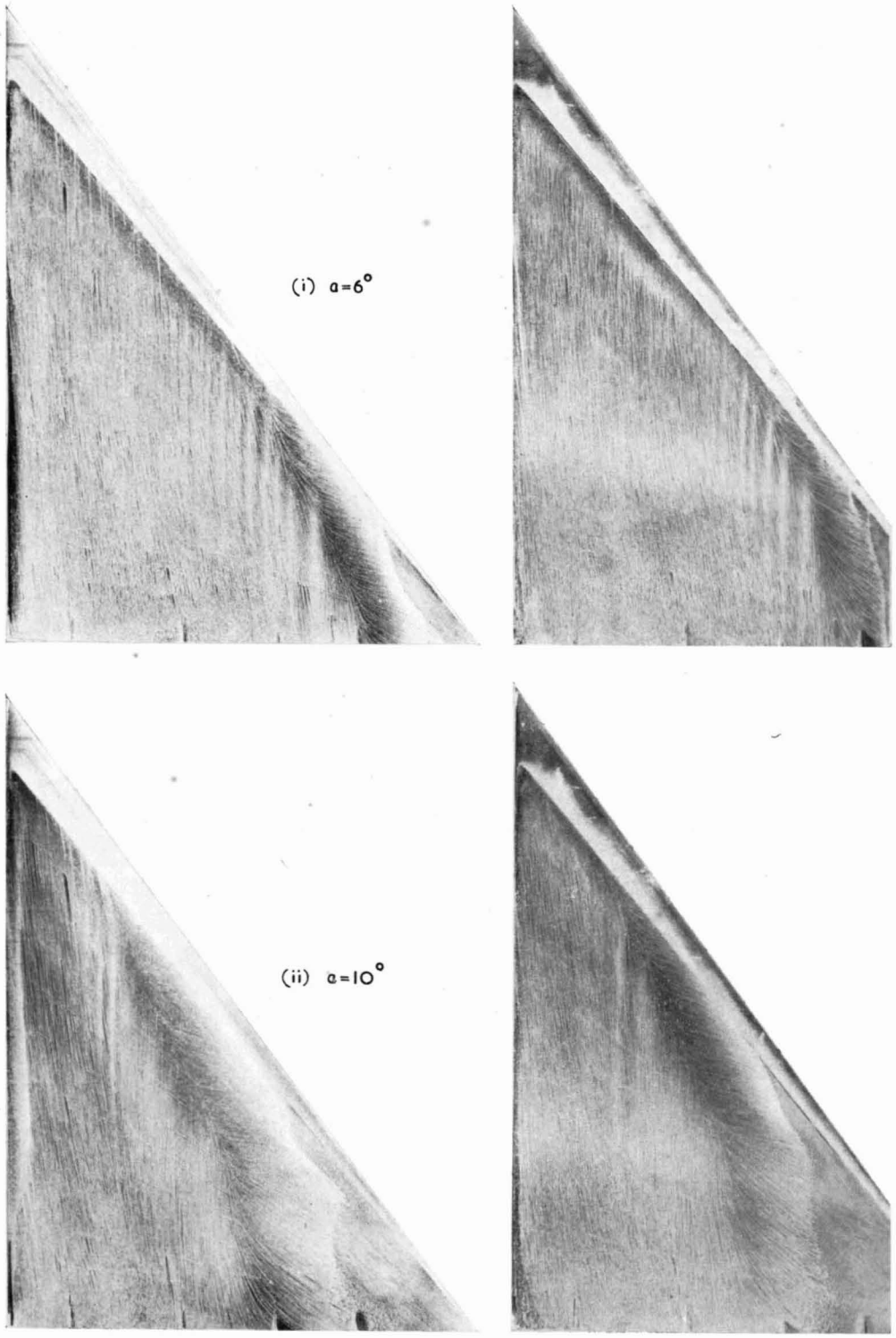

FIG. 37a. Comparison of upper-surface oil-flow patterns before and after cropping: $M_0 = 0{\cdot}80$.

(85536)

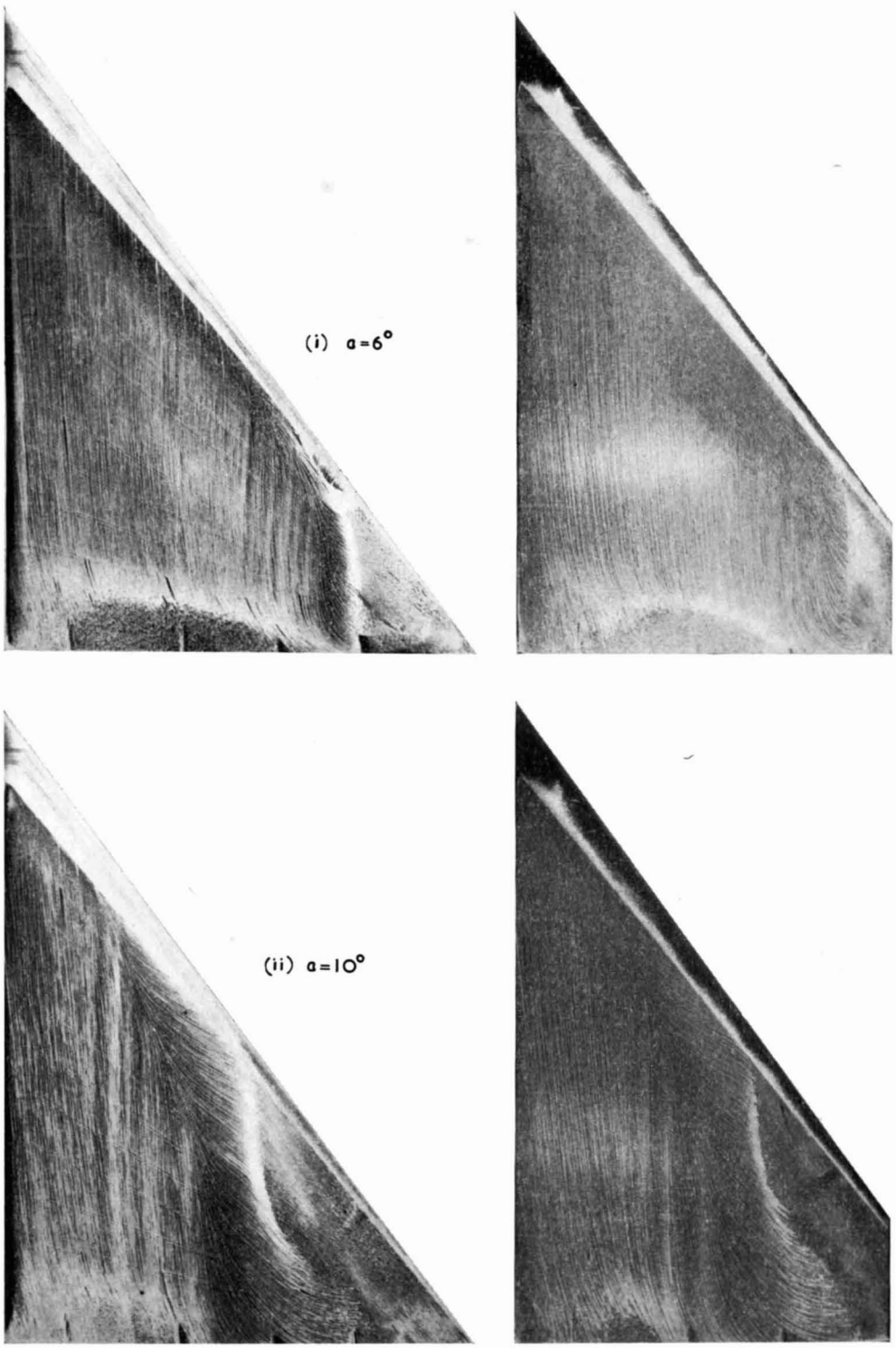

FIG. 37b. Comparison of upper-surface oil-flow patterns before and after cropping: $M_0 = 1{\cdot}00$.

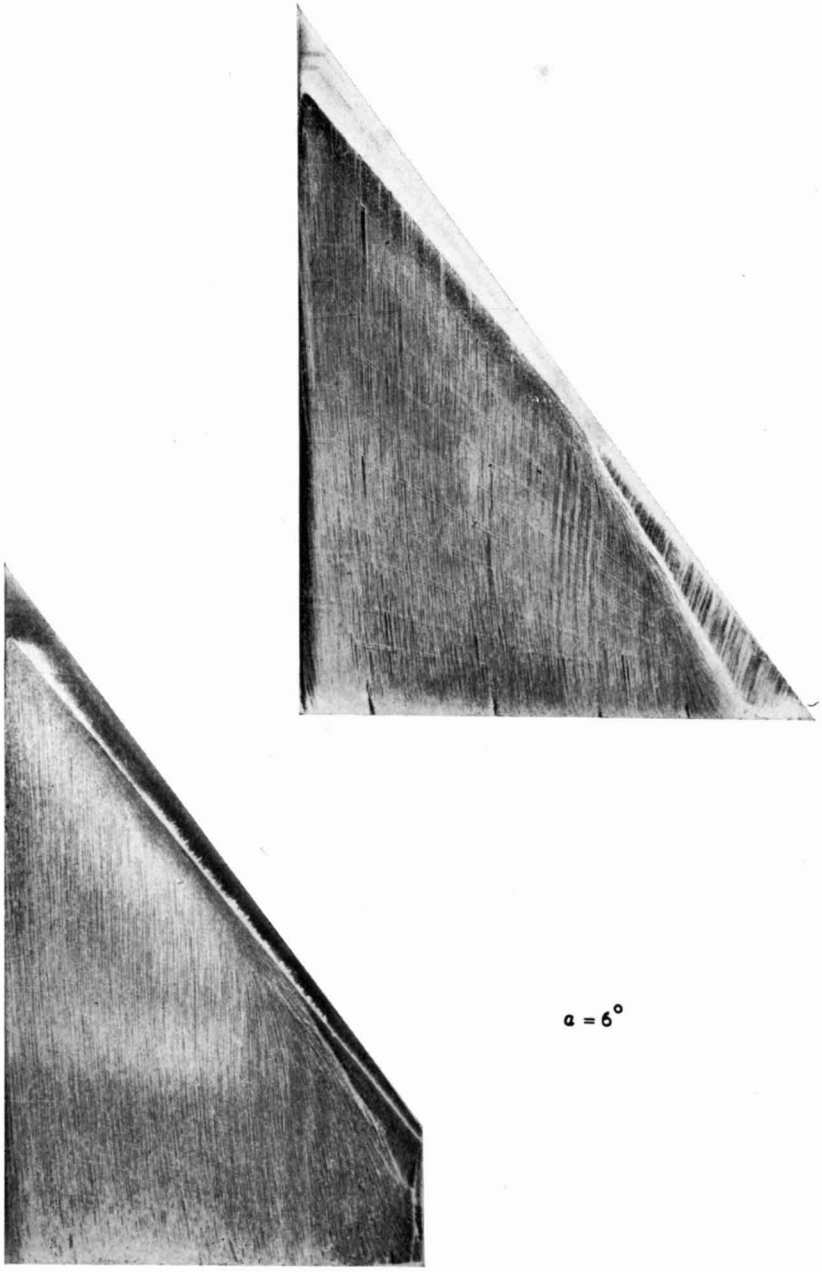

FIG. 37c. Comparison of upper-surface oil-flow patterns before and after cropping: $M_0 = 1 \cdot 11$.

(85536) Wt. 64/1857 K. 5 10/62 Hw.

Publications of the Aeronautical Research Council

ANNUAL TECHNICAL REPORTS OF THE AERONAUTICAL RESEARCH COUNCIL (BOUND VOLUMES)

1942 Vol. I. Aero and Hydrodynamics, Aerofoils, Airscrews, Engines. 75*s.* (post 2*s.* 9*d.*)
Vol. II. Noise, Parachutes, Stability and Control, Structures, Vibration, Wind Tunnels. 47*s.* 6*d.* (post 2*s.* 3*d.*)

1943 Vol. I. Aerodynamics, Aerofoils, Airscrews. 80*s.* (post 2*s.* 6*d.*)
Vol. II. Engines, Flutter, Materials, Parachutes, Performance, Stability and Control, Structures. 90*s.* (post 2*s.* 9*d.*)

1944 Vol. I. Aero and Hydrodynamics, Aerofoils, Aircraft, Airscrews, Controls. 84*s.* (post 3*s.*)
Vol. II. Flutter and Vibration, Materials, Miscellaneous, Navigation, Parachutes, Performance, Plates and Panels, Stability, Structures, Test Equipment, Wind Tunnels. 84*s.* (post 3*s.*)

1945 Vol. I. Aero and Hydrodynamics, Aerofoils. 130*s.* (post 3*s.* 6*d.*)
Vol. II. Aircraft, Airscrews, Controls. 130*s.* (post 3*s.* 6*d.*)
Vol. III. Flutter and Vibration, Instruments, Miscellaneous, Parachutes, Plates and Panels, Propulsion. 130*s.* (post 3*s.* 3*d.*)
Vol. IV. Stability, Structures, Wind Tunnels, Wind Tunnel Technique. 130*s.* (post 3*s.* 3*d.*)

1946 Vol. I. Accidents, Aerodynamics, Aerofoils and Hydrofoils. 168*s.* (post 3*s.* 9*d.*)
Vol. II. Airscrews, Cabin Cooling, Chemical Hazards, Controls, Flames, Flutter, Helicopters, Instruments and Instrumentation, Interference, Jets, Miscellaneous, Parachutes. 168*s.* (post 3*s.* 3*d.*)
Vol. III. Performance, Propulsion, Seaplanes, Stability, Structures, Wind Tunnels. 168*s.* (post 3*s.* 6*d.*)

1947 Vol. I. Aerodynamics, Aerofoils, Aircraft. 168*s.* (post 3*s.* 9*d.*)
Vol. II. Airscrews and Rotors, Controls, Flutter, Materials, Miscellaneous, Parachutes, Propulsion, Seaplanes, Stability, Structures, Take-off and Landing. 168*s.* (post 3*s.* 9*d.*)

1948 Vol. I. Aerodynamics, Aerofoils, Aircraft, Airscrews, Controls, Flutter and Vibration, Helicopters, Instruments, Propulsion, Seaplane, Stability, Structures, Wind Tunnels. 130*s.* (post 3*s.* 3*d.*)
Vol. II. Aerodynamics, Aerofoils, Aircraft, Airscrews, Controls, Flutter and Vibration, Helicopters, Instruments, Propulsion, Seaplane, Stability, Structures, Wind Tunnels. 110*s.* (post 3*s.* 3*d.*)

Special Volumes

Vol. I. Aero and Hydrodynamics, Aerofoils, Controls, Flutter, Kites, Parachutes, Performance, Propulsion, Stability. 126*s.* (post 3*s.*)
Vol. II. Aero and Hydrodynamics, Aerofoils, Airscrews, Controls, Flutter, Materials, Miscellaneous, Parachutes, Propulsion, Stability, Structures. 147*s.* (post 3*s.*)
Vol. III. Aero and Hydrodynamics, Aerofoils, Airscrews, Controls, Flutter, Kites, Miscellaneous, Parachutes, Propulsion, Seaplanes, Stability, Structures, Test Equipment. 189*s.* (post 3*s.* 9*d.*)

Reviews of the Aeronautical Research Council

1939–48 3*s.* (post 6*d.*) 1949–54 5*s.* (post 5*d.*)

Index to all Reports and Memoranda published in the Annual Technical Reports

1909–1947 R. & M. 2600 (out of print)

Indexes to the Reports and Memoranda of the Aeronautical Research Council

Between Nos. 2351–2449	R. & M. No. 2450 2*s.* (post 3*d.*)
Between Nos. 2451–2549	R. & M. No. 2550 2*s.* 6*d.* (post 3*d.*)
Between Nos. 2551–2649	R. & M. No. 2650 2*s.* 6*d.* (post 3*d.*)
Between Nos. 2651–2749	R. & M. No. 2750 2*s.* 6*d.* (post 3*d.*)
Between Nos. 2751–2849	R. & M. No. 2850 2*s.* 6*d.* (post 3*d.*)
Between Nos. 2851–2949	R. & M. No. 2950 3*s.* (post 3*d.*)
Between Nos. 2951–3049	R. & M. No. 3050 3*s.* 6*d.* (post 3*d.*)
Between Nos. 3051–3149	R. & M. No. 3150 3*s.* 6*d.* (post 3*d.*)

HER MAJESTY'S STATIONERY OFFICE

from the addresses overleaf

Printed and published by
HER MAJESTY'S STATIONERY OFFICE

To be purchased from
York House, Kingsway, London W.C.2
423 Oxford Street, London W.1
13A Castle Street, Edinburgh 2
109 St. Mary Street, Cardiff
39 King Street, Manchester 2
50 Fairfax Street, Bristol 1
35 Smallbrook, Ringway, Birmingham 5
80 Chichester Street, Belfast 1
or through any bookseller

Printed in England

S.O. Code No. 23-3286